

Analog and Digital Co-design Methods for Future Wireless Transmitters

Millaniyage Sidath Priyanka Madhuwantha

BEng, PG. Dip, MIET

Master of Engineering (Research) Degree



**Maynooth
University**

National University
of Ireland Maynooth

Department of Electronic Engineering

National University of Ireland, Maynooth

Ireland

August 2018

Head of the Department: Prof. Ronan Farrell

Supervisors in research: Dr. John Dooley and Prof. Ronan Farrell

Abstract

Increasing demand to provide higher data rates with spectral purity sets high standards for future mobile communication systems. Future wireless communication transmitters are challenged to improve their performance with reduced power consumption. Work performed in this thesis aims at improving several key areas of a wireless transmitter architecture to be more efficient and reliant on their power consumption.

A novel calibration technique based on constellation mapping of a quadrature amplitude modulated (QAM) signal is proposed to alleviate the analog impairments within a wireless transmitter at system level. This technique facilitates the mixed-signal approach towards building efficient, linear transmitters.

A primary front-end component of a wireless transmitter is the Power Amplifier (PA). Advanced architectures for PAs with improved power efficiency need to be explored for these future wireless communication systems. Ameliorations made towards improving the hardware structure in literature provides a variety of advanced power amplifier architectures. In analyzing the needs for the future mobile communication standards, and the complex nature of the signals involved, the Doherty power amplifier (DPA) architecture has indicated promise over the years. In this work, further improvements have been made on existing state-of-the-art Doherty PA architectures to aid wider-bandwidth operation to transmit at higher data rates. A distributed structure of four-way digitally controlled inputs has been suggested and its operation was tested at Ku-band frequency range.

Furthermore, in simulating advanced PA architectures such as mentioned above, the time taken to perform a single simulation for a PA is significant. As a result, in-order to perform a system level simulation of a transmitter with several PA's and other components will be even more apparent and less convenient. Therefore, for futuristic applications such as distributed arrays, a method of behavioral modeling of a fabricated asymmetrical DPA is suggested and tested.

Declaration

I, Millaniyage Sidath Priyanka Madhuwantha, certify that the Thesis is my own work and I have not obtained a Degree in the University or elsewhere on the basis of this Research Thesis. Information derived from published or unpublished work has been acknowledged within and a list of references is provided.

A handwritten signature in black ink that reads "S. Madhuwantha". The signature is written in a cursive style and is underlined with a single horizontal line.

Signature

21/ 11/ 2018

Date

This work is dedicated to my mother and father, for their love and trust in me.

Acknowledgment

For the past two years, there have been so much support and encouragement to successfully conclude this work. I would first like to thank my thesis supervisor Dr. John Dooley for his advice and guidance. Secondly, I would like to thank my co-supervisor Prof. Ronan John Farrell for his support and helpful suggestions.

All this work would not have been possible without the help and support of the team at Maynooth. My sincere thanks to Prasad Ramabadran who has helped me with his vast experience and valuable insight as a mentor, James Kinsella whose support that I really appreciate in the fabrication of boards in debugging, and support in casual/helpful conversations at challenging times. To Mrs. Joanna O'Grady for her valuable help with administration work and for friendly conversations.

I would also like to extend my thanks to the good company of my colleagues which was helpful throughout my stay at Maynooth Dr. Shawaiz Iqbal, Pavel Afanasyev, Declan Byrne, Dr. Sara Adel, Sara Hesami, Joseph Finnegan, Ziming Wang, Minh Thuy Pham, Meabh Loughman, Anqi Hu, Dr. Somayeh Mohammady, and Abdulrahman Alqadami.

For the work that I performed along with the company Benetel, I would like to thank Kyriaki Niotaki and John Doyle. Additionally, I would also like to extend my gratitude to Mr. Ken Collins from Rohde & Schwarz for his help with additional laboratory equipment and in answering related questions. And to all other companies and individuals who supported and helped us with devices and their services.

Table of Contents

Analog and Digital Co-design Methods for Future Wireless Transmitters.....	i
Abstract.....	ii
Declaration.....	iii
Dedication.....	iv
Acknowledgment.....	v
Table of Contents.....	vi
List of Figures.....	x
List of Tables.....	xiv
List of Acronyms.....	xv
List of Publications.....	xvii
Chapter 1 Introduction.....	1
1.1. Background.....	1
1.2. Motivation.....	6
1.3. Thesis Outline and Research Contributions.....	6
1.3.1. Chapter 2.....	6
1.3.2. Chapter 3.....	7
1.3.3. Chapter 4.....	8
Chapter 2 Novel Calibration Technique for RF Transmitters.....	9
2.1. RF Path Calibration.....	9

2.2. Summary of Previous Calibration Techniques.....	12
2.3. Experimental Validation Indicators of Performance Improvement.....	14
2.3.1. Visual Inspection Techniques.....	14
2.3.1.1. Error Vector Magnitude (EVM).....	15
2.3.1.2. Visual Analysis of The Receiver Spectrum.....	15
2.4. Constellation Mapping for RF Path Calibration.....	18
2.5. Identifying Distortion Components Using Constellation Mapping.....	22
2.6. Weakly Nonlinear System Testing at S-band.....	23
2.6.1. A Test Case of an 8-PSK Signal.....	23
2.6.2. A Test Case of a 256-QAM Signal.....	24
2.7. Weakly Nonlinear System Testing at Ku-band.....	25
2.7.1. Testing for Consistency.....	26
2.7.2. A Test Case of an 8-PSK and 256-QAM Signals.....	28
2.8. Strongly Nonlinear System Characterization.....	29
2.8.1. Two Separate Test Setups Used.....	29
2.8.2. Strongly Nonlinear System Driven with a Small Signal.....	30
2.8.2.1. Testing with 8-PSK Signal.....	32
2.8.2.2. Strongly Nonlinear System Driven with Large Signal Input.....	33
2.9. Conclusions.....	41
Chapter 3 N-way Digitally Driven Doherty Power Amplifier For Ku-band Applications.....	42
3.1. Need for a N-Way Digitally Driven DPA.....	42
3.2. Existing Doherty Power Amplifier Topologies.....	44

3.2.1. Symmetrical Doherty Power Amplifier.....	45
3.2.2. Asymmetrical Doherty Power Amplifier.....	46
3.2.3. Digitally Driven Doherty Power Amplifier.....	47
3.2.4. N-Way Doherty.....	48
3.2.4. N-way Digitally Driven Doherty Power Amplifier.....	50
3.3. Summary of The Design Procedure.....	54
3.3.1. Concept of Load-modulation.....	57
3.4. Conclusions.....	66
Chapter 4 Behavioral Modeling.....	67
4.1. Behavioral Modeling of RF Power Amplifiers.....	67
4.2. Memory effect of a PA.....	69
4.3. Estimation of Model Accuracy.....	69
4.4. Memory-less Modeling Techniques.....	70
4.4.1. AM/AM and AM/PM.....	70
4.4.1.1. Saleh Model.....	71
4.4.1.2. Polynomial Model.....	72
4.5. Models that capture memory-effects of PA's.....	74
4.5.1. Hammerstein Model.....	74
4.5.2. Alternate Models.....	75
4.5.2.1. Weiner-Hammerstein Model.....	75
4.6. Volterra Series.....	76
4.6.1. Memory Polynomial.....	77
4.7. Neural Networks (NN).....	79

4.7.1. A Piecewise Segmented Polynomial.....	81
4.7.2. Vector Partitioning.....	82
4.7.2.1. K-Means.....	82
4.7.2.2. Kohonen’s Self-Organized Maps (SOM).....	84
4.8. Conclusions.....	87
Chapter 5 Conclusions and Future work.....	88
5.1. Conclusions.....	88
5.2. Future Work from Novel Calibration Technique.....	92
5.3. Future Work from N-way Digitally Driven Doherty Amplifier	93
5.4. Future Work from Behavioral Modeling.....	94
References.....	95
Appendix.....	102

List of Figures

Fig. 1. An example figure of individual blocks of an RF transmitter used for weakly and strongly nonlinear system characterization. 10

Fig. 2. Illustration of AMAM distortion. 10

Fig. 3. Illustration of AMPM conversion effects. 11

Fig. 4. An example illustration of the concept EVM, ideal symbol point lies on path in blue and received/measured point lies on path in red (dashed). 15

Fig. 5. An example of the uncalibrated and calibrated magnitude spectrum of 256-QAM signal at Ku-band. 16

Fig. 6. An example of the uncalibrated and calibrated magnitude spectrum of 256-QAM signal within passband. The figure was captured at Ku-band. (blue trace) uncalibrated signal, (black) calibrated signal. 17

Fig. 7. Designed 64-QAM Constellation with the inclusion of all unique Permutations, as seen from the figure all transitions between points have been accounted for. 19

Fig. 8. Magnitude and phase of the calibration signal in the frequency domain. 19

Fig. 9. Constellation of the calibration signal/ideal symbol location (red - *) and the captured signal (blue - o) and the correction of vector positioning of the symbol (black - o). Constellation is presented by means of a polar plot to indicates the advantages of both amplitude and phase positions of the 64-QAM signal stimuli. 20

Fig. 10.(a) The plot of the constellation of the strongly nonlinear system indicating outer constellation symbols subjected to AMAM distortion and inner symbols subjected to AMPM. (b) Constellation plot of a weakly driven nonlinear system where outer symbols have been subjected to AMPM conversion. Both figures are from experimentation test cases, each case is presented in-detail in section 2.8. 20

Fig. 11.8-PSK constellation (a) before and (b) after calibration. 23

Fig. 12.8-PSK constellation zoomed view of constellation points (a) before and (b) after calibration 24

Fig. 13. 256-QAM constellation (a) before and (b) after calibration.....	24
Fig. 14. Enlarged figure of constellation in Fig. 13 (a) before and (b) after calibration.	25
Fig. 15. Test results for different 64-QAM signal inputs.....	26
Fig. 16. (a) Captured un-calibrated 64-QAM signal (for each iteration the constellation for un-calibrated case was observed to be similar, for simplicity only the first capture is shown), (b) – (g) presents demodulated constellation for each of the six individual 64-QAM signals after performing RF path calibration...26-27	26-27
Fig. 17. Calibrated cases at 14.32 GHz (a) 8-PSK signal (b) 256-QAM signal	28
Fig. 18. Strongly nonlinear system characterization with high input power.....	29
Fig. 19. Strongly nonlinear system characterization at a low input power level with the wide-bandwidth input signal.....	30
Fig. 20. The amplitude response of the test-setup as assembled in Fig. 19, of 64-QAM calibrated and un-calibrated signal magnitude spectrum. Two traces: uncalibrated (blue) calibrated (black). (a) Passband zoomed view, (b) carrier and image view.	30
Fig. 21. Strongly nonlinear system driven with the wideband small signal input of different 64-QAM signals (Test setup as indicated in Fig. 19).....	31
Fig. 22. (a) Uncalibrated case (b) calibrated case, demodulated 64-QAM constellation (Different QAM modulated signal to that of the stimulus).....	32
Fig. 23. (a) Uncalibrated case (b) Calibrated case, demodulated 8-PSK constellation..	32
Fig. 24. Magnitude Spectrum of uncalibrated strongly (+5 dBm) and weakly (-10 dBm) driven DPA.	34
Fig. 25. The uncalibrated response of weakly nonlinear DPA (input signal power of -10 dBm)	35
Fig. 26. Magnitude Spectrum of uncalibrated strongly (+5 dBm) mildly (0 dBm) weakly (-5 dBm) driven DPA.....	36
Fig. 27. Uncalibrated test-setup (Fig. 18 type) indicating an EVM of ~11 % and SNR of 18.7 dB at strongly nonlinear conditions (+5dBm input)	37
Fig. 28. Calibrated test-setup (Fig. 18 type) indicating an EVM of 4.4 % and SNR of 27 dB at strongly nonlinear conditions (+5dBm input)	37
Fig. 29. Demodulated constellation view of uncalibrated test setup under strongly nonlinear conditions. (as in test-setup described by Fig. 27).....	38

Fig. 30. Demodulated constellation view of calibrated test setup under strongly nonlinear conditions. (as in test-setup described as in Fig. 28) 38

Fig. 31. Demodulated constellation view of uncalibrated test setup under weakly nonlinear conditions. AMPM conversion can be clearly observed from the constellation rotation..... 39

Fig. 32. Demodulated constellation view of calibrated test setup under weakly nonlinear conditions..... 39

Fig. 33. A visual illustration of different types of power conversions of a power amplifier. 42

Fig. 34. A tree-map chart of power consumption in the percentage of that of a base-station 43

Fig. 35. General topology of a single input symmetrical Doherty Power Amplifier. 45

Fig. 36. An example architecture of a digitally driven DPA..... 47

Fig. 37. N-way architecture of a Doherty Power Amplifier, with a N-way power splitter and a combiner and at the input and output respectively..... 49

Fig. 38. N-way architecture of a Doherty Power Amplifier, with a N-way power splitter and a combiner and at the input and output respectively..... 50

Fig. 39. An example design flow for a design of symmetrical DPA and a comparison of measured and modeled performance of S-parameters of the device used. 55

Fig. 40. An example arrangement of a symmetrical DPA schematic diagram [29]..... 56

Fig. 41. An example setup of load-modulation operation. Which takes place on a two-way symmetrical Doherty PA design. Two amplifiers are represented by Voltage Controlled Current Sources (VCCS). 57

Fig. 42. The characteristic plot for output current vs voltage plot of the device. R_L – load impedance seen by the device been characterized. 58

Fig. 43. The test-setup used to investigate the best possible characteristic impedance value of the impedance converter [29]..... 59

Fig. 44. Results from simulation in Fig. 43, with output power vs impedance sweep values [29]..... 60

Fig. 45. (a) Loadpull contours obtained for simulations of carrier-branch on a Smith chart centered at a center at a chosen impedance for peaking-branch. Impedance sweep

points/surface samples (black dots), Power contours (red), PAE contours (blue), impedance inverter response (green circle).	60
(b) Indicates the overlapping of chosen impedance point (red) on the VSWR circle without the contours, as an image that can be used to see the proximity to an actual maximum of PAE (marker m_4).....	61
Fig. 46. Testing of offset line impedance for the peaking path presenting a high impedance at the designed frequency of 15 GHz.	61
Fig. 47. An example of test-bench which can be used for single tone measurements. Additionally, RF power presented to each of the branches can also be swept [29].....	62
Fig. 48. Simulation results of the overall two-way Doherty power amplifier [29].....	63
Fig. 49. PAE vs output power curve for two-way and four-way DPA architectures [29]....	64
Fig. 50. Transmitted (Tx) and received (Rx) constellation diagram of the 64-QAM signal. (Tx- red, Rx-blue) [29].	65
Fig. 51. Magnitude spectrum of the output spectrum [29] (Input signal – red, Low-power mode output, High-power mode).....	65
Fig. 52. AM/AM-AM/PM model characterizing the output signal of the DPA in AM/AM distortion curve [42].....	73
Fig. 53. AM/AM-AM/PM model characterizing the output signal of the PA in AM/PM distortion curve [42].....	73
Fig. 54. Hammerstein model block diagram	74
Fig. 55. Weiner model.....	75
Fig. 56. Classic Volterra model characterizing the output signal of the PA in AM/AM distortion curve [42].....	78
Fig. 57. Classic Volterra model characterizing the output signal of the PA in AM/PM distortion curve [42].....	78
Fig. 58. Block diagram of TDNN model	80
Fig. 59. Example of a piecewise segmentation of each sample in a signal into different zones base on its magnitude.....	81
Fig. 60. Euclidean distance calculation.....	83

Fig. 61. Neuron structure of a SOM, with several weights (ω_i), inputs ($X(n)$ is the discrete input signal.) and monotonic binary function.	85
Fig. 62. The magnitude of frequency domain plots of output from each model compared with the measured results [42]	85
Fig. 63. K-means and SOM model characterizing the output signal of the PA in AM/AM distortion curve.	86
Fig. 64. K-means and SOM models characterizing the output signal of the PA in AM/PM distortion curve.	86
Fig. 65. Overall view of research performed placed in relation to the RF transmit path.....	91
Fig. 66. 8-PSK uncalibrated constellation test result at Ku-band.....	102
Fig. 67. 256-QAM uncalibrated constellation test at Ku-band. SNR of the signal is lower than that of the Shannon limit for correct demodulation of 256-QAM signal constellation.....	102
Fig. 68. 64-QAM uncalibrated constellation with DPA at linear conditions at a very low input power level (-10dBm).....	103
Fig. 69. Magnitude spectrum of uncalibrated and calibrated strongly nonlinear system (with DPA, driver amplifier and DAC board – example test setup is Fig. 19) driven with 80 MHz 64-QAM modulated calibration signal captured at 500 MHz of span (RBW 100 kHz, VBW 1 MHz and SWT 75 ms).....	103

List of Tables

Table 1. Comparison of different test setups; linear, weakly nonlinear and strongly nonlinear.	40
Table 2. Comparison of different Power amplifiers and topologies used in similar applications.	52
Table 3. Comparison of linear performance of the DPA.	54
Table 4. Models with their NMSE values in comparison to the measured output [42]..	70

List of Acronyms

3GPP, 3rd Generation Partnership Project
ACLR, Adjacent Channel Leakage Ratio
ANN, Artificial Neural Network
AM, Amplitude Modulation
CAD, Computed Aided Design
CFR, Crest Factor Reduction
CO₂, Carbon Dioxide
dB, decibel
dBm, dB with respect to one milliwatt
DPA, Doherty Power Amplifier
DPD, Digital Predistortion
DSP, Digital Signal Processing
DUT, Device Under Test
DVB, Digital Video Broadcasting Standard
ET, Envelope Tracking
EVM, Error Vector Magnitude
FIR, Finite Impulse Response
IMD, Intermodulation Distortion
IQ, Inphase and Quadrature phase
ITU, International Telecommunication Union
LEO, Low Earth Orbit Satellite
LO, Local Oscillator
LRRM, Line-Reflect-Reflect-Match
LTE, Long Term Evolution
LTI, Linear Time Invariant
MATLAB, Matrices Laboratory

MEO, Medium Earth Orbit
MHz, Mega Hertz
MIMO, Multiple input Multiple output
MLP, Multilayer Perceptron
MMIC, Monolithic Microwave Integrated Circuits
NMSE, Normalized mean square error
OFDM, Orthogonal Frequency Division Modulation
PA, Power Amplifier
PAE, Power Added Efficiency
PAPR, Peak to Average Power Ratio
PM, Phase Modulation
PRBS, Pseudo-Random Binary Sequence
QAM, Quadrature Amplitude Modulation
RF, Radio Frequency
RMS, Root-mean Square
Rx, Received signal
SLOT, Short-Open-Load-Reciprocal
SNR, Signal To Noise Ratio
SOLAR, Short-Open-Load-Reciprocal
SOM, Self-Organized Maps
TDNN, Time-delay Neural Network
TRL, Thru-Reflect-Line
Tx, Transmitted signal
VNA, Vector Network Analyzer
VSA, Vector Signal Analyzer
VSV, Vector Switched Volterra

List of Publications

1. S. Madhuwantha, P. Ramabadran, R. Farrell, and J. Dooley, “Novel Calibration Technique for Wideband Transmitters using Constellation Mapping,” submitted to (unpublished) 92nd ARFTG Microwave Measurement Conference, Orlando, Florida, January 20-23, 2019.
2. S. Madhuwantha, P. Ramabadran, R. Farrell, and J. Dooley, “N-way Digitally Driven Doherty Power Amplifier Design and Analysis for Ku band Applications,” presented at the Conf. in 29th Irish Signals and Systems Conference, Queens University Belfast, UK, June. 21-22, 2018.
3. S. Madhuwantha, J. Dooley, P. Ramabadran, D. Byrne, K. Niotaki, J. Doyle, R. Farrell “Behavioural Models for Distributed Arrays of High-Performance Doherty Power Amplifiers,” presented at the Conf. in 29th Irish Signals and Systems Conference, Queens University Belfast, UK, June. 21-22, 2018.
4. P. Ramabadran, S. Madhuwantha, P. Afanasyev, R. Farrell, L. Marco, S. Pires and J. Dooley, “Digitally Assisted Wideband Compensation of Parallel RF Signal Paths in a Transmitter,” 91st ARFTG Microwave Measurement Conference, Philadelphia, PA, USA, 2018.
5. P. Ramabadran, S. Madhuwantha, P. Afanasyev, R. Farrell, J. Dooley, “Wideband Interleaved Vector Modulators for 5G Wireless Communications,” IEEE MTT-S International Microwave Workshop Series on 5G Hardware and System Technologies, Dublin, Ireland, 30th -31st August 2018.
6. S. M. Alqadami, S. Madhuwantha, R. Farrell and J. Dooley, “A 5 W high-efficiency Class AB power amplifier for LTE base station application,” 28th Irish Signals and Systems Conference (ISSC), Killarney, 2017, pp. 1-5.

Chapter 1

Introduction

1.1. BACKGROUND

Wireless transmitter and receiver hardware components are governed by the laws of physics in their operation, which limits their performance. For example, a limited operational band of hardware components introduces spectral impurity. Moreover, as described by laws of electromagnetics physical components in close quarters interact with each other electrically (under permitting conditions) thus resulting in undesired performance such as signal distortion and loss in efficiency as the useful transmit signal is coupled elsewhere. To address the challenges of future mobile communication systems it is of the utmost importance that the physical components used in the communication system operate at their optimum capability.

In addition to the hardware components used in the physical layer, present-day modulation schemes are also designed to provide high-throughput as well as being spectrally efficient to meet the demands of mobile communication standards. An example is Long Term Evolution (LTE) which is an international standard used in cellular communication systems aimed at providing service of fourth-generation mobile broadband systems. LTE-Advanced and LTE-Advanced Pro are derived standards developed by the 3rd Generation Partnership Project (3GPP¹) in exceeding the fourth-generation radio-communication standard defined by International Telecommunication Union (ITU) [5]. Orthogonal Frequency Division Multiplexing (OFDM) is a modulation technique in which a digital data is arranged across different multiple orthogonal sub-

¹ <http://www.3gpp.org/about-3gpp>

carriers in the frequency domain consisting of highly spectrally efficient and distortion resilient modulation scheme [6]. It is widely used in digital television, audio broadcasting, broadband internet services etc [6].

In terms of a system level point of view, it is of vital importance that both hardware components and modulated input signals that drive the hardware both are at their optimum capability in performance. However, it is a well-known fact that hardware components such as a nonlinear power amplifier performs best with constant envelope modulated signals at saturation operating regime providing higher efficiencies. Although, spectrally efficient modern-day modulation schemes operate with varying envelopes maximizing their capacity in-accordance with information theory. Signals with varying envelopes consist of higher and lower amplitude levels. Meaning the hardware components that the signal propagates through must be able to handle efficiently both signal levels (or multiple levels) without incurring clipping or introducing a distortion which leads to loss of information in the transmitted signal.

As an integration platform for both hardware and modulated input signals (radio frequency signals carrying useful information), digital signal processing (DSP) techniques can be identified. A few common DSP techniques are crest factor reduction (CFR), digital pre-distortion (DPD), and Calibrating of the hardware impairments. The purpose of CFR techniques is to reduce the peak to average power ratio (PAPR) of the transmitted signal while preserving the quality of the transmitted signal. Reduction of the peak to average ratio of the signal allows the power amplifier to be operated at or near the compression point thus resulting in higher efficiency. Clipping and windowing, peak windowing are a few CFR techniques that are commonly used [1], [2]. Digital predistortion can use a model of the device generated by physical, circuit level or behavioral modeling and uses an inverse function of the nonlinear impairments introduced into the signal by the power amplifier when the RF signal propagates through the device. Therefore, this inverse function then can be applied to reduce distortion present in the modeled power amplifier in practice, facilitating the further improvement of its performance. Performing a path calibration allows the identification of In-phase and Quadrature-phase (IQ) imbalances present within the transmit or receive path and pre-compensate them by incorporation of the imbalance into the RF input signal. In summary, all of the above-mentioned techniques

help comply with spectral mask and error vector magnitude (EVM) requirements set by wireless communication standards as well as improving the overall efficiency of the entire system.

In terms of analog hardware components, the power amplifier is the main component that is operated in a nonlinear operating regime. Several advanced structures have been proposed more recently in the literature to deliver higher efficiency power amplifiers for future communication systems. An outphasing power amplifier uses two phase modulated input signals with constant amplitude to drive the PA. Constant amplitude feeding to the PA assures higher power efficiency. However, one major concern with this technique is that the bandwidth expansion caused by phase modulation [4]. In addressing modern communication signals with higher bandwidths with an increase in information, the resultant bandwidth expansion is several times the original signal bandwidth, this causes complications within the entire transmit chain. Envelope tracking (ET) is another advanced PA architecture which improves the power efficiency of the PA. Principle in ET is to extract the RF envelope of the input signal by an envelope detector and use it to modulate the supply voltage to the PA. Several challenges exist in this methodology, for example, the time delay between the envelope path and RF path needs to be equal. ET power supply bandwidth needs to be higher than that of the envelope of the signal, to ensure the linear efficient performance of the PA [3]. Another PA architecture is the Doherty power amplifier (DPA) configuration. A DPA incorporates two paths (namely carrier and peaking/auxiliary) for the input signal to propagate and amplify through, the outputs are then recombined. The carrier path is biased in class AB and can amplify an average level of signal input and the auxiliary path is biased at class C and is turned on at the peaks of the input signal. This combined operation of both paths of an DPA, helps to handle signals with high PAPR.

In order to address the above-mentioned challenges, this research work presents three different solutions. First, is to provide an integration platform between hardware and input drive signals (software) using a novel RF path calibration technique incorporating DSP techniques. Secondly, to improve the existing hardware within the RF transmitter (specifically the PA), a method of using several small signal amplifiers in a digitally driven N-way Doherty topology to achieve the performance of a single large signal PA

with even greater flexibility is introduced. Finally, to address the challenge of increased complexity and simulation time expected for highly efficient power amplifiers deployed as distributed arrays in advanced telecommunications systems such as 5G a behavioural modelling solution is presented as a viable option with experimental validation with an asymmetrical DPA.

It is of vital importance when considering a system level architecture of the RF transmitter that each hardware component operates at its maximum efficiency without introducing heavy distortion into the information signal, thus resulting in a reliable information transfer through the RF transmit chain. This can be achieved by digitally pre-compensating (DSP technique) the input modulated signal (a method similar to pre-distortion) to alleviate the RF path impairments (which are introduced by the hardware components in the transmitter) when the signal propagates through the RF blocks. After performing pre-compensation, the signal received at the end of the RF transmit path is an amplified, quadrature up-converted and a non-distorted version of the original signal, hence the system can now be termed as a calibrated RF transmitter. The novel calibration technique is a non-iterative method which comprises of a specially designed 64-QAM modulated test signal. Since this modulation format closely resembles a standard modern communication signal used in practice using a 64-QAM modulation provides an additional advantage of the technique being suitable to be applied in many test scenarios such as; characterization of both weakly and strongly nonlinear systems. A modulated stimulus signal such as 64-QAM consisting of multiple amplitude levels and phases in the time domain can identify both power and frequency dependent RF path impairments. Compensation is achieved for the identified distortion components in the form of an finite impulse response (FIR) filter. This filter transfer function is then convolved with the intended transmit signal, thus resulting in a perfect non-distorted signal at the output of the transmitter upon transmission.

As explained earlier power amplifier is a component in the RF transmitter which consumes a considerable portion of the input power supply. Power efficient operation, the capability of handling wideband spectrally efficient signals and linear operation are major concerns in choosing a base station PA for satellite-based applications in Ku-band. To handle these concerns a futuristic method of using a combination of several small signal

PA's in a Doherty type topology has been identified. This method offers performance similar to that of a using a single large signal PA with additional advantages such as the flexibility to turn-off and turn-on its paths as per the user requirements. This is helpful in scenarios such as operating the system with the limited amount of input power which requires an efficient signal amplification or to adjust the number of paths based on the input signal characteristics such as operating with input signals consisting of a variety of PAPR levels. In this work, a detailed analysis of existing methods and the design methodology of the presented technique in comparison with prior-art has been presented. The technique has been validated using signal bandwidths up to 800 MHz at Ku-band.

High-efficiency PA topologies in distributed networks with increased complexity are required to provide the additional increase in performance required for 5th generation telecommunications. However, in doing so simulation time and hence production time will also increase proportionally. The concept of using a behavioral model instead of a circuit level or physical model for a DPA is suggested. Behavioral modeling provides a software-based characterization of a hardware component based on its input and output responses. The method is tested using the input-output responses of a fabricated asymmetrical Doherty power amplifier while operating at its nonlinear operating region offering amplification with higher power efficiency. A variety of behavioral modeling techniques were used in order to prove their ability and the suitability for accurate characterization of the device.

In observing the trends of future wireless communications standards that facilitate the needs of the future customer, it can be understood the need for higher efficiency and greater reliability in both hardware and software segments in a transmitter. As mentioned above the contribution of this research work is to implement methods of co-design of hardware and software for better integration, thus improving the performance of the wireless transmitters.

1.2. MOTIVATION

The objective for the research work performed in this thesis is to address the problems as described above by integrating DSP techniques and advanced hardware architectures to overcome physical and operational limitations that are present in a wireless communication system. As an outcome of improving the physical components and their overall performance, it is expected to help meet the stringent requirements of future mobile communication standards.

1.3. THESIS OUTLINE AND RESEARCH CONTRIBUTIONS

1.3.1. CHAPTER 2

In chapter 2, an existing problem of IQ imbalance and path impairments in relation to RF path of a wireless transmitter has been identified. A novel technique for calibration of RF transceivers based on constellation mapping of a 64-QAM test signal is proposed. A brief history of different calibration techniques is presented. Specific advantages of the stimulus itself includes the ability to detect impairments such as AMAM, AMPM, Inter-symbol interference (ISI) etc. has been identified and explored in detail. The concept has been validated for both weakly and strongly nonlinear test conditions with a variety of test signals.

The use of a modulated test signal closely resembles a real application, therefore in comparison to other test signals applying a modulated test signal provides a better test case.

1.3.2. CHAPTER 3

Chapter 3 presents an interesting challenge in enhancing the performance of the power amplifier. A power amplifier is known to be a high power consuming device in a base-station. Therefore, it is of vital importance that the power amplifiers are made to operate efficiently. However, with the increase in complexity in present and future modulation schemes, significant improvements are necessary in-order to facilitate the specifications as well as to conserve power in operation. Based on the state-of-the-art methods a further advanced solution of a digitally-driven four-way Doherty power amplifier with a unique impedance transformation ratio at Ku-band has been proposed as a potential solution to address the above-mentioned challenges. The design was tested using a 64-QAM modulated input signal of 800 MHz bandwidth at Ku band frequency range. From this analysis, it is identified that the design has potential for scalability, operate with improved efficiency and with reduced power consumption.

The design is aimed at providing a viable solution for Low Earth Orbit (LEO) and Medium Earth Orbit (MEO) satellites where problems such as high efficiency, higher linearity are of greater concern.

In concluding the work performed a paper publication was presented at 29th ISSC Irish Signals and Systems Conference.

S. Madhuwantha, P. Ramabadran, R. Farrell, and J. Dooley, “N-way Digitally Driven Doherty Power Amplifier Design and Analysis for Ku band Applications,” presented at the Conf. in 29th Irish Signals and Systems Conference, Queens University Belfast, UK, June. 21-22, 2018.

1.3.3. CHAPTER 4

Advanced system architectures such as Massive Multiple Input Multiple Output (Massive-MIMO) have been identified to overcome challenges faced by future mobile communication systems such as the simulation of large numbers of power amplifiers. Realising these systems requires the incorporation of a distributed array of power amplifiers within the transmitter. However, with the increase in complexity of the design, the time taken for production or to perform system level testing is significantly higher. As a solution to this problem behavioral modeling techniques can be used to perform a system level simulation of the design with reduced time and sufficient accuracy. As an efficient power amplifier, an asymmetrical Doherty power amplifier (single input single output system) was fabricated and utilized for this work to compare numerous behavioral models. Work performed experimentally extracts computationally efficient models for the mentioned high efficiency asymmetrical DPA architecture. Historical aspects of behavioral modeling and concepts were also presented. The Doherty power amplifier was modeled using several modeling techniques. The results and metrics used were explained in identifying a suitable solution for modeling an asymmetrical Doherty power amplifier².

In concluding the work performed a paper publication was presented at 29th ISSC Irish Signals and Systems Conference.

S. Madhuwantha et al., “Behavioural Models for Distributed Arrays of High-Performance Doherty Power Amplifiers,” presented at the Conf. in 29th Irish Signals and Systems Conference, Queens University Belfast, UK, June. 21-22, 2018.

² This work was performed along with a company named Benetel <http://www.benetel.com/>

Chapter 2

Novel Calibration Technique for RF Transmitters

The aim of this chapter is to present a novel calibration technique which uses a 64-QAM modulated input signal designed with all possible permutations of its constellation points to calibrate the signal path for both weakly nonlinear and strongly nonlinear systems. Comprehensive testing was performed consisting of a variety of test cases to prove the validity of the proposed technique.

2.1. RF PATH CALIBRATION

Due to increasing demand for higher data rates to support of modern communication systems such as high-definition television, satellite communication, online real-time games, and real-time video broadcasts; the need for reliable information transfer is of significant importance. Wireless transceivers such as those used in base-stations are widely deployed in cellular networks. A wireless communication system encompasses hardware components, signal processing techniques, and standardized communication layers. These technologies are responsible for allowing the transmission of information in an efficient and reliable manner. Physical impairments of RF hardware components within a transmitter or a receiver chain can contribute to the loss of information and losses in efficiency in most communication systems. One solution to this issue is to intelligently apply digital signal processing methods to alter the transmission signal to mitigate physical limitations existent on the RF transmit path.

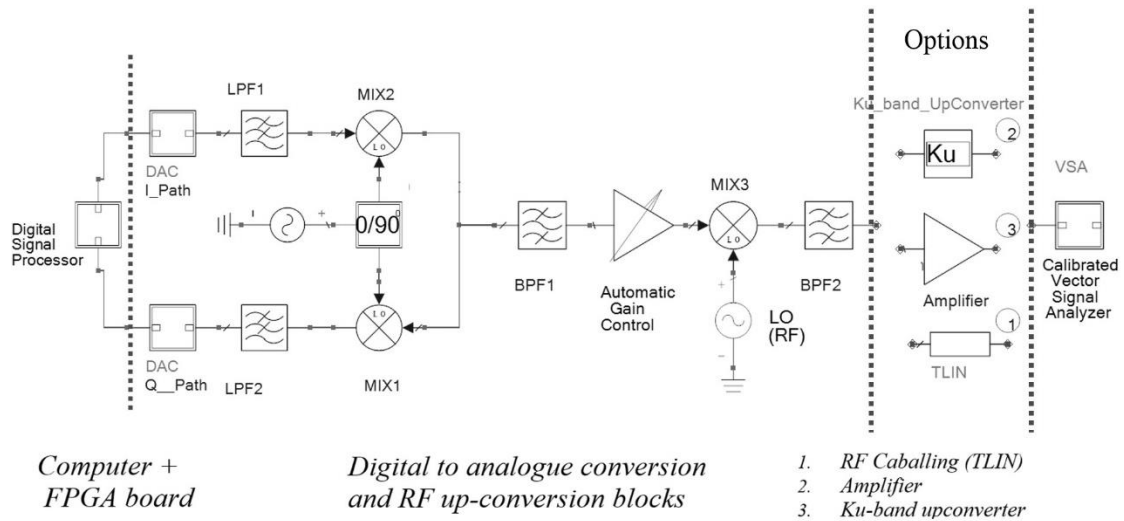


Fig. 1. A block diagram of an RF transmitter used for weakly and strongly nonlinear system calibration.³

Phenomena such as AMAM, AMPM conversion, IQ imbalance, local oscillator (LO) leakage, group delay and sinc roll-off exists in most practical RF transmit and receive paths. IQ imbalance and LO leakage are both frequency independent distortions while group-delay and amplitude roll-off are frequency dependent nonlinear distortion factors. Compensation for the above-mentioned phenomena is necessary as it significantly affects the quality of the information signal sent through the RF paths.

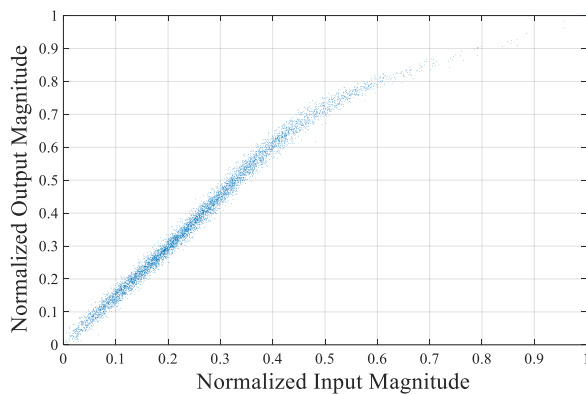


Fig. 2. Illustration of AMAM distortion.

Fig. 2 is a plot of the ratio of normalized output amplitude to the normalized input amplitude plotted for each sample. This plot illustrates the concept of AMAM distortion

³ Figure as shown above is only for indicating block level components of an RF transmitter, results obtained in all testcases are from practical testing.

caused by a power amplifier. As can be seen from Figure 2 above, operation of 1dB compression point, the PA will exhibit strongly nonlinear behavior. As a result, the gain of the PA is affected therefore linear response of the output amplitude with respect to the input amplitude is no longer held.

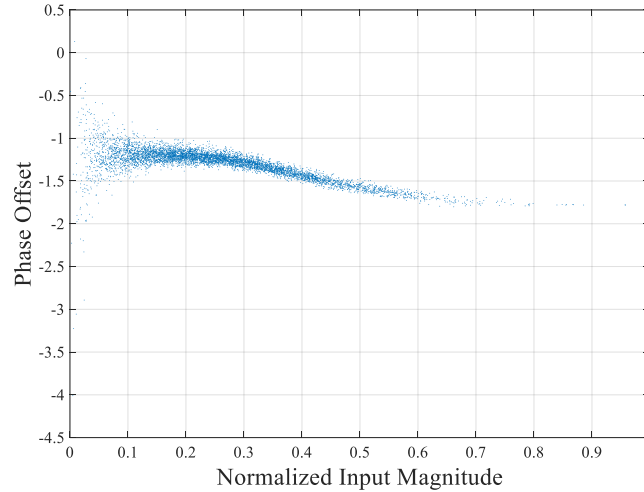


Fig. 3. Illustration of AMPM conversion effects.

In Fig. 3 AMPM conversion effects are highlighted. The relationship of input amplitude with the output phase is plotted in the above figure. As seen by the figure once the higher amplitude levels are reached the phase response of the example system is no longer linear thus AMPM distortion effects are said to be in effect. As can be seen from Fig. 10. (a) before the application of the path calibration, the constellation points are packed closer together in the output signal constellation illustrating AMAM effect. Similarly, in Fig. 10. (b) AMPM effect is displayed by a rotation of the constellation points with respect to their ideal locations.

In Fig. 1, the mixers 1,2 (MIX1, MIX2) in combination with the Local Oscillator forms the quadrature modulator whose performance is critical to the integrity of the vector modulated signal generated. These mixers, however, introduce frequency independent amplitude offsets between the paths owing to offsets in the gains of the mixers, frequency dependent impairments such as amplitude ripple and tilt over the band of interest, IQ phase errors owing to the deviations in the phases of the LO signals from quadrature condition at the LO input ports of the mixers. Under ideal conditions the gain of the two mixers should be equal and phase difference between them should be an exact quadrature relation. The mixer 3 (MIX3) which is a part of the RF up-converter section also

introduces additional amplitude ripple and tilt along with non-linear phase response over the bandwidth of interest. The impact is summarized in Fig. 5 in where an undesired image carrier is observed due to quadrature gain and phase errors and a tilt is observed in the desired carrier owing to a non-uniform gain of the mixers over the band of interest. Additionally, distortions introduced by BPF2 are manifested as amplitude-ripple and tilt as indicated by Fig. 6 in section 1.

2.2. SUMMARY OF PREVIOUS CALIBRATION TECHNIQUES

A variety of calibration procedures exist in the RF domain for the use in various applications. The main use-cases for such methods are;

1. Identify a mathematical, behavioral (or another) type of a model for the device under test (DUT).
2. Accurate verification of the performance of a DUT.
3. Transmit and receive information with greater accuracy and efficiency.

An example is, the pre-calibration routine of a Vector Network Analyzer VNA testbed, to accurately measure a system model of transmission lines, passive networks etc. using analysis performed with the help of a VNA. Routines enable the engineer to pre-calibrate the measurement system to allow corrections for cables and RF components upto the reference plane of the DUT. Thereby, when measuring the performance of the DUT itself, the measurement path data (error terms) that were stored in the memory of the VNA are recalled and necessary corrections are applied to the measured signal through the DUT allowing measurement of the DUT performance only. In-terms of vector network analysis multiple calibration methods exist based on the nature of the DUT; Short-Open-Load-Reciprocal (SLOT), Thru-Reflect-Line (TRL), Line-Reflect-Reflect-Match (LRRM), Short-Open-Load-Reciprocal (SOLAR) are a few calibration methods [7]. Additionally, in the characterization of power amplifiers or such nonlinear systems methods such as enhanced vector calibration using loadpull measurements are possible [8]. The advantage in the application of the latter technique is it allows for the creation of an accurate model of the DUT.

Another scenario where calibration is applied is in modeling the RF channel. Advanced signal processing algorithms based on channel estimation and training are widely presented in the literature as to pre-compensate impairments existent in the channel; interested readers are referred to [9], [10], [11], [12]. In [14] authors describe using wideband sinc and chirp pulses for characterization of RF transmit paths, for weakly and strongly nonlinear systems respectively.

Reference [72] uses a method of time-domain characterization of a polar transmitter architecture using a Schroeder-phased multi-sine signal. This method requires the use of a four-channel digitizer consisting of four track and hold amplifiers and a high sampling oscilloscope. Transition into higher frequency bands such as Ka-band is expected for future wireless communication systems to facilitate the need for higher data rates. Therefore, the use of higher sample rate equipment as mentioned above at these frequency bands are expensive. Reference [73] uses a technique which mixes I and Q portions of LO with RF signal to generate a baseband representation of an RF signal and subsequently generates a calibration signal in an iterative manner as a frequency sweep technique. The time required for calibration using an iterative frequency swept technique for spectrally efficient signals such as wideband, and multi-carrier signals will increase proportionally to the number of frequency components involved. In [13], first an arbitrary signal generator is used to generate the quadrature baseband signals (digitally controlled), then upconverted to an RF frequency using an IQ modulator. The resulting output is supplied to a spectrum analyzer which computes the carrier and image power. Then an algorithm is used to calculate gain and phase offsets by taking in carrier-to-signal power ratio and image-to-signal power ratios iteratively, allowing compensation for the mismatches in the gain and phase of the IQ modulator. This technique is iterative and for wideband signals with increased number of frequency components it is time consuming.

Calibration of a hardware testbench and in a cellular network basestation would benefit from real-time calibration. When advanced digital signal processing techniques are incorporated for calibration, it is possible to overcome the hardware limitations to an acceptable level.

The novel method proposed uses a modulated waveform which closely resembles a standard wireless communication signal. This offers the added advantage of using the

proposed technique for testbench calibration as well as transmit path calibration over the air.

For the work carried out in this section a heterodyne transmitter architecture is considered with digital Intermediate Frequency (IF). It is possible to adopt and implement a homodyne architecture for the concept as well. Novelties of the proposed technique are, in using a well-defined 64-QAM modulated signal input with the arrangement of constellation symbols to include all possible permutations. Design of the test signal itself enables the technique to be used for path calibration of weakly and strongly nonlinear modules as a non-iterative technique.

2.3. EXPERIMENTAL VALIDATION INDICATORS OF PERFORMANCE IMPROVEMENT

2.3.1. VISUAL INSPECTION TECHNIQUES

To compare the effectiveness of the system with and without calibration applied, a scientific method that can capture both amplitude and phase characteristics of the nonlinear system is of paramount importance. Therefore, the main advantage of using 64-QAM signal stimulus is that the calibration can be verified instantly by observing the demodulated output at a receiver and observing the constellation captured of the stimulus itself. For this purpose, it is possible to use a quantity that captures both amplitude and phase errors called “Error Vector Magnitude (EVM)”. Additionally, to fulfill the requirements for different broadcasting standards, it is possible to analyze the spectral characteristics of the system at the output. Moreover, the quantity “Signal to Noise Ratio (SNR)” can also be used in determining the quality of the level of the information of the signal when compared to the noise level.

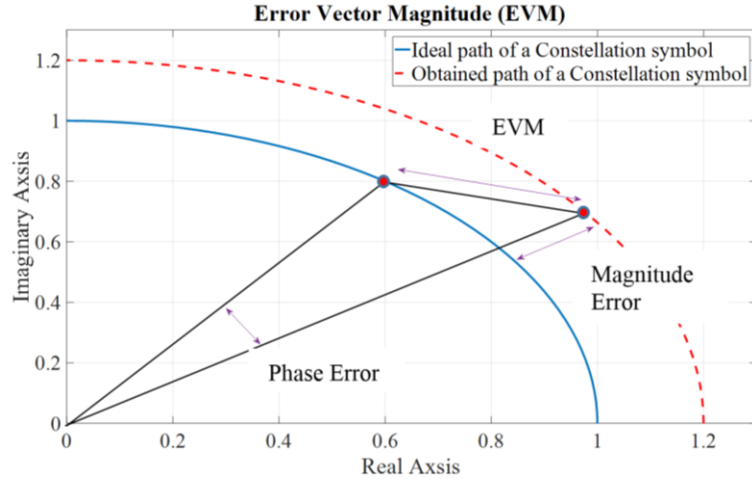


Fig. 4. An example illustration of the concept EVM, ideal symbol point lies on path in blue and received/measured point lies on path in red (dashed).⁴

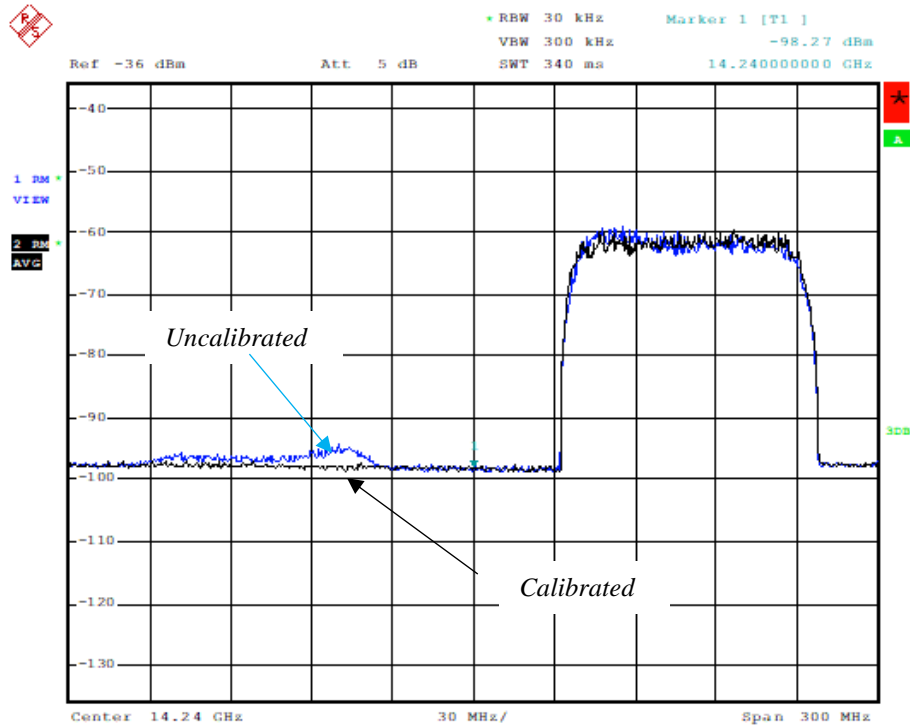
2.3.1.1. ERROR VECTOR MAGNITUDE (EVM)

EVM is a quantity that quantifies the vector difference between the ideal constellation points and the measured constellation points obtained at the reference pre-calibrated receiver [56]. An example visual description can be seen in Fig. 4 (In this work Rohde and Schwarz R&S FSQ-40 with a vector demodulation bandwidth of 120 MHz was used).

2.3.1.2. VISUAL ANALYSIS OF THE RECEIVER SPECTRUM

Fig. 5 indicates the sideband image component arising from IQ amplitude and phase frequency independent imbalances of the modulator. As a result of this impairment crosstalk between I and Q paths occurs. Following procedures set out in [16] and [14], it is possible to test the IQ correction by observation of improvement in adjacent channel leakage ratio (ACLR). ACLR is commonly termed as the relative filtered mean power of an adjacent channel to that of the transmit channel power [17]. For each of the tests, this metric provides an indication of the level of IQ imbalance. Attached below in Fig. 5, presents a calibration scenario of 256-QAM signal at Ku band.

⁴ References used in understanding EVM – [56]

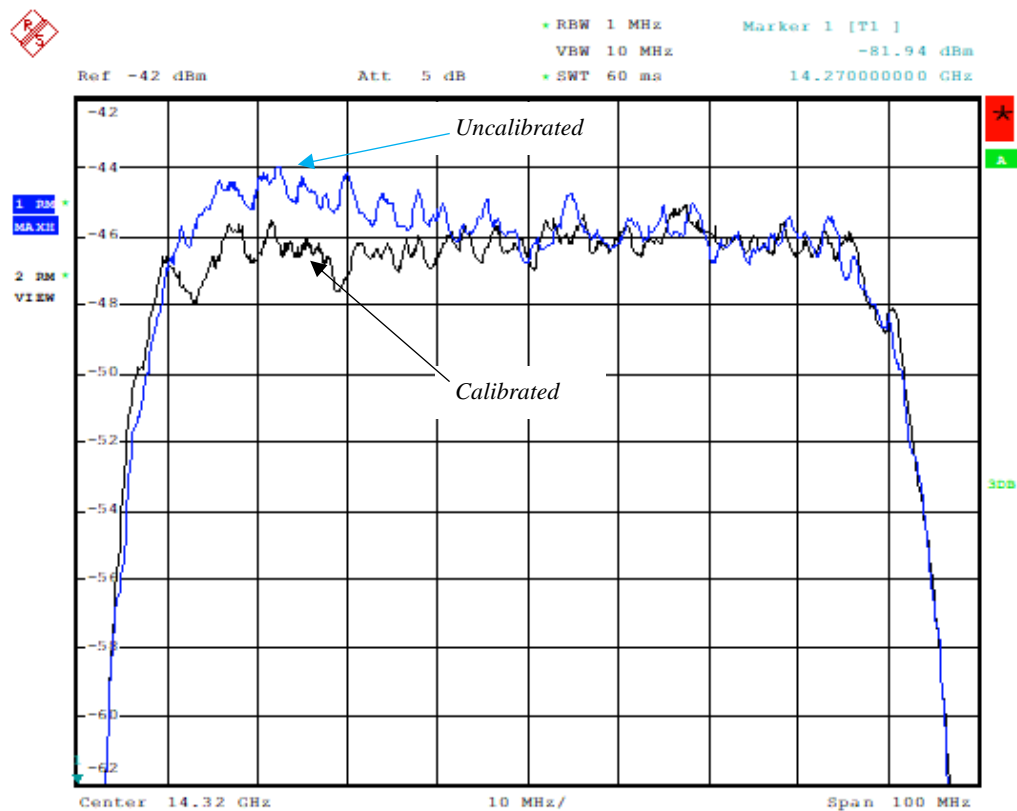


Date: 12 JUN 2018 18:21:57

Fig. 5. An example of the uncalibrated and calibrated magnitude spectrum of 256-QAM signal at Ku-band.

Fig. 5 indicates the full screen capture of the magnitude spectrum over a bandwidth of 300 MHz. A successful rejection of the sideband image component in the adjacent channel can be observed. The figure was captured at Ku-band with the center frequency of 14.24 GHz uncalibrated signal (blue trace), calibrated signal (black trace). Compensation of amplitude tilt present within passband is also visible. A better visual indication of this can be achieved by zoomed view of the passband itself as in Fig. 6.

Another visual analysis method; is to observe the magnitude spectrum before and after calibration within the pass-band. An example is indicated in the figure below for amplitude tilt, which can be explained as a variation in amplitude along with frequency. As depicted in Fig. 6 amplitude tilt has been compensated well after calibration yielding a flatter amplitude response. Amplitude roll-off may also occur due to the nonlinear frequency dependent performance of an RF path and due to the sampling process of the transmitter, this phenomenon is also known as the sinc roll-off.



Date: 12 JUN 2018 18:27:10

Fig. 6. An example of the uncalibrated and calibrated magnitude spectrum of 256-QAM signal within passband. The figure was captured at Ku-band. (blue trace) uncalibrated signal, (black) calibrated signal.

2.4. CONSTELLATION MAPPING FOR RF PATH CALIBRATION

Present-day digital transmissions by radio waves incorporate quadrature amplitude modulation (QAM) schemes, which is a form of vector modulation. QAM modulation is achieved by applying amplitude modulation to two time-domain vectors namely: quadrature and in-phase [15].

In this work a novel technique uses a 64-QAM modulated input signal, inherently having multiple amplitude levels and phase angles in the time domain allow the stimulus to emulate a variety of signals used in different applications. In comparison to 16-QAM, a 64-QAM modulation type is chosen after considering the greater number of amplitude levels in time-domain in contrast to that of 16-QAM a calibration signal that is developed using the same technique as it may not be as accurate in its performance when characterizing a highly complex test signals such as 256-QAM⁵ whereas the increased in amplitude levels of a 64-QAM signal allows characterization of a 256-QAM modulation signal as observed by the conducted test results that are presented in later chapters. A 256-QAM signal could also be used in to develop a calibration signal however, it is at the expense of the computational effort and requires higher channel capacity requirements (Signal to Noise Ratio - SNR) to perform a demodulation under distorted conditions in comparison with the 64-QAM modulation scheme. Moreover, a properly designed 64-QAM signal is capable of capturing frequency transitions to a sufficient detail within the passband of the stimulus as shown in Fig. 8. Stimuli may also be designed to have high dynamic range to allow characterization of highly nonlinear systems. The calibration signal is designed to contain all possible combinations of unique transitions of a 64-QAM constellation. To capture memory effects of a nonlinear system under test (e.g. hysteresis) required permutations were calculated (1-2). Therefore, all possible transitions are included in designing the calibration signal. In the following equation “n” is the number of different constellation symbols, and “r” stands for the number of different choices.

$${}^n P_r = \frac{n!}{(n-r)!} \quad (1)$$

$${}^{64} P_2 = \frac{64!}{(64-2)!} = 4032 \quad (2)$$

⁵ For the purpose of usage and abbreviation N-QAM signal means and N-QAM modulation applied signal

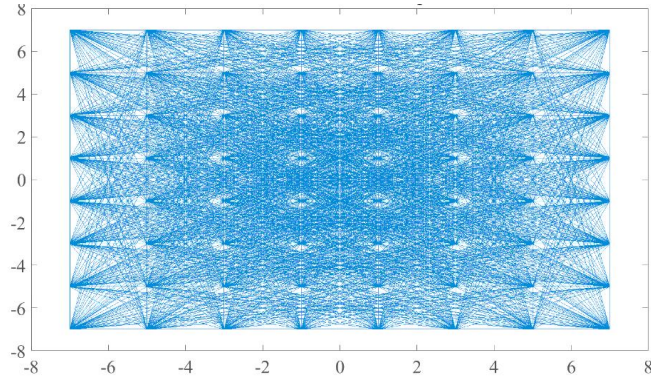


Fig. 7. Designed 64-QAM Constellation with the inclusion of all unique Permutations, as seen from the figure all transitions between points have been accounted for.⁶

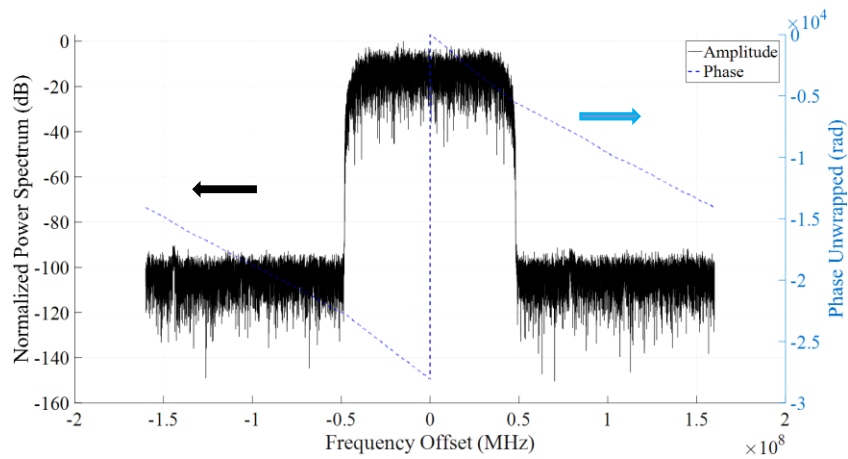


Fig. 8. Magnitude and phase of the calibration signal in the frequency domain.

Calibration technique implemented is based on the principles of design of the constellation as described above, capturing the transmitted signal, and digitally correcting its vector positioning of symbols. The procedure for calibration includes designing the calibration signal itself. Then the signal is transmitted through the system and captured from a calibrated vector receiver vector signal analyzer (VSA). However, capturing through a noncalibrated receiver is still possible as the calibration signals characteristics are well designed. The captured distorted signal is analyzed for IQ impairments. The vector of the difference between the distorted signal constellation point and the desired constellation point is logged. Subsequent to this a corrected signal is generated by applying the vector offset required to the distorted signal to position it on the desired

⁶ All possible permutations account for 4032 values, in practice for the ease of implementation 4036 transitions were programmed. Matlab function `permn` [74] can be used to calculate the individual permutations.

constellation point as seen in Fig. 9. This signal was then subjected to circular convolution with any other type of a signal to mitigate impairments present in the test setup.

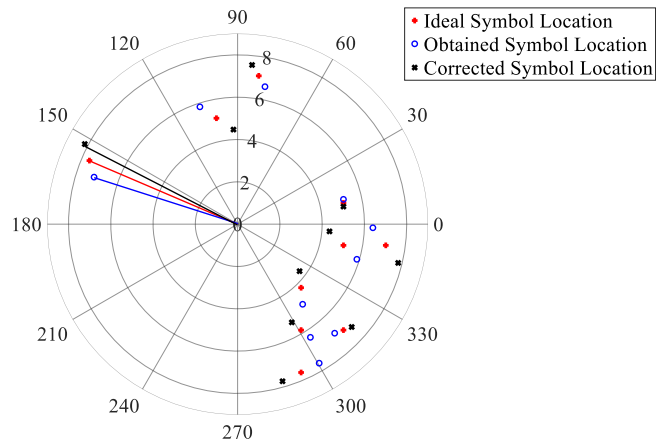


Fig. 9. Constellation of the calibration signal/ideal symbol location (red - *) and the captured signal (blue - o) and the correction of vector positioning of the symbol (black - o). Constellation is presented by means of a polar plot to indicate the advantages of both amplitude and phase positions of the 64-QAM signal stimulus.

The main advantage of this technique is that the captured demodulated stimulus itself can be used as an indicator of multiple impairments for both weakly and strongly nonlinear system behavior by analyzing the position of the constellation points. Additionally, the overall technique is noniterative and requires a shorter amount of time in comparison to iterative techniques. Following [15], six types of distortions can be identified by using a 64-QAM constellation.

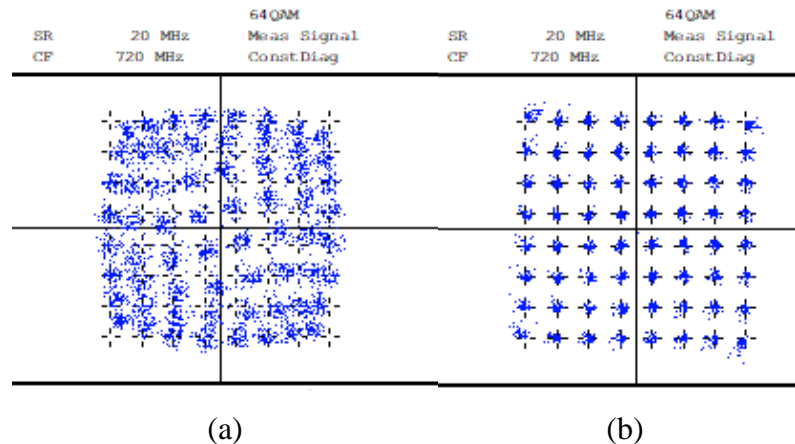


Fig. 10. (a) The plot of the constellation of the strongly nonlinear system indicating outer constellation symbols subjected to AMAM distortion and inner symbols subjected to AMPM. (b) Constellation plot of a weakly driven nonlinear system where outer symbols have been subjected to AMPM conversion. Both figures are from experimentation test cases, each case is presented in-detail in section 2.8.

1. AMAM distortion – AMAM distortion is where an amplitude modulated signal is subjected to further amplitude modulation due to highly nonlinear system behavior. This causes the constellation symbol to have a shorter vector radius than its ideal location. Observe Fig. 10 plot (a).
2. AMPM distortion – AMPM distortion is where an amplitude modulated signal undergoes phase modulation due to nonlinear system behavior. This results in the symbol point to have the same vector radius but to be moved in its angle along the vicinity of the ideal location. When this occurs by observing the four corners (and nearby points) of the constellation it can be clearly observed that all four symbols are rotated in the same direction. Observe Fig. 10 plot (b).
3. Delay distortion - received constellation point distorted in respect with ideal constellation point due to inter-symbol interference.
4. Random noise – causes the demodulated individual points to have a scatter around its ideal location (without overlapping with another symbol).
5. Interference – the result of other spurious signals coupled with the transmission line, causes the symbol to have a circular movement around its ideal location.
6. Phase noise – introduces an angular movement of the constellation point. This phenomenon is different from AMPM distortion and random noise. As this is a type of an angular distortion which happens at both directions of the ideal symbol location. The primary source of phase noise is non-ideal spectral characteristics of the local oscillator.

Interested readers are referred to reference [15] for a more detailed description of advantages in using a 64 QAM modulated signal in identifying contributors of errors to the desired RF signal. In the section 2.3.1 other visual inspection techniques that can be used to evaluate the existing impairments such as characteristics of the magnitude spectra, were presented and these observations are common to most calibration signals, however, the observations presented above are special signal characteristics displayed by the calibration signal itself (and other QAM modulation types).

2.5. IDENTIFYING DISTORTION COMPONENTS USING CONSTELLATION MAPPING

Effect of IQ imbalance, group-delay, and amplitude roll-off on the RF transmit and receive paths can be observed by analyzing the above-mentioned visual inspection techniques as described in section 2.3.1. Demodulation of the 64-QAM signal can be performed by analyzing the IQ parts of a signal capture from a receiver or by performing demodulation through a calibrated receiver such as a VSA (in this case R&S FSQ). After a successful run of the calibration on the RF signal paths, the demodulated 64-QAM constellation (or any other suitable signal) should indicate an improvement of both EVM and in SNR values on the VSA in addition improved spectral characteristics. Additionally, as explained in section 2.4 properties of calibration signal itself can be used as well (demodulation of the stimuli itself by a VSA – useful in practice for the application engineer to perform an immediate verification).

To experimentally validate the advantages of the presented calibration technique, it of vital importance to use appropriate test cases. the following inputs were used; a different 64-QAM modulated input signals with random transitions between their constellation points, Phase Shift Keying modulated signal (8-PSK), 256-QAM modulated signal (Complicated test scenario with very high susceptibility for error).

Fig. 1 portrays the general architecture of a heterodyne transmitter⁷. In practical testing signals were generated using MathWorks MATLAB tool, the signal was transmitted via Texas Instruments DAC34SH84 board (or through a calibrated Signal Generator R&S SMU 200A8) and captured through a calibrated VSA. Rohde and Schwarz FSQ were used to perform the function of the calibrated VSA. In this test bench test signals were transmitted at an RF frequency of 2.24 GHz for applications in S-band. For the applications in Ku-band signals were further upconverted to a center frequency of 14.32 GHz. The test signals were created to have 80 MHz in bandwidth with a roll-off factor of 0.2. This will result in an overall bandwidth of 96 MHz of bandwidth. Therefore, the IQ capture of signals was performed at 100 MHz of the span of the carrier signal,

⁷ With Digitally generated IF.

⁸ Sampling rate of 100MHz and at an IF of 30MHz

which is well within the vector demodulation bandwidth of the chosen VSA. Signals were transmitted at a sampling rate of 320 MHz, in correspondence with near maximum capturing sampling rate of the calibrated receiver.

2.6. WEAKLY NONLINEAR SYSTEM TESTING AT S-BAND

Test cases mentioned below were chosen to prove the validity of the method in characterizing different input signals under weakly nonlinear characteristics. Structure of a weakly nonlinear system can be viewed from Fig. 1, case 1 and 2. Applications in S-band are Wireless-LAN, mobile communications, and avionics. Proving of current calibration technique is within this frequency band also suggest the possibility of future applications for this type of a technique.

2.6.1. A TEST CASE OF AN 8 PSK SIGNAL

Considering the difference in 64-QAM and 8-PSK modulation schemes especially in-terms of their time domain characteristics (levels of amplitude and chosen phase angles) their constellations are different. Testing under this condition would provide valuable insight into the application of the calibration method to a different complex envelope modulated signal input of a different arrangement to that of the stimuli.

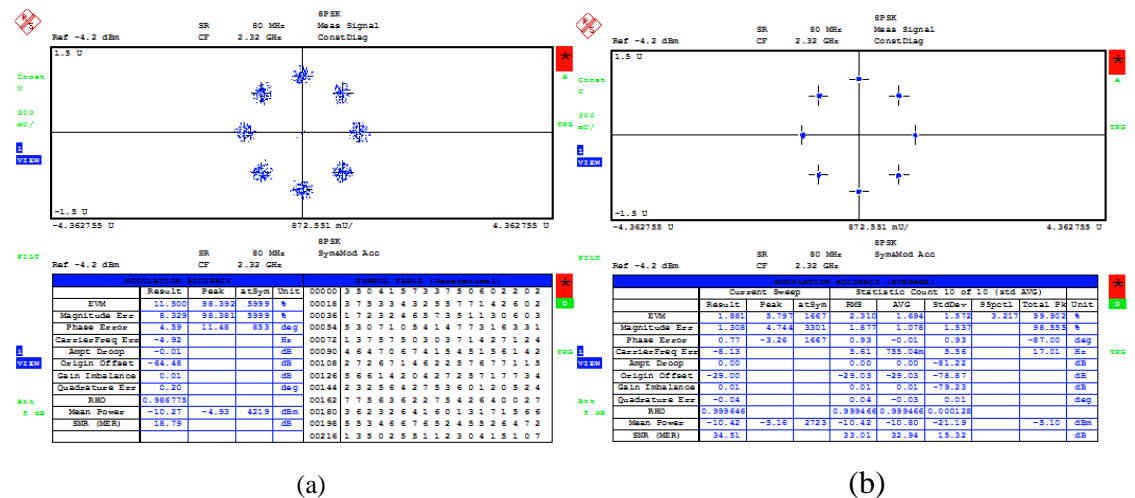


Fig. 11. 8-PSK constellation (a) before and (b) after calibration.

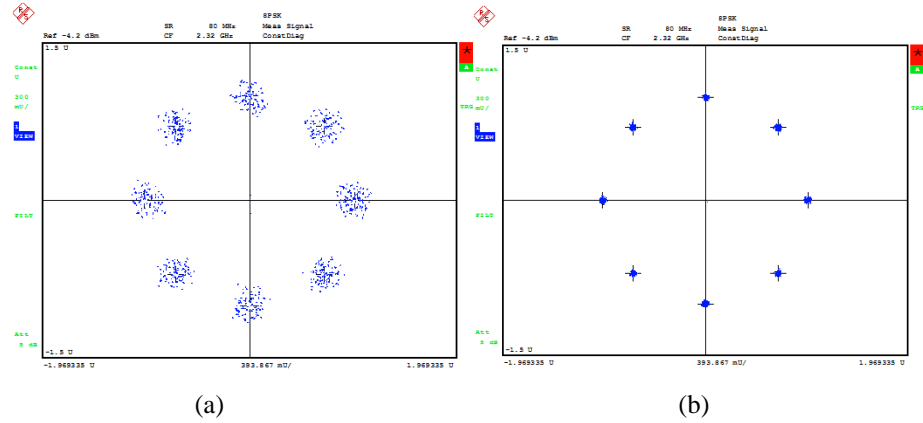


Fig. 12. 8-PSK constellation zoomed view of constellation points (a) before and (b) after calibration

Results from the 8-PSK test indicate a successful validation of the technique, as there is a significant improvement in EVM by 9.62 % and SNR by 15.72 dB.

2.6.2. A TEST CASE OF A 256 QAM SIGNAL

In comparison with the 64-QAM signal, a 256-QAM signal has twice the number of levels for its amplitude and a more widely spread phase angles in its constellation. In terms of time domain characteristics having a spread-out and detailed constellation results in a complicated stepped waveform. Having higher number and a variety of transitions forming a detailed constellation 256-QAM in comparison to 64-QAM leads to higher number of unique frequency components that correspond to its characteristics.

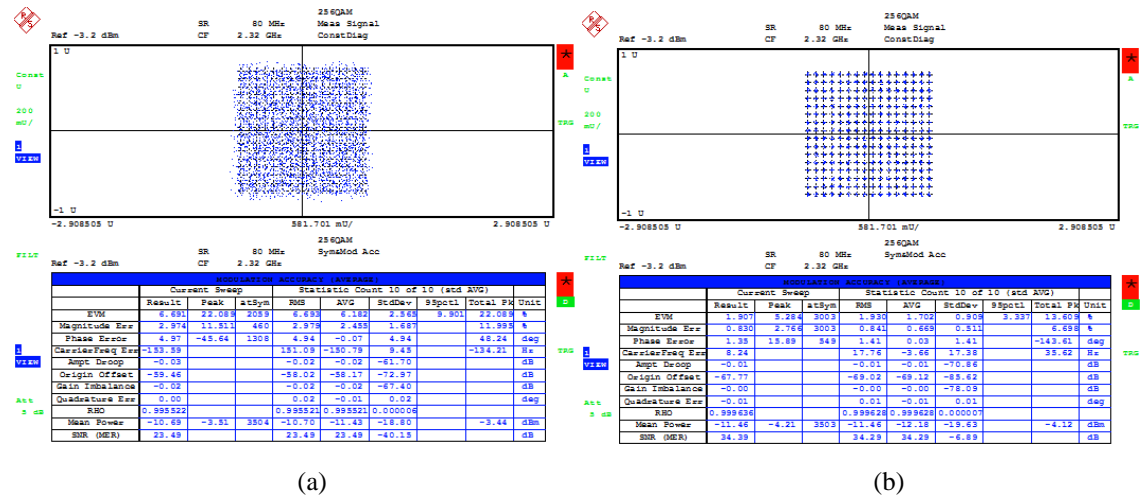


Fig. 13. 256-QAM constellation (a) before⁹ and (b) after calibration.

⁹ Following Shannon limit on channel capacity for 256-QAM modulation, EVM for the uncalibrated case was not considered.

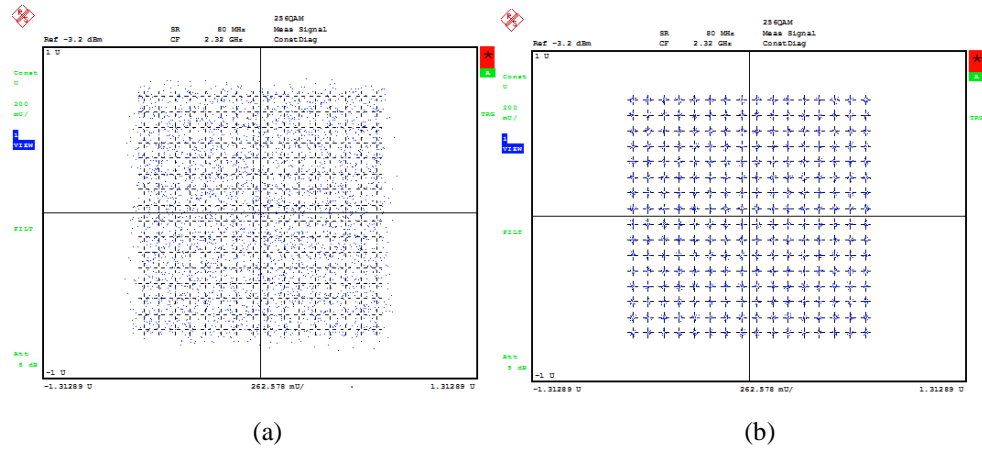


Fig. 14. Enlarged figure of constellation in Fig. 13 (a) before and (b) after calibration.

Results from the 256-QAM test indicate an improvement of SNR by 10.9 dB validating the usefulness of the technique. As can be observed in Fig. 13, Fig. 14 after performing calibration to compensate for nonlinearities the quality of the RF signal in the RF transmits path has been restored.

2.7. WEAKLY NONLINEAR SYSTEM TESTING AT KU-BAND

Blocks of hardware components present in the Ku-band¹⁰ test-bench can be identified as section 2.1 Fig. 1, In the Ku-band test bench cavity-filter, presents higher group delay and higher amplitude roll-off. Testing for Ku-band is useful in satellite communications applications and future mobile communication systems. Please refer to Fig. 6 in section 1 to observe the noticeable tilt in amplitude detected while testing in Ku-band experiments.

¹⁰ Ku-band upconverter was developed by RF team at Maynooth University

2.7.1. TESTING FOR CONSISTENCY

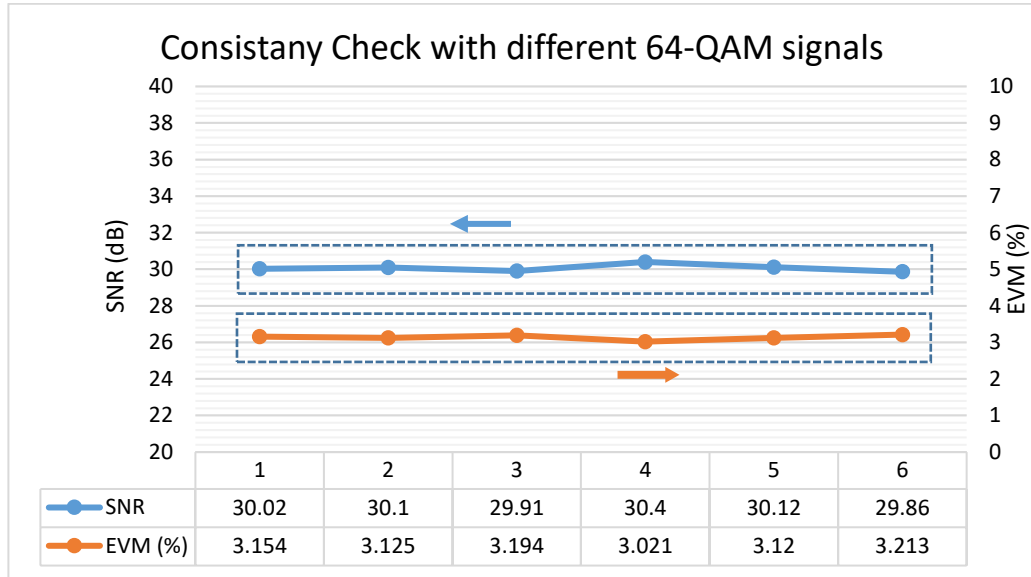
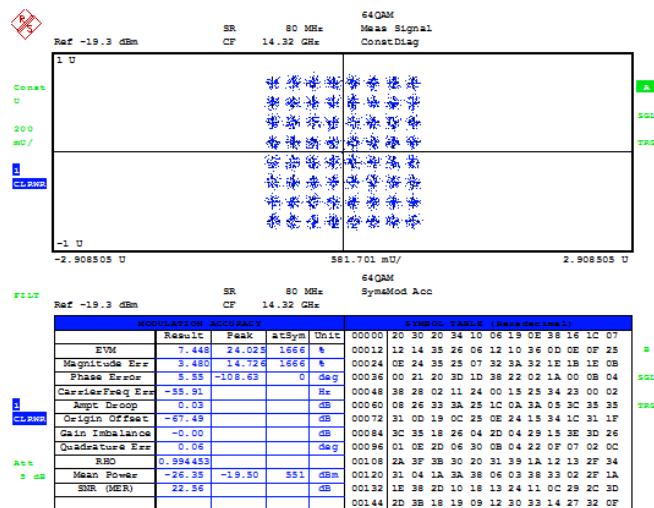


Fig. 15. Test results for different 64-QAM signal inputs.

In addition to the testing performed with 256-QAM and 8-PSK test signals. To present a greater certainty of the repeatability of the technique, the calibration was performed for six unique 64-QAM modulated signals generated by random allocation of constellation points and was tested with the use of the same hardware test setup under similar test conditions. As expected SNR level and EVM readings indicate consistent operation throughout the testing Fig. 15.



(a)

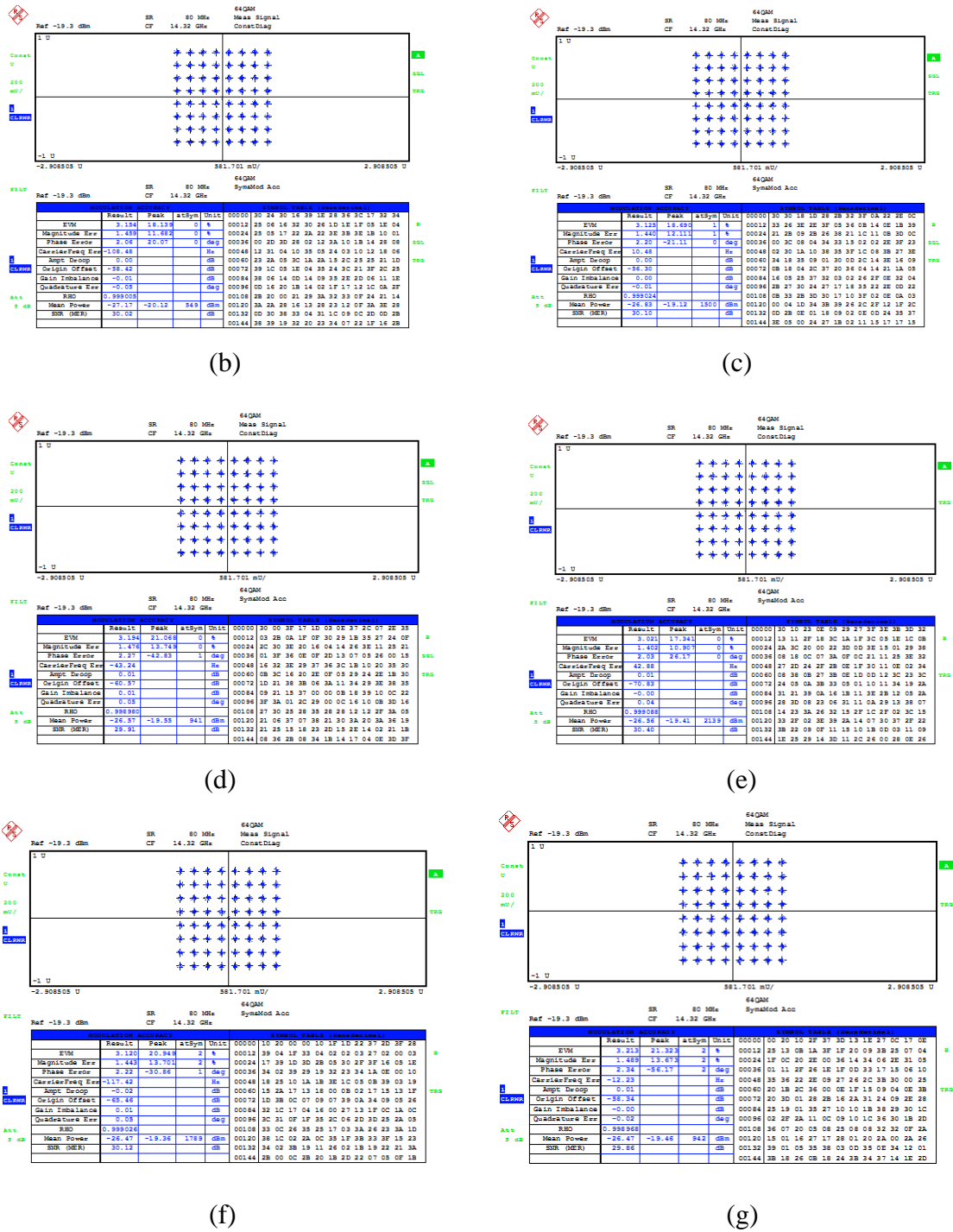


Fig. 16. (a) Captured un-calibrated 64-QAM signal (for each iteration the constellation for un-calibrated case was observed to be similar, for simplicity only the first capture is shown), (b) – (g) presents demodulated constellation for each of the six individual 64-QAM signals after performing RF path calibration.

2.7.2. A TEST CASE OF AN 8-PSK AND 256-QAM SIGNALS

Comparable to testing performed in S-band Ku-band test for 8-PSK and 256-QAM signal testing was also performed.

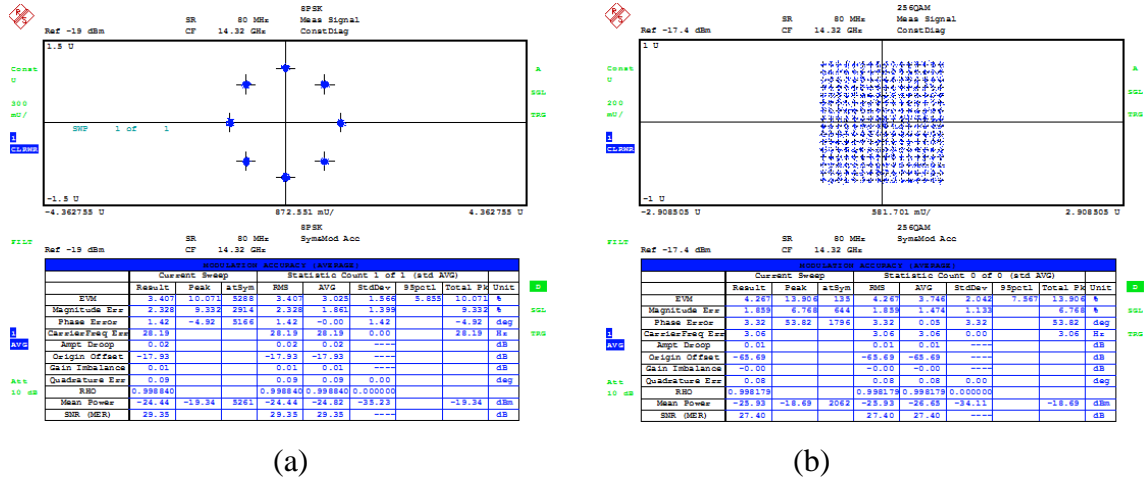


Fig. 17. Calibrated cases at 14.32 GHz (a) 8-PSK signal (b) 256-QAM signal

In an overall analysis of Ku-band test results, Fig. 6, indicates the amplitude spectrum compensation achieved for the desired passband. It can be clearly observed that amplitude remains relatively flat for the entire bandwidth of operation. Fig. 15, and Fig. 16 justifies the repeatability of the technique indicating consistent test results. Fig. 17 depicts the ability of the technique to certify its validity among more challenging modulation schemes such as 256-QAM modulation and suitability in a general test case of an 8-PSK modulated test signal with a different arrangement of constellation points. For an 8-PSK test case, an improvement of 8.02 dB of SNR is seen, with 5.531% EVM. For 256-QAM a 3.59 dB of improvement in SNR is achieved. Different test cases of 64-QAM yielded an average improvement of 7.508% in EVM and an average improvement of 4.31 dB of SNR. In-terms of further analysis into signal constellation random noise can be observed.

2.8. STRONGLY NONLINEAR SYSTEM CHARACTERIZATION

Strongly nonlinear systems provide the ultimate testing in calibration performance. Additional effects such as AMAM and AMPM conversation effects that which does not provide significant distortion to an RF signal in a weakly nonlinear system can be clearly recognized to influence the RF signal fed through a strongly nonlinear RF transmitter. A setup of a strongly nonlinear system can be achieved by having a power amplifier driven into its nonlinear operation regime. A more challenging case is when the main nonlinear module is an asymmetrical Doherty Power Amplifier (DPA). In addition to the RF signal being driven through a nonlinear path in-terms of a DPA, the RF signal propagating though two separate amplifier modules and get recombined at a combiner. Therefore, in total there are three nonlinear operations in a DPA.

2.8.1. TWO SEPARATE TEST SETUPS USED

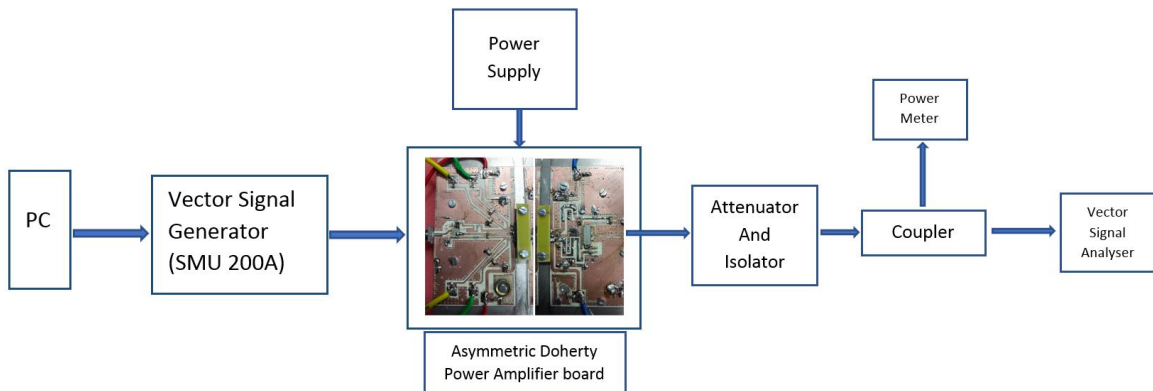


Fig. 18. Strongly nonlinear system characterization with high input power

The asymmetric Doherty power amplifier board was fabricated in-house and uses an NXP dual stage LDMOS power amplifier A2I08H040NR1 at 700 MHz 5G frequency band.

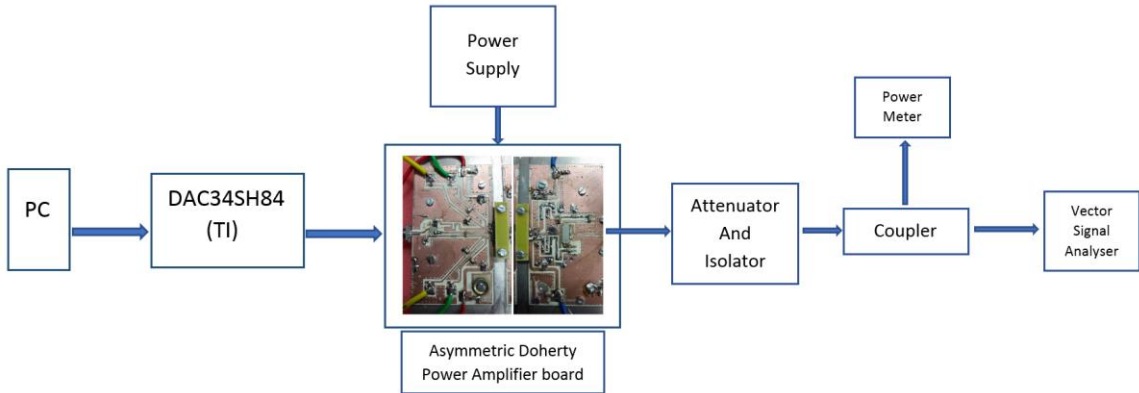


Fig. 19. Strongly nonlinear system characterization at a low input power level with the wide-bandwidth input signal

2.8.2. STRONGLY NONLINEAR SYSTEM DRIVEN WITH A SMALL SIGNAL

Fig. 19, describes the setup used to test the system under weakly nonlinear excitations. Although the DPA itself can be classified to be a strongly nonlinear device, when driven with a small signal input it operates at low power regime, in this instant overall system behaves as a weakly nonlinear system. Purpose of this test is to observe the performance of the technique for a weakly nonlinear system with a DPA operating in a low power regime excited with a wideband signal.

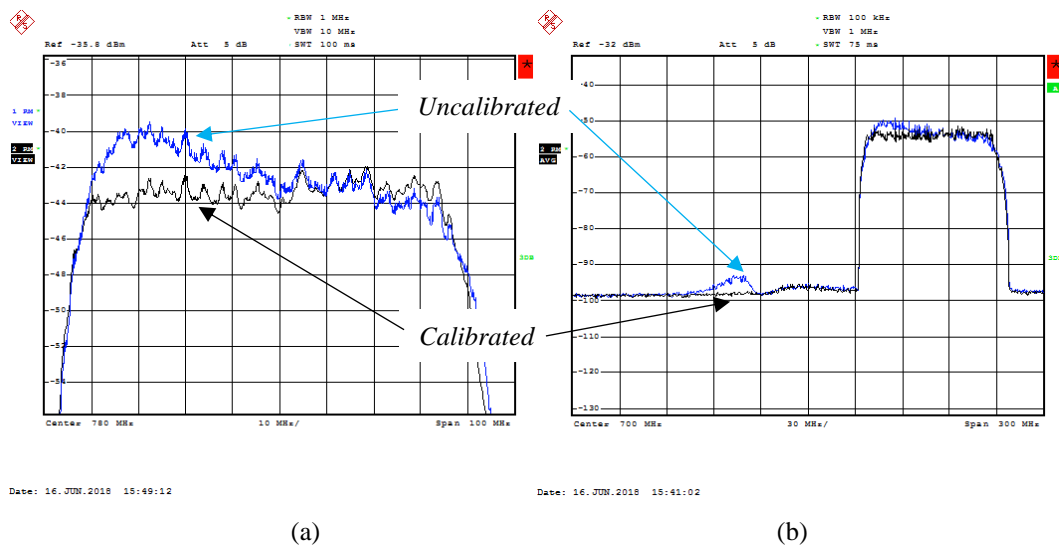


Fig. 20. The amplitude response of the test-setup as assembled in Fig. 19, of 64-QAM calibrated and uncalibrated signal magnitude spectrum. Two traces: uncalibrated (blue) calibrated (black). (a) Passband zoomed view, (b) carrier and image view.

In Fig. 20, the DPA was driven with a signal that allows it to operate in “low power mode” for a Doherty power amplifier. This is further identified by observing the spectrum and no visible compression of the passband magnitude is seen. It can be observed in Fig. 20 (b) that the image component is fully suppressed for the input signal placed at 80 MHz in IF (Image component, if any should appear at a center of 620 MHz). Moreover, as indicated by figure Fig. 20 (a) amplitude roll-off has also been well compensated with about ~3 dB correction. Meaning, that the calibration has been successful in compensating for both frequency independent and dependent distortion effects.

In validating the consistency of the proposed method, for the system as assembled in Fig. 19, a calibration was performed using the stimuli and then its performance was tested for ten uniquely different 64-QAM signals to be certain of the consistency of the test method Fig. 21.

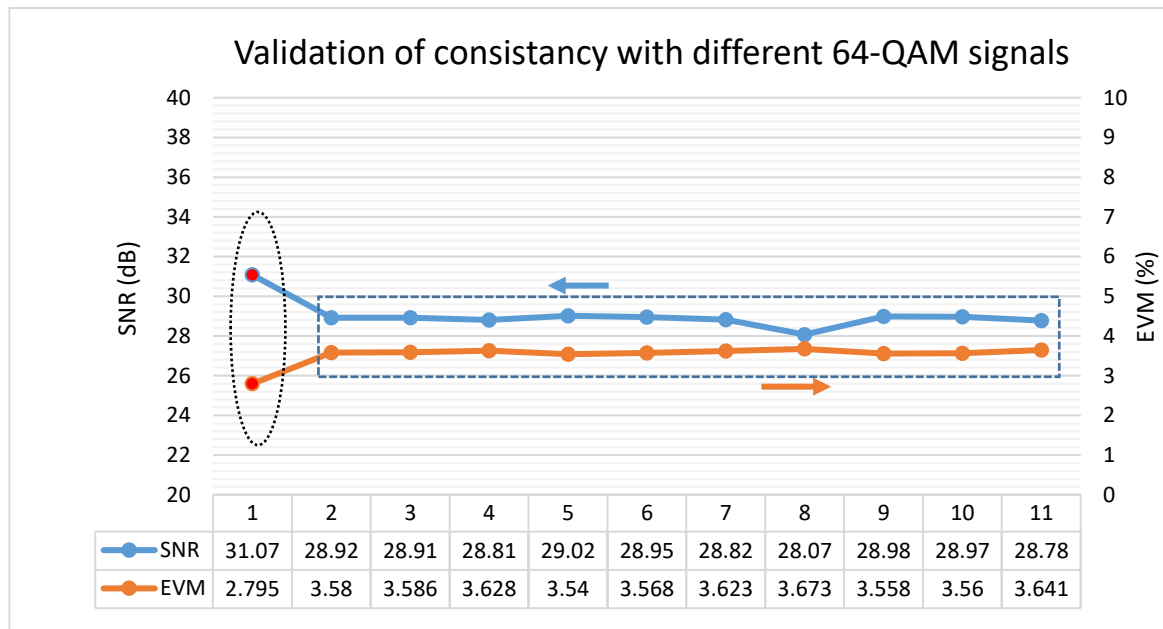


Fig. 21. Strongly nonlinear system driven with the wideband small signal input of different 64-QAM signals (Test setup as indicated in Fig. 19).

Fig. 21, indicates the response of the weakly nonlinear calibrated system with the DPA operating at lower power levels with improved SNR and EVM readings. As observed by the flat response in (2-11 points) both results we can conclude that the results are consistent, with SNR being within 1dB of variation and EVM calculated to have <1% of deviation. The first test result was on purpose selected to be the calibration signal itself,

as expected it shows better EVM (lower value) SNR (higher value) performances in comparison to other test signals.

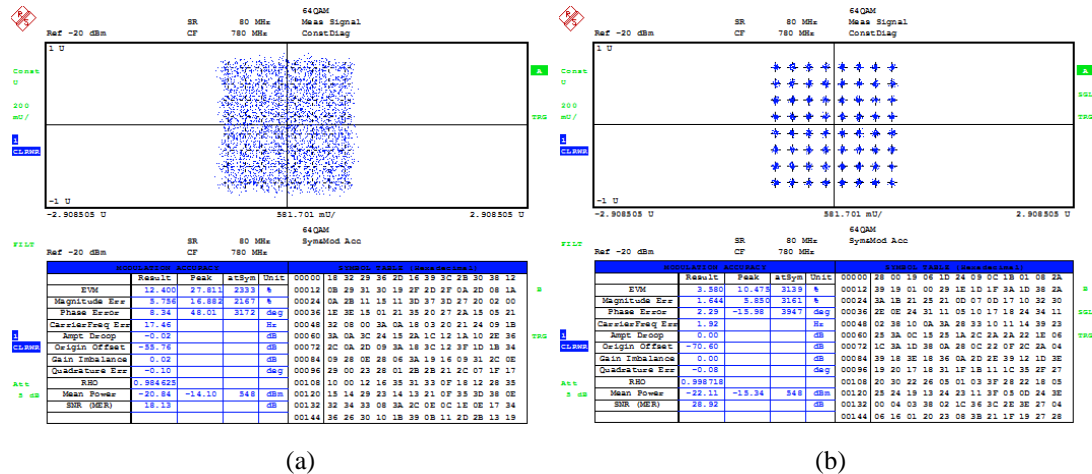


Fig. 22. (a) Uncalibrated case (b) calibrated case, demodulated 64-QAM constellation (Different QAM modulated signal to that of the stimulus)

For all the different 64-QAM signals uncalibrated case indicated an EVM of ~12 % and SNR of ~18 dB. On average an improvement of 8.7 % for EVM and 10.6 dB for SNR can be obtained after performing calibration on the system with the DPA.

2.8.2.1. TESTING WITH 8-PSK SIGNAL

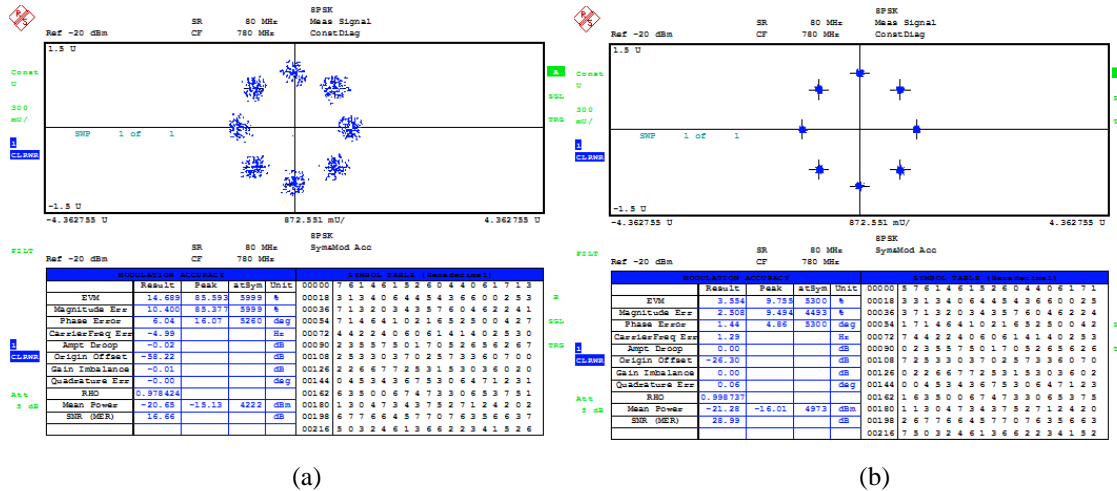


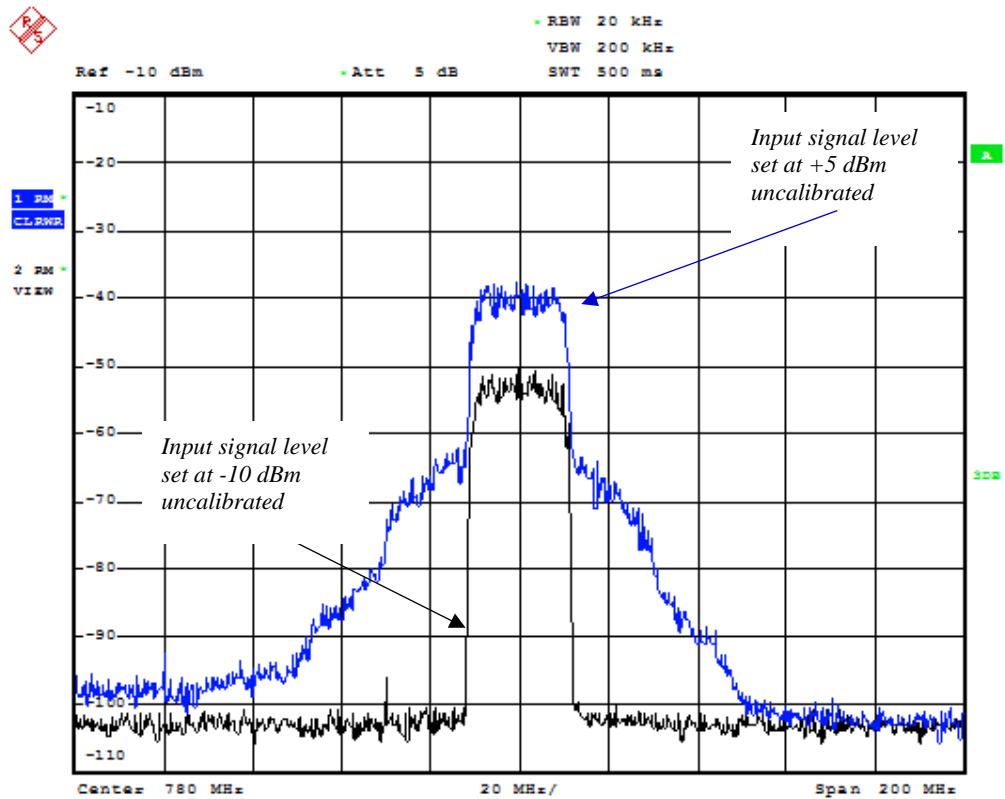
Fig. 23. (a) Uncalibrated case (b) Calibrated case, demodulated 8-PSK constellation

Testing was performed for an 8-PSK input as well. As seen by analysis performed by the demodulator an improvement of SNR of 12.33 dB and an improvement of EVM of 11.135 % was obtained. In comparison to calibrated case uncalibrated case indicates a

random variation of all symbols within their vector space in the constellation. In analyzing the entire transmitter chain, even though the signal was amplified by the amplifier further undesired noise could be introduced to the information signal when it propagates in RF channel over the air or during capture in the receiver. Therefore, in a real-time practical application above signal as captured by the uncalibrated case is highly susceptible to noise, therefore to further improvement of the signal is essential to maintain the integrity of information transmitted through.

2.8.2.2. STRONGLY NONLINEAR SYSTEM DRIVEN WITH LARGE SIGNAL INPUT

In validating any calibration technique, it is necessary to perform testing under both weakly and strongly nonlinear presence to understand the applications that it is valid for. As mentioned in section 2.5, a variety of advantages exists in using a 64-QAM signal. However, in this section, it is the intention of the author to make use of an even more challenging case. An asymmetrical DPA presents an even greater challenge to a non-iterative calibration technique as it has two paths for the RF signal to propagate. The first path is a class AB biased PA and the second path is a class C biased nonlinear PA, input signal propagates through both and finally gets combined at the combiner. Under strong input signal excitation in an asymmetrical DPA, there are three nonlinear units. Calibration not only has to account for distortion in one path with an amplifier but also to two separate paths and for the constructive summation of signals between those paths.



Date: 24 JUN 2018 12:48:56

Fig. 24. Magnitude Spectrum of uncalibrated strongly (+5 dBm) and weakly (-10 dBm) driven DPA.

The above figure indicates nonlinear compression characteristics of the DPA operating at strongly nonlinear regime with higher power level (+5dBm) with the raised side-lobes present in the spectrum with intermodulation distortion (IMD) components.

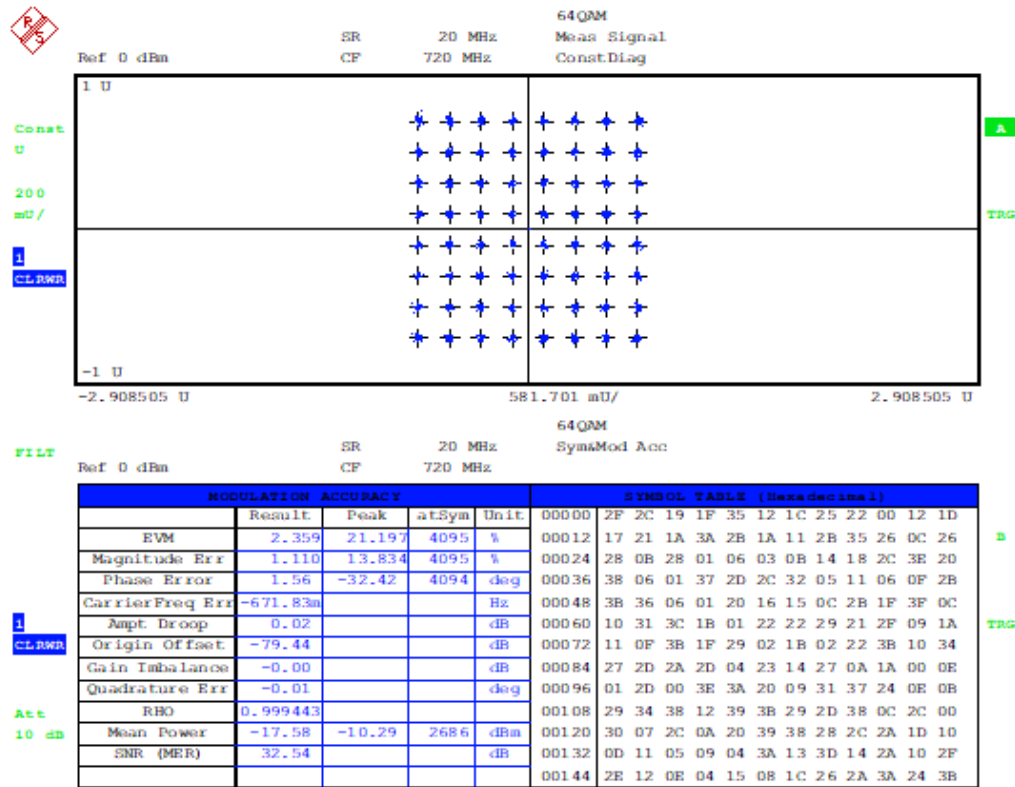


Fig. 25. The uncalibrated response of weakly nonlinear DPA (input signal power of -10 dBm)

After comparing both Fig. 24 and Fig. 25 at lower power level the entire system indicates linear characteristics at a lower power level for this type of clean input signal level the calibration is unnecessary. However, power amplifiers are more efficient and deliver more output power while operating at a nonlinear regime therefore application-wise input signals with higher levels must be used to achieve better Power Added Efficiency PAE and output power. Corresponding to power level of +5 dBm. However, as portrayed by Fig. 24 this results in loss of linearity/dynamic range in magnitude spectrum and as observed by Fig. 29 degradation of signal quality, as useful information (symbols in the constellation) have now undergone severer distortion.

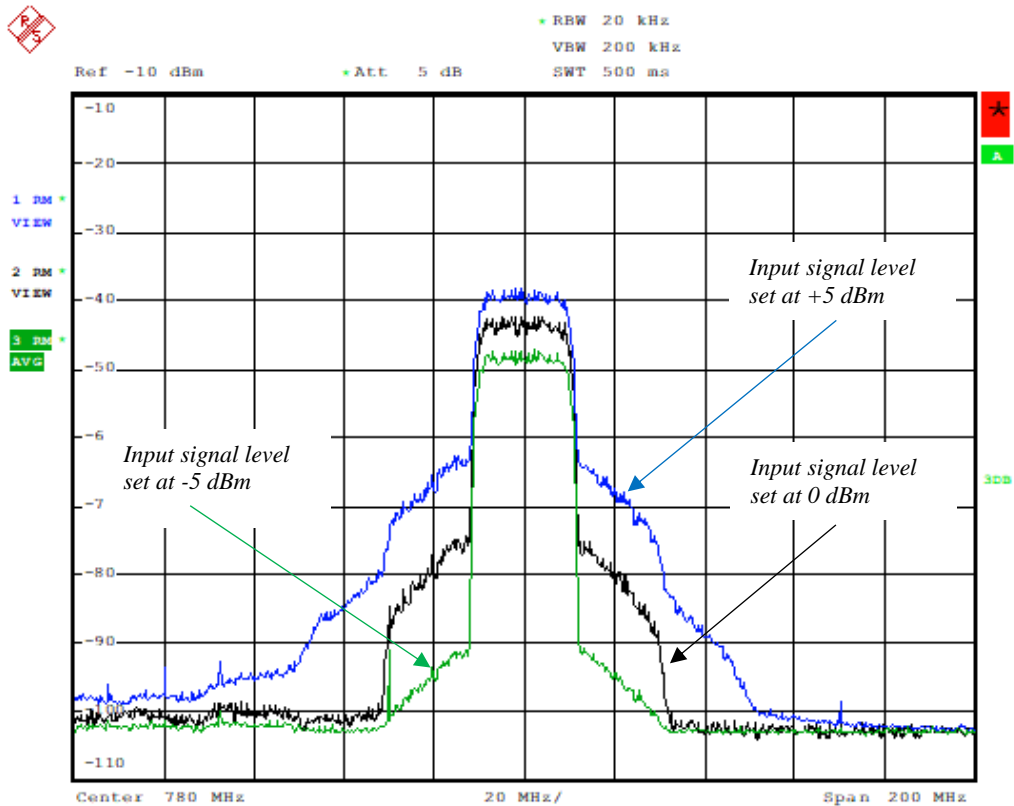


Fig. 26. Magnitude Spectrum of uncalibrated strongly (+5 dBm) mildly (0 dBm) weakly (-5 dBm) driven DPA.

To better present the case Fig. 26, encapsulates the spectral view of nonlinear system operating at several power levels. Uncalibrated signal capture after demodulation at the input power level of +5 dBm indicates an output power of approx. 31.25 dBm. At this frequency range (center placed at 720 MHz) the DPA gain was tested to be of 30 dB, therefore the DPA is operating beyond the P_1 dB compression point at an input power level of +5 dBm. As observed by the frequency spectrum in Fig. 26 the DPA operating at +5 dBm indicates a higher level of distortion components/ side-lobes around its passband thus greatly compromising the SNR level to an approximate of 10 dB (refer to Fig. 29, Fig. 31).

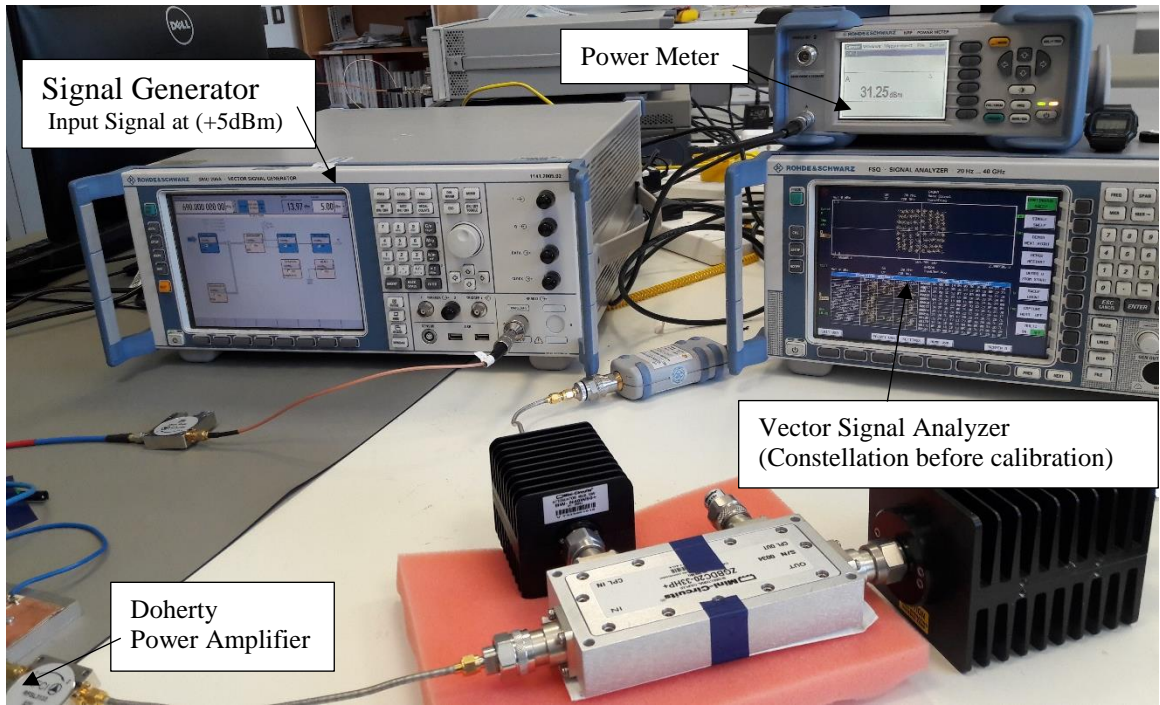


Fig. 27. Uncalibrated test-setup (Fig. 18 type) indicating an EVM of ~11 % and SNR of 18.7 dB at strongly nonlinear conditions (+5dBm input)

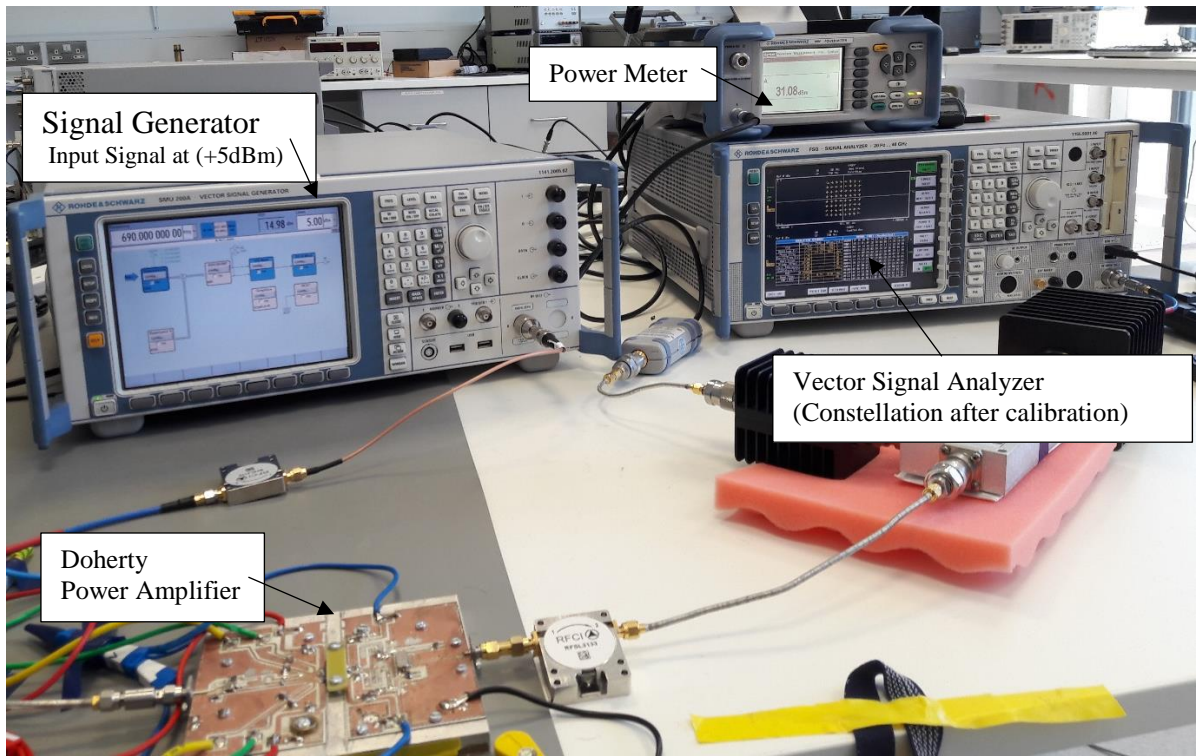


Fig. 28. Calibrated test-setup (Fig. 18 type) indicating an EVM of 4.4 % and SNR of 27 dB at strongly nonlinear conditions (+5dBm input)

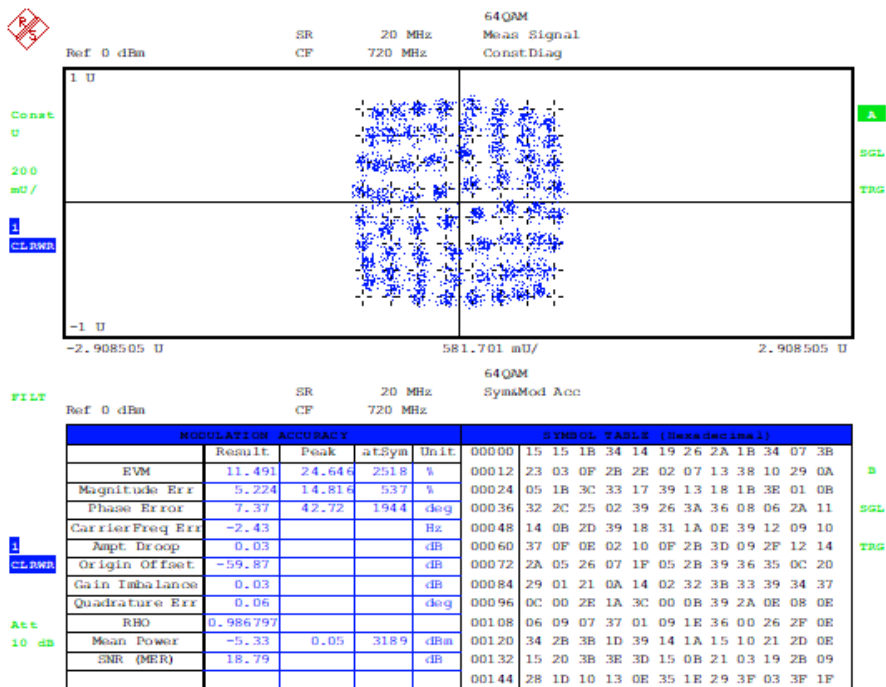


Fig. 29. Demodulated constellation view of uncalibrated test setup under strongly nonlinear conditions. (as in test-setup described by Fig. 27)

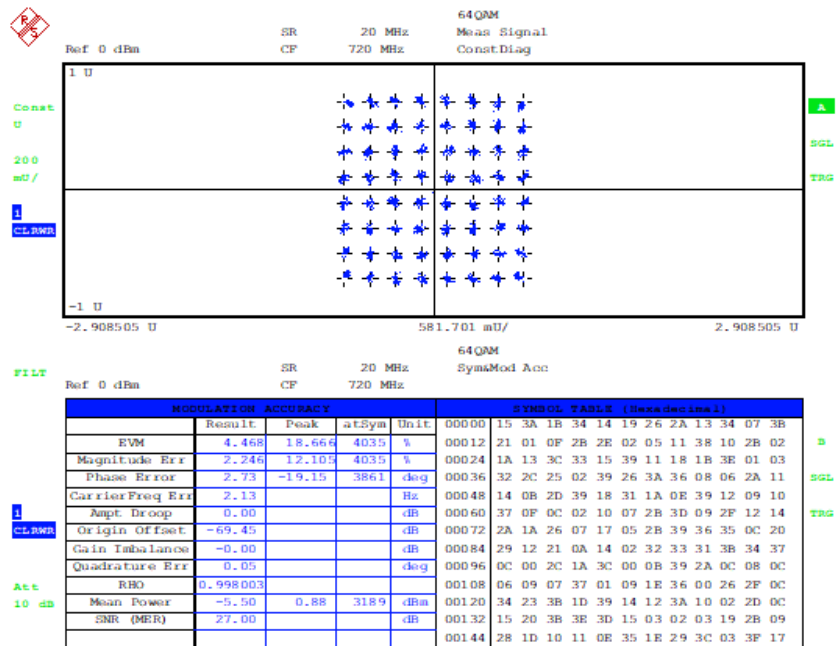


Fig. 30. Demodulated constellation view of calibrated test setup under strongly nonlinear conditions. (as in test-setup described as in Fig. 28)

Following Fig. 31 and Fig. 32 AMPM conversion has been fully compensated after performing of calibration along with the 3dB improvement of SNR and 1.2 % of the reduction in EVM.

Table 1 Comparison of different test setups; linear, weakly nonlinear and strongly nonlinear.

Metric	Linear (-10 dBm)	Weakly nonlinear (-5 dBm)		Strongly nonlinear (+5dBm)	
	Uncalibrated (Fig. 68)	Uncalibrated (Fig. 31)	Calibrated (Fig. 32)	Uncalibrated (Fig. 29)	Calibrated (Fig. 30)
EVM (%)	2.359	4.503	3.252	11.491	4.468

After comparing test results indicated by uncalibrated strongly nonlinear case (Fig. 29), calibrated strongly nonlinear case (Fig. 30) and weakly nonlinear uncalibrated case (Fig. 31) based on EVM, view of demodulated constellation points performance of the calibrated strongly driven nonlinear system (+5dBm input) performs better/similar than that of an uncalibrated weakly nonlinear system driven at an input power of -5dBm. In other words, in-terms of linearity it is as if though if the nonlinear system is driven by a lower level of input power (of -5dBm) but delivers a higher level of output power that corresponds to an input of +5 dBm.

Notably, it was observed in practice that the AMPM distortion (Fig. 31 test-setup driven at an input power level of -5 dBm) occurs before AMAM distortion (Fig. 29 test-setup driven at an input power level of +5 dBm) as explained in reference [15].

2.9. CONCLUSIONS

Challenges present in RF path calibration described in Section 2.1, have been successfully addressed by experimental tests with the use of four different test-setups presenting both weakly and strongly nonlinear system impairments with the use of a variety of test cases (section 2.5 to section 2.8). Impairments that exist within an RF transmitter path occur due to individual components and have been identified and presented (in section 2.1). A novel calibration technique based on constellation mapping has been invented as well as characterizing weakly nonlinear behavior the technique has also proven to capture phenomena such as memory effects that indicate a significant presence in strongly nonlinear systems as depicted by experimental test results. In comparison with existing methods, specific advantages of the proposed method were highlighted and were experimentally validated (section 2.4 and section 2.5-2.8). Additionally, other methods such as magnitude spectrum characteristics were discussed in identifying impairments and as a method to observe the correction performed after calibration in section 2.3.1 From the experimental test results obtained; a few noteworthy mentions are, for weakly nonlinear testing at S-band 8-PSK test signal and 256 QAM signal yielded EVM of near 1.9 % with an SNR of ~34 dB (improvement was ~10 dB). For weakly nonlinear testing at Ku-band six different 64-QAM signals resulted in an approximate EVM of 3.14 % and average SNR of 30 dB, with 7.5 % average increase of EVM, and of the average increase in 4.235 dB of SNR. Testing performed with Doherty power amplifier with small signal input indicates an average improvement of 10.6 SNR and 8.7 % in EVM leading to ~3.6 % and SNR of 28.8 dB. Most importantly a strongly driven nonlinear system at +5dBm indicated an improved linear performance in-terms of EVM and SNR values as if though it was driven by -5 dBm input that equates to the performance of the uncalibrated mildly nonlinear system.

Chapter 3

N-way Digitally Driven Doherty Power Amplifier For Ku-band Applications

The aim of this chapter is to present a novel design of a four-way digitally driven Doherty power amplifier (DPA) for Ku-band applications aimed at conserving power with increased efficiency. This is achieved by building a large signal amplifier using several small signal transistors arranged in a four-way digitally driven Doherty amplifier architecture. The proposed DPA is intended for future wireless communication applications in satellite communication services such as Lower Earth Orbit (LEO) and Medium Earth Orbit Satellite (MEO) constellations.

3.1. NEED FOR A N-WAY DIGITALLY DRIVEN DPA

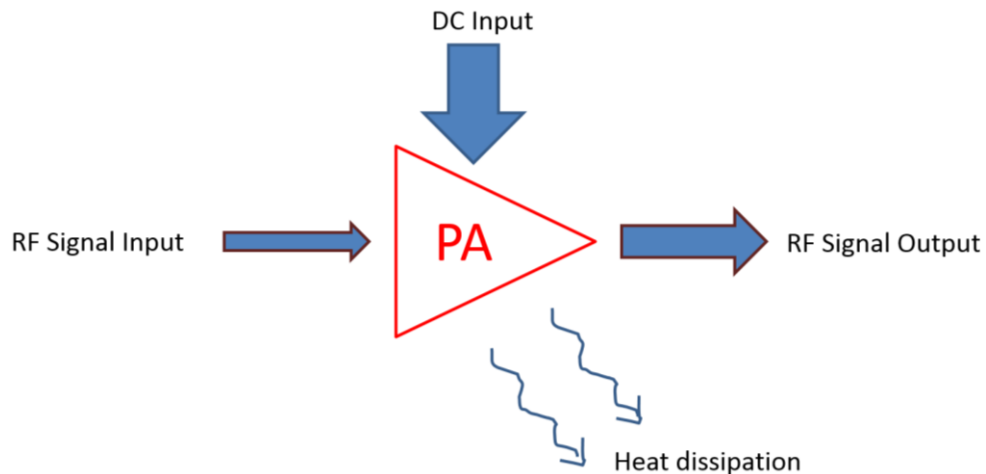


Fig. 33. A visual illustration of different types of power conversions of a power amplifier.

A power amplifier (PA) is a component that is used in a base-station which amplifies the useful RF signal that carries information to be transmitted wirelessly allowing communication (in the case of a wireless transmitter). As with most physical systems, the

power amplifier is not 100% efficient, there is a loss of power in its power-transfer mechanism. As visually illustrated by Fig. 33, the DC input power supplied to the PA is larger in comparison to the RF signal output (signal with information) meaning; energy into the system is much more than the energy that has been converted into a useful output. According to [54] and [55], a significant portion of power is consumed by a power amplifier in a base-station, leading to a value of 65% of the overall power consumed by the base-station. Therefore, the efficient operation of a power amplifier is of vital importance as it saves a lot of energy while meeting the user demand. Percentage distribution of power consumption in a base-station can be illustrated by a tree-map as in Fig. 34. [55].

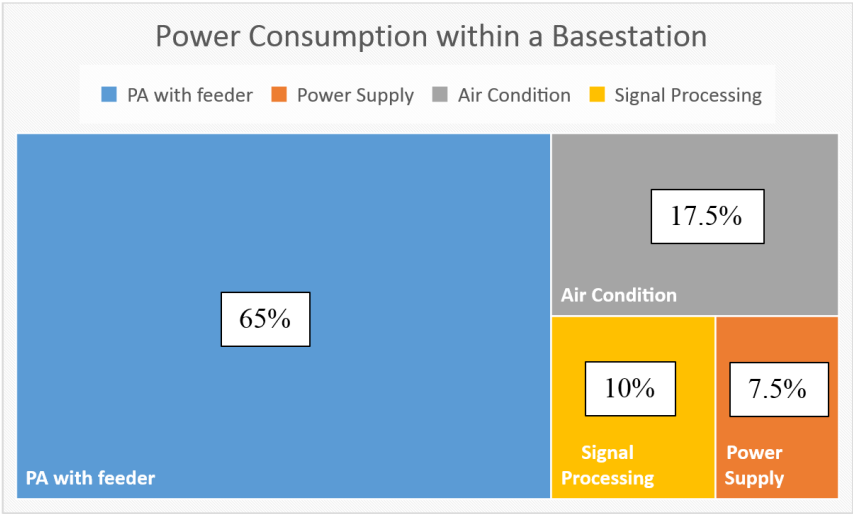


Fig. 34. A tree-map chart of power consumption in the percentage of that of a base-station

As highlighted in [55] it has been identified that mobile base-stations and mobile switching centers are contributors to the CO₂ emissions (electricity usage) and the number of such facilities has and are set to increase rapidly over the next few years. Therefore, any improvement in efficiency and linear performance of a power amplifier would result in greater savings of energy and would help to minimize the effect on the climate posed by the base-stations.

In contrast to issues of power wastage in base-station transmitters, there needs to be a platform to address the needs of the customer while preserving energy efficiency. For example, modern-day user habits expand to on-demand streaming applications such as broadband internet access, online gaming, etc. Additionally, the emphasis has also been

on connected broadband wireless infrastructure on all areas across the globe covering even the furthest rural areas. Not only a service such as satellite-based communication service helps to fulfill the requirements of the modern user but also helps to better allocate resources and to provide better connections in much-needed disaster management situations even in access limited areas. Low earth orbit (LEO) and medium earth orbit (MEO) satellite constellations have been identified as a possible solution to address service requirements above. Both LEO and MEO operate below geostationary orbit, meaning transmission at a lower power is sufficient to establish a communication link as the path loss is much less. Satellite manufacturers are leaning towards smaller size and low-cost deployments of satellites in constellations to cover the earth. Therefore, in supplying the high demand requested by the user wireless base-station transmitters emphasis is more focused on efficiency and linearity with low power output. Integral to this application is the Ku-band operating frequency range, that has already been and is further expected to be widely used by communication satellites. It is expected that a four-way DPA configuration would supply a linear amplified output response for a wideband signal at Ku-band frequency range as a four-way configuration is well suited at handling signals with varying PAPR levels. Implementing digital control over the input power distribution would allow efficient and linear operation of the overall DPA. Therefore, in conclusion, to meet the demand a four-way or further derived an N-way digitally driven Doherty configuration can be identified as a suitable choice for the proposed application and for future communications where higher data rates and spectrally efficient highly complex signals are being used incorporating multicarrier and multi-standard solutions.

3.2. EXISTING DOHERTY POWER AMPLIFIER TOPOLOGIES

As described in section 1.1, to meet the challenges of the future wireless communication systems, RF hardware needs to be well designed to integrate well with the needs of the spectrally efficient complex envelope modulated input signals that are designed to meet the future mobile communication standards. It has been identified that a DPA consisting of two different amplifiers operating on the principle of load-modulation (described in section 3.3) provides amplification for signals with different amplitude levels while maintaining an acceptable level of efficiency. Therefore, Since the invention

of DPA in 1936 by William Doherty [18] there has been a large body of work in applying doherty configuration into solid-state power amplifiers (SSPA).

3.2.1. SYMMETRICAL DOHERTY POWER AMPLIFIER

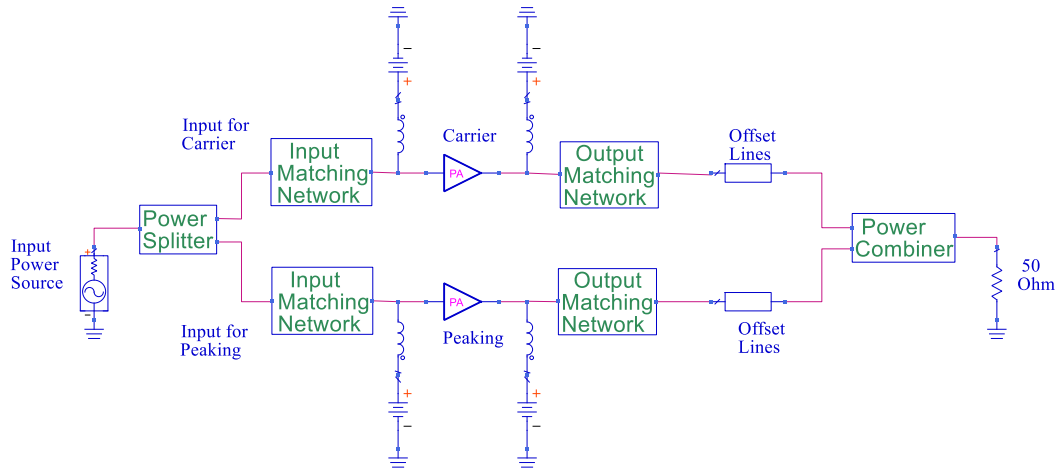


Fig. 35. General topology of a single input symmetrical Doherty Power Amplifier.¹¹

The simplest topology of a DPA is the symmetrical single input Doherty Power Amplifier. First the analogue power splitter divides the input power into the two paths. For a symmetrical design it is a 3dB split providing equal power to both power amplifiers. Input and output matching networks help to match the impedance of the device to that of the desired input and output impedance values. These are generally matched to 50 Ohms or that of the power splitter and the output match depends on the topology of the power combiner. The carrier and peaking power amplifiers themselves are chosen to be equal in their nature. If there are any phase offsets between the two paths due to manufacturing process or etc. tuning of offset lines provides balance between the paths. A Doherty power combiner takes the amplified output signal from both paths and sums them constructively. Additionally, it also provides the impedance match between the junction impedance to the output load impedance, which is typically set as 50 Ohms. A detailed discussion of the power combiner will be given in section 3.3 with basic load-modulation. In terms of the proposed application of using DPA in a LEO and MEO satellite communication link,

¹¹ (Power combiner shown is a Doherty Power Combiner with the inclusion of the impedance inverter and impedance converter, functions of these are discussed in-detail in subsequent pages)

there exists several advantages and disadvantages of using this architecture. Even-though a symmetrical DPA indicates suitability in handling signal with two amplitude levels such as 16-APSK modulated DVB-S2 (Commonly used for satellite communications) signal in-contrast to a single PA module, along with higher amplitude levels such as 32-APSK modulated DVB-S2 signal with an approximate PAPR level of ~8dB or even further, loss in efficiency and power is expected.

3.2.2. ASYMMETRICAL DOHERTY POWER AMPLIFIER

The main characteristic of an asymmetrical DPA is that the ratio of the resultant output power given from the two amplifiers are not similar. Instead in general in an asymmetrical design the peaking amplifier path is designed to deliver output power over a wider range than the carrier amplifier [42], [19]. If we list the maximum output power from the carrier amplifier as $P_{carrier}$ and power generated from the peaking path as $P_{peaking}$,

$$\alpha = P_{carrier}/P_{peaking} \quad (3)$$

For a symmetrical DPA $\alpha = 0.5$, meaning equal amount of output power is generated by the two paths. However, it is also possible to have a different value for α . For example, $\alpha = 0.25$, meaning more output power is generated by the peaking path relative to that of the carrier. Having an $\alpha = 0.5$, would suggest that one-fourth of the total output power of the DPA is generated at the low power region by the carrier amplifier. This means the turning on of the peaking path takes place at -6 dB in relation to the maximum output power generated by the DPA, this is commonly termed as output back-off level (OBO) in the literature. As shown in (4), the relationship can be written as [42], [19],

$$OBO = -20 \cdot \log_{10}(1/\alpha) \quad (4)$$

Which is an acceptable scenario when a signal with lower PAPR level is driving the DPA. In terms of our application for future satellite communications, as anticipated the PAPR of the input drive signals can be ~8 dB or more (anticipated). Therefore, an asymmetrical design is plausible for example an $\alpha = 0.25$ following equation (4) will

yield a back-off level of -12.04 dB. Meaning the peaking path is able to facilitate a signal with high PAPR. However, due to different classes of operation of the two devices the resultant gain of both paths is not guaranteed to be similar. In the analogue domain this can be mitigated by using a relatively high-power device for the peaking path as explained by [68] or by using an uneven power drive. However, as mentioned in [21], [22], [24] the use of analog splitter at the input even-though the power division ratio can be adjusted between the two paths, it does however, waste some amount of power till the auxiliary paths are fully turned on. The best method to mitigate this is to have digital control over the input powers on each branch, which enables saving of power that would have otherwise been wasted in a conventional analog only input structure by allowing signal into the auxiliary path at high enough drive level. Because of having digital control over the paths, it has been reported in the literature that improved load modulation performance can also be obtained due to the effective distribution of power in both branches [21]. Therefore, for the proposed application, having digital control of input paths is beneficial as power conservation is of significant concern for the application.

3.2.3. DIGITALLY DRIVEN DOHERTY POWER AMPLIFIER

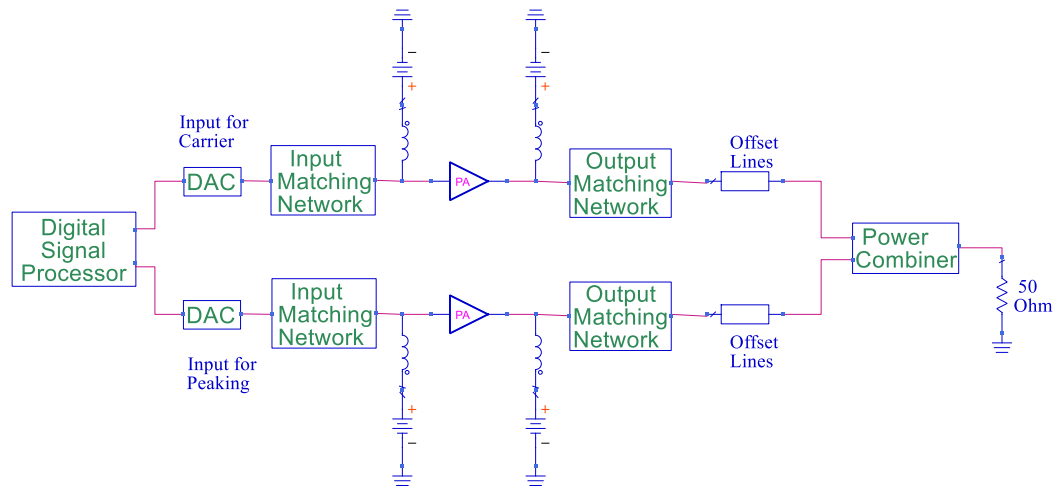


Fig. 36. An example architecture of a digitally driven DPA.

In accordance to Fig. 36, an example architecture of a DPA is presented. In the literature, examples such as [21], [22], [24] demonstrate the function of the digitally

driven DPA. Digital signal processors allow the distribution of the input signal into two paths, additionally it can also provide digital alignment of the phases for the two paths. Meaning analogue impairments that are existent in the paths and between the paths can be compensated. Allowing digital input power supply as described in [21], [22], [24] reduces the power wastage into peaking/auxiliary branch when it is not in use at a lower level of amplitude of the input signal. This helps to increase the overall efficiency of the DPA. The above mentioned practical usefulness of having digital control enhances constructive summation of the signals propagated within the paths at the DPA combiner thus yielding greater linear performance. The digital to analog converter (DAC) performs the signal conversion from the digital domain to the analog domain and does the up-conversion to feed the DPA board (an example block diagram highlighting the individual components of the DAC and the up-conversion block can be viewed from Fig. 1). Input and output matching networks and the power combiner functions as mentioned earlier in sections 3.2.1 and in sections 3.2.2.

Advantages in having a digitally driven DPA for the proposed application can be summarized as; improved power conservation thus improved efficiency, suitability of adjusting the input signals to allow impairments of an individual RF paths separately (as described in section 2.1). [21], [22], [24].

3.2.4. N-WAY DOHERTY

Advantages of a digitally driven architecture for DPAs can be well identified from their superior performance in comparison to fully analogue DPAs. However, they can only perform to the maximum extent that the hardware allows. Reconfigurability in a wireless system is necessary to meet the criteria for the future wireless communication standards. This is where the proposed concept of utilizing several small signal devices to develop a large signal amplifier would be helpful as with digital control the individual small signal devices can be turned on or off or individually controlled. i.e. If a path can be identified in the future to be defective the power distribution to that path can be switched-off. Additionally, several small signal amplifiers designed for maximum linear

operation when combined effectively can achieve the output power required for a power transistor with better linearity. In applications such as LEO or MEO this operation is often desired.

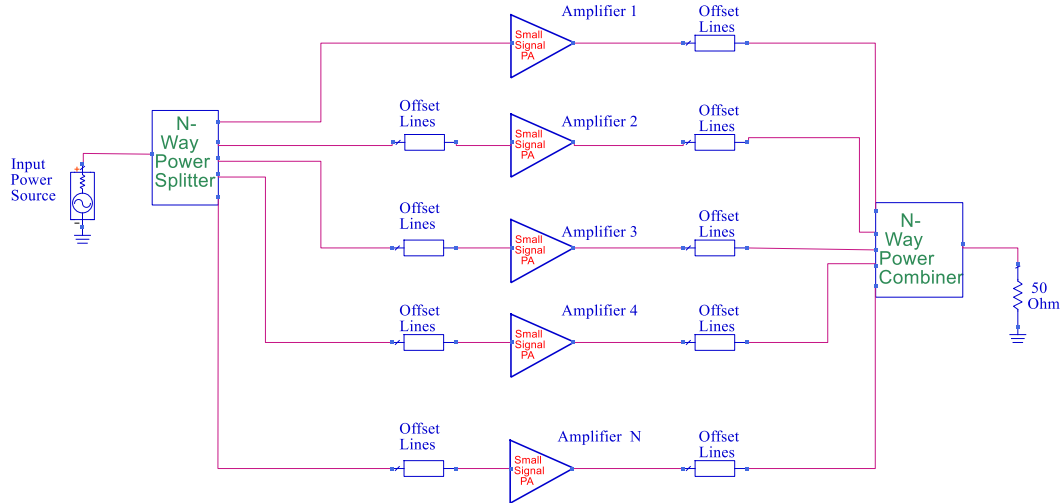


Fig. 37. N-way architecture of a Doherty Power Amplifier, with a N-way power splitter and a combiner and at the input and output respectively.

Reference to Fig. 37, conventionally amplifier 1 is selected as the carrier, amplifiers 2 to N will be peaking paths and correspondingly the combiner and power splitters will be designed. The conventional purpose in having an N-way architecture as well described in [19] is to have superior performance at back-off levels. Meaning when a signal with high PAPR is supplied to the N-way DPA. Carrier path will be handling the signals the lowest amplitude and each of the other paths will correspondingly get activated for a sufficient enough input power level for them to conduct. This operation will help to maintain performance of the overall DPA across a wide range of amplitudes.

A three-way Doherty structure can also be incorporated in a die assembly [23]. As mentioned in [23] the advantage of such a structure is to obtain a wide bandwidth performance and higher efficiency at several back-off levels in comparison to a two-way structure. As an advancement to conventional three-way structures, a three-way concept of a digital Doherty transmitter capable of achieving extended bandwidth is explored in [22].

Although, an N-way fully analog DPA architecture has more flexibility in design in comparison to the symmetrical or asymmetrical DPA. However, like a symmetrical DPA the analogue input power distribution causes losses and imperfections as described earlier. An analogue power splitter does not allow flexibility in the input signals to the separate branches of the DPA, i.e. in a situation where more output power is needed, reconfiguration of one of the peaking paths into a carrier path thus yielding continuous operation through the input waveform is not possible to achieve. A digitally controlled input however, would have been able to overcome this by digitally supplying the phase offsets and provide the function of the output impedance inverter to an acceptable extent¹². Moreover, individual attention to mitigate the impairments of each of the separate RF paths to yield a better performance cannot be offered, therefore, for the proposed application N-way architecture alone would not suffice.

3.2.4. N-WAY DIGITALLY DRIVEN DOHERTY POWER AMPLIFIER

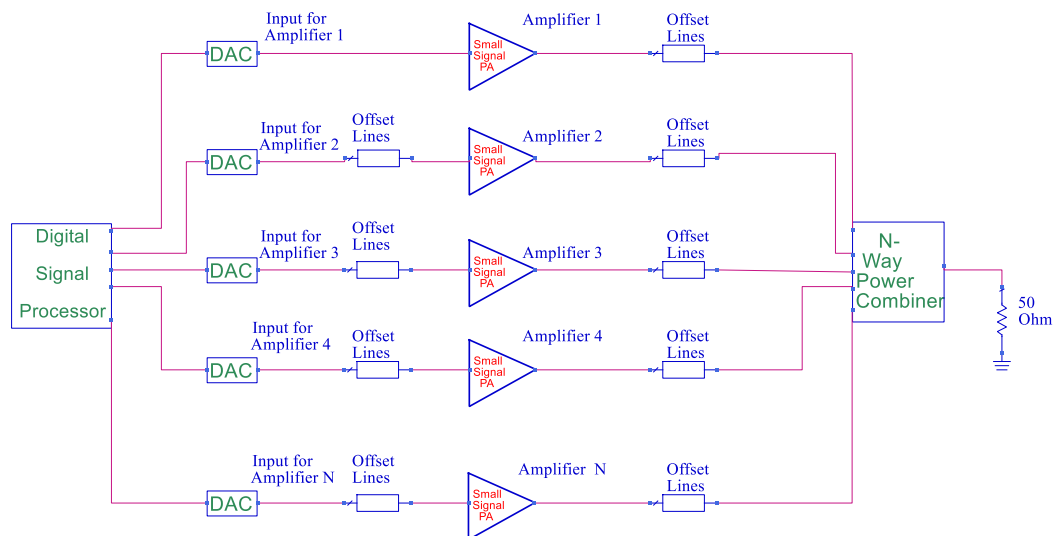


Fig. 38. N-way architecture of a Doherty Power Amplifier, with a N-way power splitter and a combiner and at the input and output respectively.

Adopting a digitally driven N-way Doherty architecture as depicted in Fig. 38 above, allows further flexibility in;

¹² A detailed study in waveform engineering is necessary to achieve such performance, however, this is beyond the scope of this work only the initial idea is proposed to justify the future possible applications.

1. Supplying path-oriented RF input signals.
2. Turning-on and turning-off the input signal at the desire of the user.
3. In addressing challenges of cases such as that of mentioned in Section 3.1 in rural areas or in disaster management situations where input power is in limited supply, all paths can be tuned to have class C bias levels and transmit RF signals at a low power with low thermal dissipation. ¹³ For the present work a simple symmetrical distribution of power was used to supply between carrier and peaking paths. The carrier was biased in class AB for linear performance and gain, peaking paths biased in class C for higher input amplitude turn-on and for efficient performance.
4. N-way architecture offers effective handing of signals with high PAPR. This allows applications such as on-demand streaming and broadband internet access, which consists of higher the data rates that results in higher modulation schemes with high PAPR to be handled comparatively better.
5. In terms of satellite applications, a spectrally efficient modulation schemes such as OFDM has been widely spoken and is set to applied over satellite transmissions. In terms of time domain view of such signal it again simplifies into a multiple input amplitude levels with a high PAPR characteristics. Therefore, a digitally controlled N-way architecture would most certainly be an option to consider for any spectrally efficient scheme.

In summary for different architectures of DPAs we have progressed through symmetrical, asymmetrical, digitally driven (two-way), and N-way Doherty, and have identified the most suitable architecture for the proposed application as a digitally assisted N-way solution. Which is a combination of N-way DPA and digitally driven architecture described in sections 3.2.3 and in 3.2.4. For illustrating the validity of the concept, a novel small signal amplifier based four-way digitally controlled architecture with a unique impedance transformation ratio combiner has been simulated in this work and is explained in detail in section 3.3.

¹³ Waveform engineered solution is necessary to maintain Doherty like operation and would be beneficial in this type of operation to gain the maximum possible performance.

Above mentioned background review of existing DPA technologies has yielded a suggestion to implement the structure of a small signal four-way digitally assisted solution to address the challenges faced in satellite applications. The viability of the proposed concept of developing several small signal amplifiers to yield the performance that of a high power large signal amplifier with improved linearity, PAE and output power can be better understood as in table below by performing a fair comparison with existing solutions which were designed to address challenges of similar applications which falls into the category of $\sim < 1W$ of output power and that are designed to operate at a similar frequency range.

Table 2 Comparison of different Power amplifiers and topologies used in similar applications.

Reference	Gain (dB)	Operational Frequency range (GHz)	Output* Power (dBm)	PAE* (%)	Process	Architecture Or Technology
[57]	8.6	9.5-18.5	~19	14.4	SiGe HBT	Differential Hybrid Cascode
[58]	~16	12-16	24.45	29.1	SiGe BiCMOS	One-stage Cascode
[59]	29	8.5-10	21	19	CMOS	Push-pull and Transformer
[60]	11.5	17.2 (17 GHz-band)	17.8	15.6	CMOS	Push-pull and Transformer
	14.5	17.2 (17 GHz-band)	17.1	9.3	CMOS	
[61]	23.6	8-13	17.3	10	SiGe BiCMOS	Two-stage Cascode
[62]	27	14.8-18.2	21.4	16.7	SiGe BiCMOS	Two-stage Cascode
[63]	12.8	13.5-14.5	30	37.5	SiGe BiCMOS	Combination of 16 unit-cell PAs
[64]	25	12.5-16	33.5	~29	pHEMT	Packaged amplifier
[65]	25	12.5-15.5	30	31	pHEMT	Packaged amplifier
[66]	19.8-20.8	11.5-13.5	28.8-29.8	52	pHEMT	Dual stage MMIC PA
[67]	17	15	27	41	GaAs pHEMT	Symmetrical DPA

[69]	8	17-18	25	40	GaAs	Single stage class D, DPA
[70]	12.5	22.8-25.2	30.9	38	GaAs	Dual stage class D, DPA
[71]	7.2	8-13 (X-band 9.5 G)	29	35-42	GaAs	Single asymmetrical stage class D, DPA
<i>This work</i>	<i>5.1-7.7^[2]</i>	<i>12-18^[1]</i>	<i>19.2^[4]</i>	<i>40^[3]</i>	<i>Hetero-Junction FET</i>	<i>Digitally Driven discrete N-way Doherty</i>

* In each case saturation point values or 1dB compression point for output power was chosen. Recorded best case at a given frequency was chosen as the corresponding PAE value for each case.

1. Following frequency sweep for two-way architecture, four-way design was successfully tested for 800 MHz wide-band signal. Fig. 51. and Reference [29] Figure 6.
2. Adjusting of peaking amplifier biasing stages allows the flexibility in obtaining better gain and PAE values for different applications. Fig. 48.
3. Four-way architecture allows a maximum of 40.367% of PAE, while two-way architectures allow 40.980%.
4. Two-way architecture allows a maximum output power of 16.921 dBm while four-way architecture allows 19.2 dBm of saturated output power.

Upon considering the output power level and design frequency concerned in the proposed application, similar such applications as observed by designs the in Table 2, structure is dominated by mostly CMOS or integrated solutions. Recent trends indicate a shift toward designs implemented with Monolithic Microwave Integrated Circuits (MMIC) or highly integrated signal or dual stage device structures. A few are of Doherty type [67], [69], [70], and [71]. In comparison to these gains and PAE of the proposed method is comparable, however in terms of output power it indicates a lower value for four-way architecture. This can be mitigated by having a higher number of stages and as demonstrated by Fig. 49 it is possible to increase the output power in-doing so without degrading the efficiency overall. Another possibility is to use a large signal power transistor itself to achieve a high-power output, however, this may compromise linearity. Therefore, in comparison with DPA architecture solutions the main differences of the proposed method are the use of discrete devices, a discrete solution may provide a controllable thermal environment at the cost of the real-estate used for the board. Another distinguishable characteristic is that all other architectures discussed use a standard symmetrical, asymmetrical or multi-stage architectures however, an N-way solution or a digitally driven solution was not indicated. The proposed design would have an advantage

(as explained in 3.2.3 and 3.2.4) in operating with information-rich signals consisting of high PAPR. Additionally, as explained before, it will also operate on a more controlled manner with the assistance from digitally controlled inputs.

In terms of linearity the small signal linear discrete devices combination indicates better performance, with the use of an N-way architecture. The following can be compared as both designs uses the same 64-QAM modulated input test signal.

Table 3 Comparison of linear performance of the DPA.

	Bandwidth (MHz)	ACPR (dBc)	Publication year
[67]	20	Before DPD -23.4 After DPD -48	2017
Proposed design *	800	Without DPD ~-50	2018

*Can be observed at Fig. 51

As can be observed by the two tables mentioned above highlighting the state of the art for a similar type of applications. The proposed design to the best of authors knowledge is the only digitally driven design, and the only distributed architecture having an N-way topology.

3.3. SUMMARY OF THE DESIGN PROCEDURE

Design steps in bringing-up of a symmetrical Doherty amplifier have been well-explored in a variety of sources in literature a few examples are [25], [26], [27], [28]. For this work, to be used as a small signal device a heterojunction Field-Effect-transistor (FET) device from NEC NE3210S0114 with its spice model implemented in Keysight's Advanced design system¹⁵ was used [29]. An example design procedure to follow can be found in Fig. 39. The initial step in the design process is to identify a suitable device for the targeted application. End-user requirements are to be considered in this step, such as frequency range of operation, desired output power level at the operation of PA at saturation, achievable maximum efficiency, thermal handling capability, size of the die or

¹⁴ © Copyright Renesas Electronics, formerly NEC Electronics Corporation.

¹⁵ © Copyright 2007-2016 Keysight Technologies. All rights reserved.

device and its possible mechanical arrangement etc. Intended application in this case for the Doherty amplifier is to be a part of a wireless transmitter base-station to establishing a communication link with LEO and MEO satellites where linearity and efficiency are of greater concern. Additionally, available resources for the designer can also be considered such as device models, S-parameter data, loadpull sweep data, data-sheet, measured data based on experimental evaluation boards provided by the device manufacture etc. All of the above-mentioned information can be used to verify the performance of the device model. An example of S-parameters sweep results is indicated in Fig. 39.

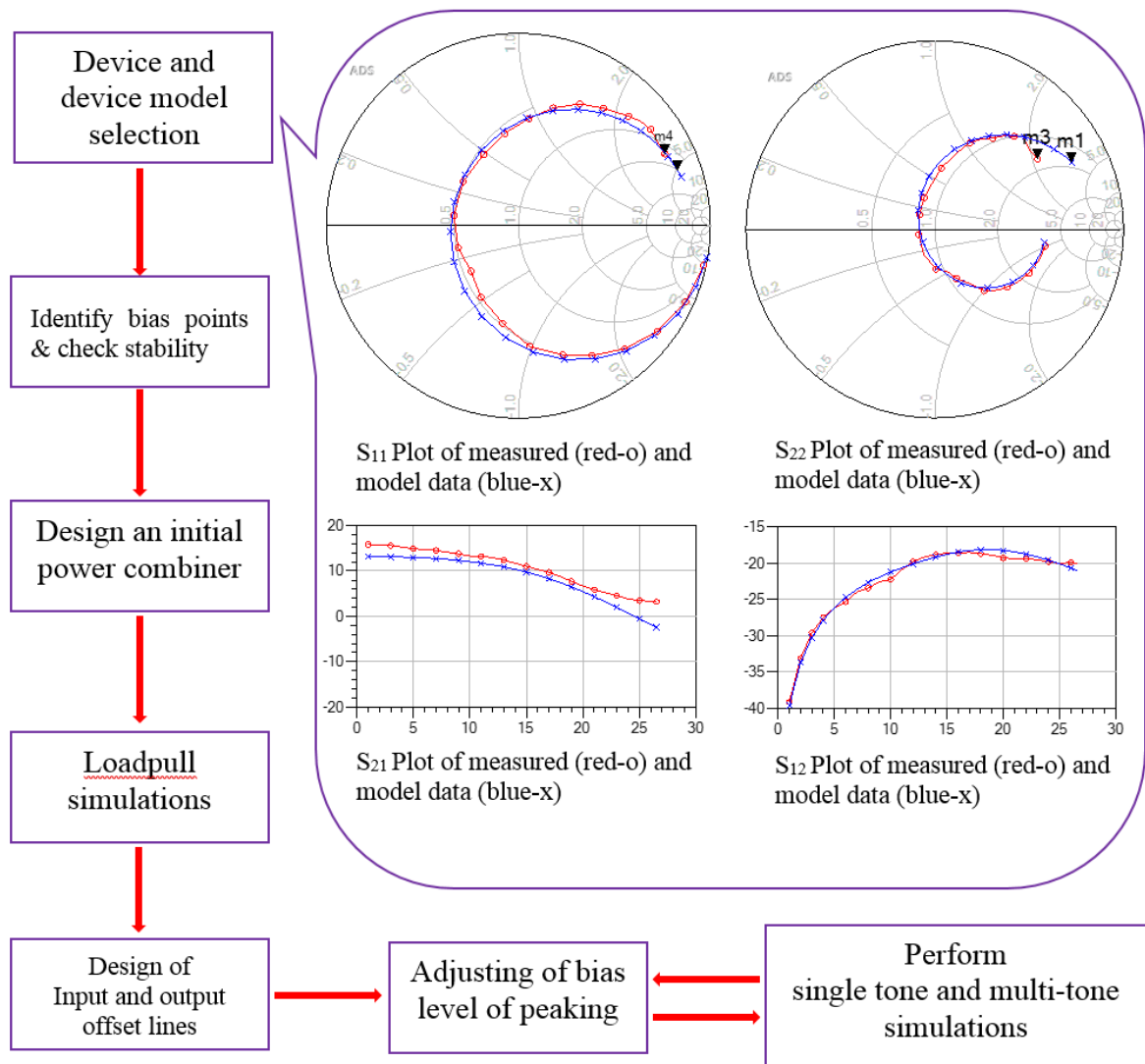


Fig. 39. An example design flow for a design of symmetrical DPA and a comparison of measured and modeled performance of S-parameters of the device used.

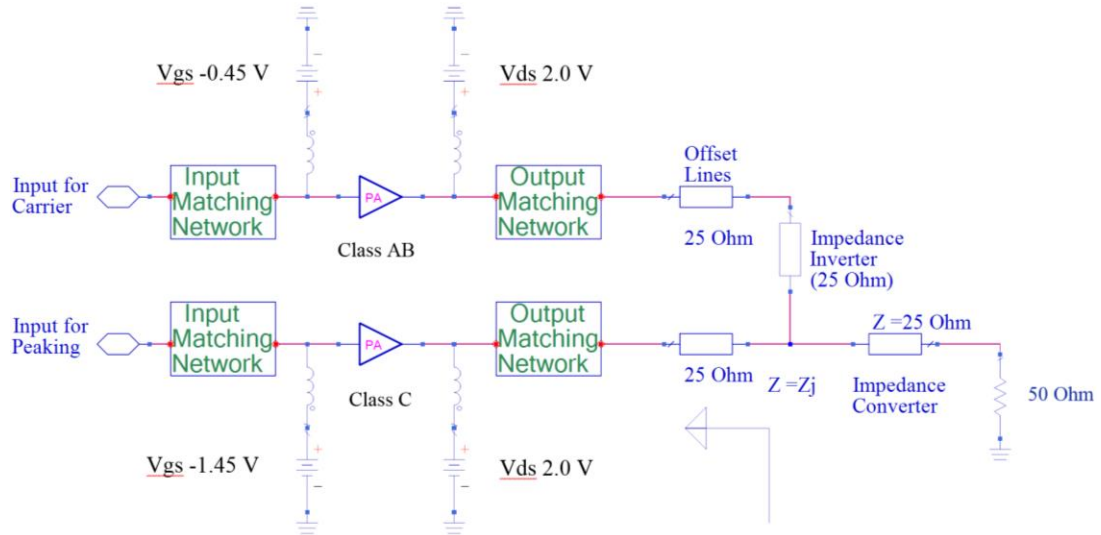


Fig. 40. An example arrangement of a symmetrical DPA schematic diagram [29].

As described by Cripps in [28], by observing the input and output characteristic curves suitable points for class AB and class C bias points can be chosen for carrier and peaking/auxiliary paths of the Doherty amplifier respectively. Doherty power amplifiers are designed such that carrier branch is expected to handle an average level of input power and peaking branch handles an above average level peak signal inputs of an information-rich complex envelope modulated input signal. Following standard Doherty configuration; as the carrier branch is biased in class AB, it is expected to deliver much needed linear performance along with linear gain to the lower levels of amplitudes. The function of the peaking branch is then to handle peaks occurring within the input signal efficiently, being biased in class C mode. However, in a symmetrical DPA, a distinctive characteristic is that input power is equally distributed to both branches at all times. As identified by [24] traditional symmetrical or in an analog DPA configuration an analog power distribution wastes the input power to the unwanted branch. E.g. a portion of input power is fed to peaking branch in lower power mode (at a lower input signal amplitude level) and vice versa. This issue, as well as phase imbalances between signal paths, can be alleviated by having a digitally driven input power arrangement as mentioned in [24].

3.3.1. CONCEPT OF LOAD-MODULATION

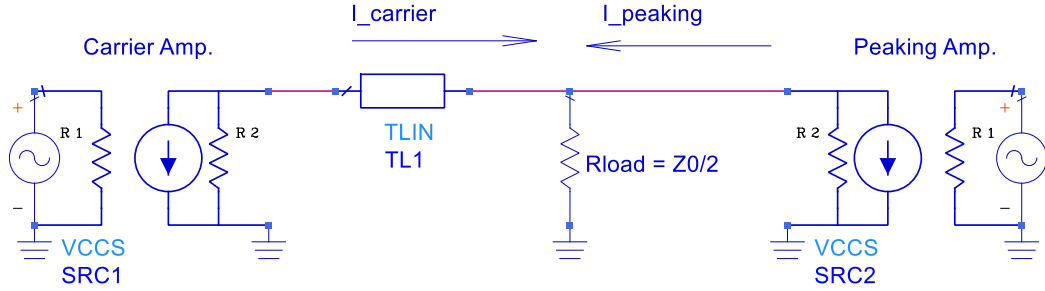


Fig. 41. An example setup of load-modulation operation. Which takes place on a two-way symmetrical Doherty PA design. Two amplifiers are represented by Voltage Controlled Current Sources (VCCS).

Essentially, there are two modes of operation of a DPA, namely, low-power mode operation and high-power mode operation. These two modes are activated by different power levels of the envelope of the input signal. If the instantaneous input signal is of average amplitude level, then the low power mode is said to be in operation. If the input signal is of an amplitude that is higher than that of the low-power mode, then the high-power mode is active. To achieve above-mentioned operation a power amplifier biased in a class AB mode that is a compromise between linear performance and efficiency is chosen as carrier amplifier. Class C biased device is chosen as a peaking amplifier as it requires higher input power level in comparison to that of a carrier amplifier to activate itself and provide an amplified output signal with higher efficiency [26], [28]. In a scenario where the instantaneous input power level is above average range, both the carrier and peaking power amplifiers will conduct. Because of this function, if both amplifiers can be assumed to deliver the same amount of load impedance (R_{load}) will be at a collective impedance of Z_0 based on principles of superposition. However, during low power mode operation, only the carrier amplifier will be active.

$$Z_0 = \sqrt{Z_{in} \cdot Z_L} \quad (5)$$

$$Z_{in} = \frac{(Z_0)^2}{Z_L} \quad (6)$$

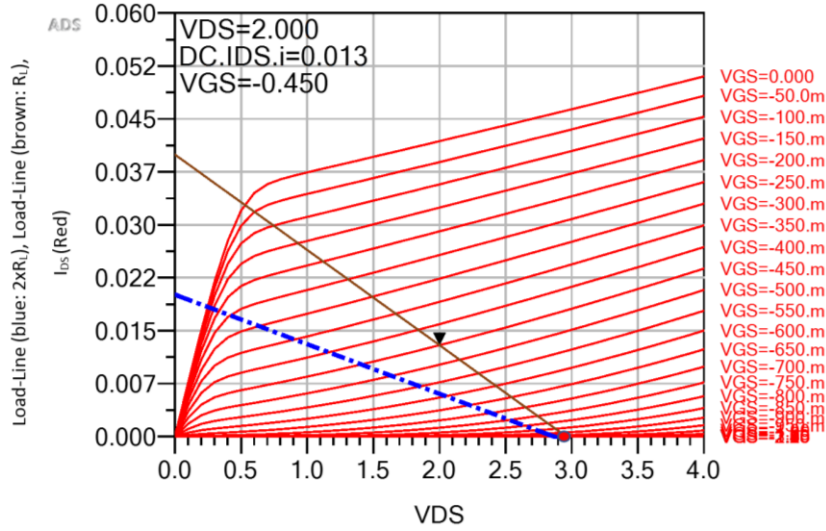


Fig. 42. The characteristic plot for output current vs voltage plot of the device. R_L – load impedance seen by the device been characterized.

In a conventional DPA during low-power region since the load impedance is much higher (x2) than that of the high-power region, load-line (in blue dashed) as presented in Fig. 42 has a different slope. The impedance seen by the carrier amplifier can be calculated by using (4).

Let us now focus on the output power combiner design of a simple two-way DPA combiner. In a DPA, the output power combiner typically consists of an impedance inverter an impedance converter. For a symmetrical DPA a characteristic impedance of 25 Ohm (Z_0) is widely used for the impedance-converter [29]. Based on transmission line equations as described by transmission line theory by equations (5) and (6) above two equations for a quarter-wave transmission line can be derived [29], [32]. In this arrangement, impedance-converter converts the output impedance of 50 Ohm (Z_L) to 12.5 Ohm (Z_{in}) for the summing node of carrier and peaking paths (6). This helps to maintain a lower transformation ratio for the output matching networks as the impedance for a device at the device reference plane is much smaller in-comparison to the output impedance of the load of 50 Ohm. The function of the impedance inverter is to perform load modulation. In summary as application of modulation in a Doherty power amplifier can be explained as: carrier amplifier observing a different output impedance to that when peaking branch is turned on. In other words, during low power drive summing junction impedance is set to be at 12.5 Ohms as calculated “impedance-inverter” itself being a

quarter-wave transmission line transforms this impedance into 50 Ohm as described by (6). However, during high power operation mode (when both carrier and peaking are active) impedance at the summing node is set to 25 Ohms as the currents from both carrier and peaking paths are summed. Therefore, a new impedance value of 25 Ohms will be presented by the impedance-transformer to the carrier amplifier. Meaning the value of the load impedance (in-respect-to the carrier path) is being modulated according to the input supply. This same concept can be further advanced into three-way Doherty power amplifier combiner design in this case, summing node impedance will be 8.33 Ohms [29]. Following equation (5), impedance converter value is 20.412 Ohm. For the four-way design summing node junction impedance is 6.25 Ohms, and by equation (5), impedance converter has a characteristic impedance of 17.678 Ohm. By performing an impedance sweep in a Harmonic Balance simulation, it is possible to investigate the best value for the characteristic impedance of the impedance converter by using the maximum power transfer theorem. This method can be used to verify the above-mentioned calculations.

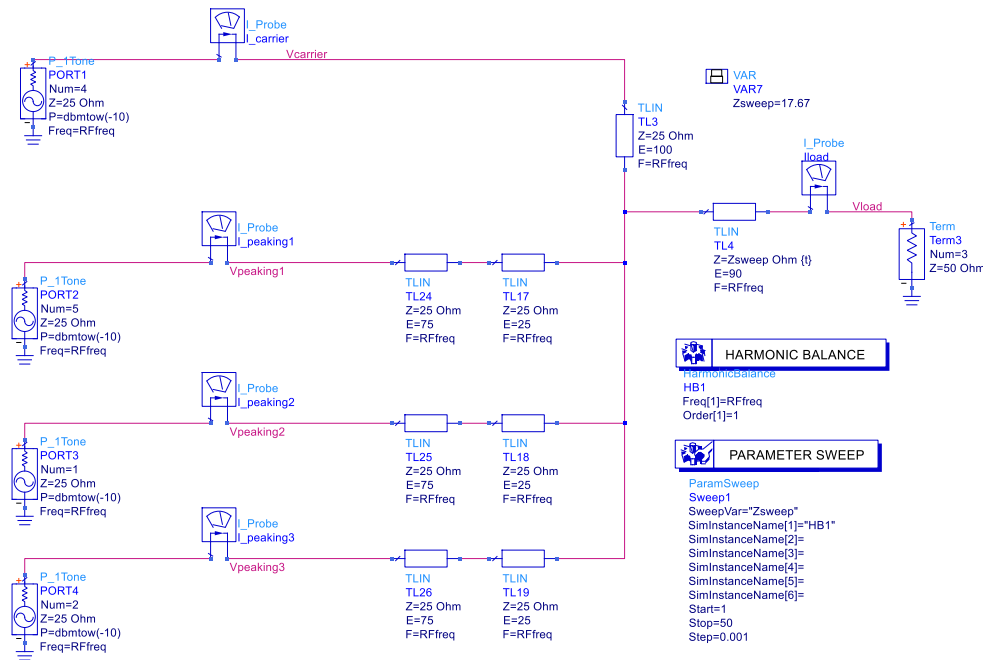


Fig. 43. The test-setup used to investigate the best possible characteristic impedance value of the impedance converter [29].

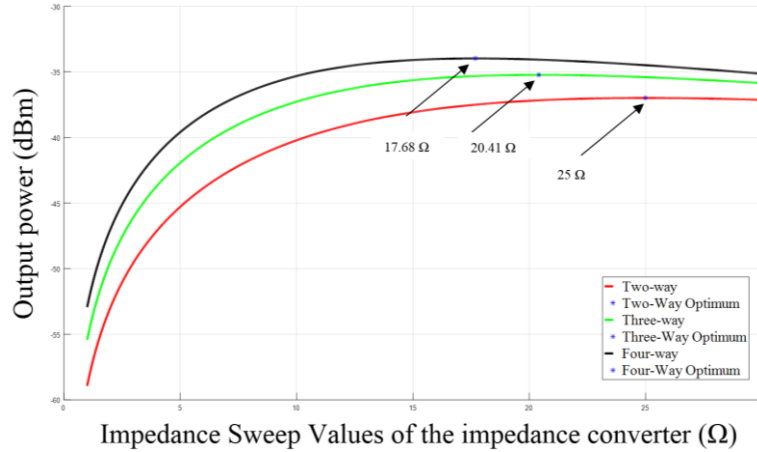


Fig. 44. Results from simulation in Fig. 43, with output power vs impedance sweep values [29].

Results indicated in Fig. 44, verifies the calculations performed in-designing the higher-level combiners. As the simulated impedance required for maximum power transfer value agrees with the calculations performed using transmission line equations.

After successfully designing the combiners, input and output matching networks can be realized. For this design it was observed initially that when the device operates well into saturation level of operation of PA, an output power level of 13.153 dBm obtained, an output loadpull impedance of $46.9-j*25.657$ Ohm was recorded at this power level. Therefore, at linear operation regime output power of approximately 10 dBm was used and recorded output loadpull impedance was $38.9-j*8.7$ Ohm.

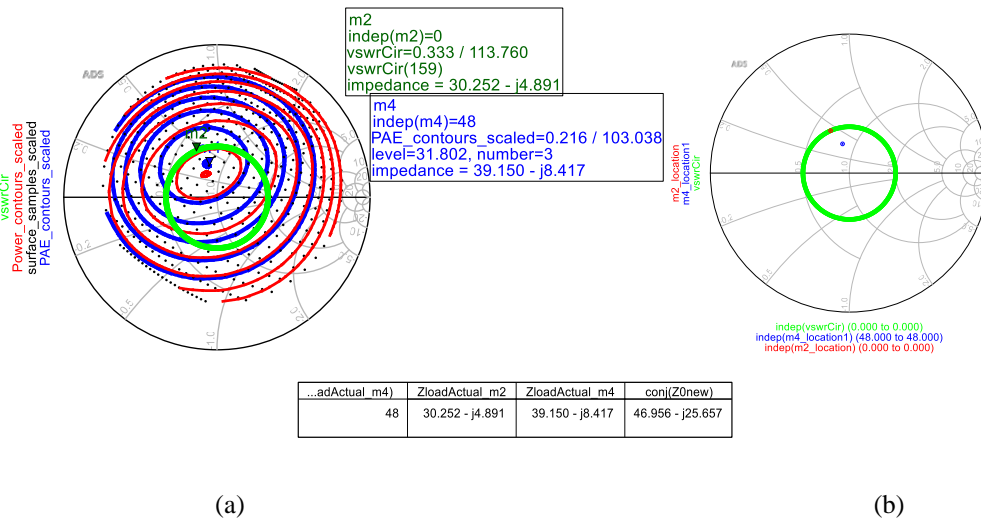


Fig. 45. (a) Loadpull contours obtained for simulations of carrier-branch on a Smith chart centered at a center at a chosen impedance for peaking-branch. Impedance sweep points/surface samples (black dots), Power contours (red), PAE contours (blue), impedance inverter response (green circle).

(b) Indicates the overlapping of chosen impedance point (red) on the VSWR circle without the contours, as an image that can be used to see the proximity to an actual maximum of PAE (marker m_4).

A setting such as that of Fig. 45, allows a trade-off between PAE and maximum output power by observing different contour levels. It can be seen from Fig. 45, that after trading-off between PAE and maximum output power the impedance transformation from high power mode to lower power mode will result in an impedance of $30.252-j*4.891$ Ohm (marker point m_2). This result is closer to what was obtained earlier ($38.9-j*8.7$ Ohm) for an output power of 10dBm, therefore approximate of 10dBm of output power is expected under the above-mentioned matching conditions. Once this process is completed impedance values obtained for both low and high-power mode can be used to design input, output matching networks and the impedance inverter [29].

The next step in the design process is to choose suitable values for the input and output offset lines for the DPA. It is of vital importance that in low-power mode operation the peaking path should be isolated from the input of the combiner in-order to make sure that load-modulation operation is not disturbed [27], [29].

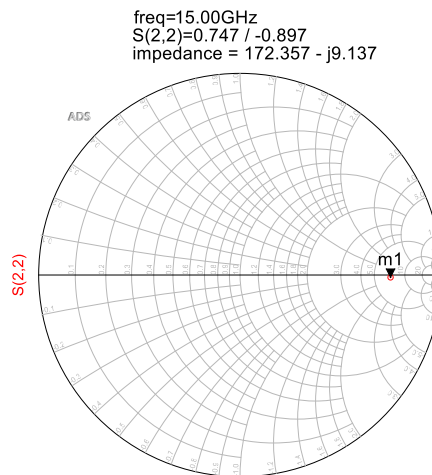


Fig. 46. Testing of offset line impedance for the peaking path presenting a high impedance at the designed frequency of 15 GHz.

Results presented in Fig. 46. Are for the tuning of output offset-line for the peaking path, indicating an open circuit at the output of the peaking path at low power mode operation. Verifying that peaking path is indeed in isolation with the combiner during low power operation. In contrast, carrier offset-lines can be placed such that both paths are balanced in phase [29].

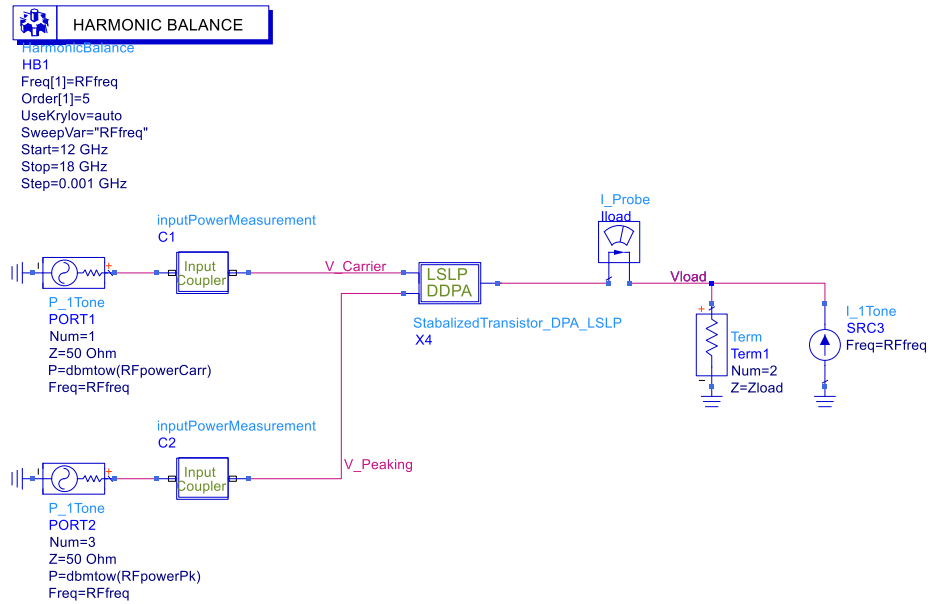


Fig. 47. An example of test-bench which can be used for single tone measurements. Additionally, RF power presented to each of the branches can also be swept [29].

The aim of using a test-bench such as that of in Fig. 47, is to identify the performance of the designed DPA. Including performance with frequency and to obtain measurements for quantities such as output power and PAE [29]. The test setup in Fig. 47 resulted in an output power of 15.0 dBm with maximum drain efficiency of 52 % for a bias level for peaking amplifier of -1.45 V. Peaking bias level set at -0.95 V yields an output power of 16.10 dBm for which the corresponding drain efficiency reported was 53.4 % along with PAE of 41% at 15 GHz.

It can be understood that the cost of increasing efficiency results in reduction of transducer power gain since the linearity of the two amplifiers are compromised when they are driven more towards operation at saturation levels at premature power levels as shown in Fig. 48. The above results indicate that the trade-off between linear performance and efficiency can be accomplished by the designer by adjusting peaking amplitude levels.

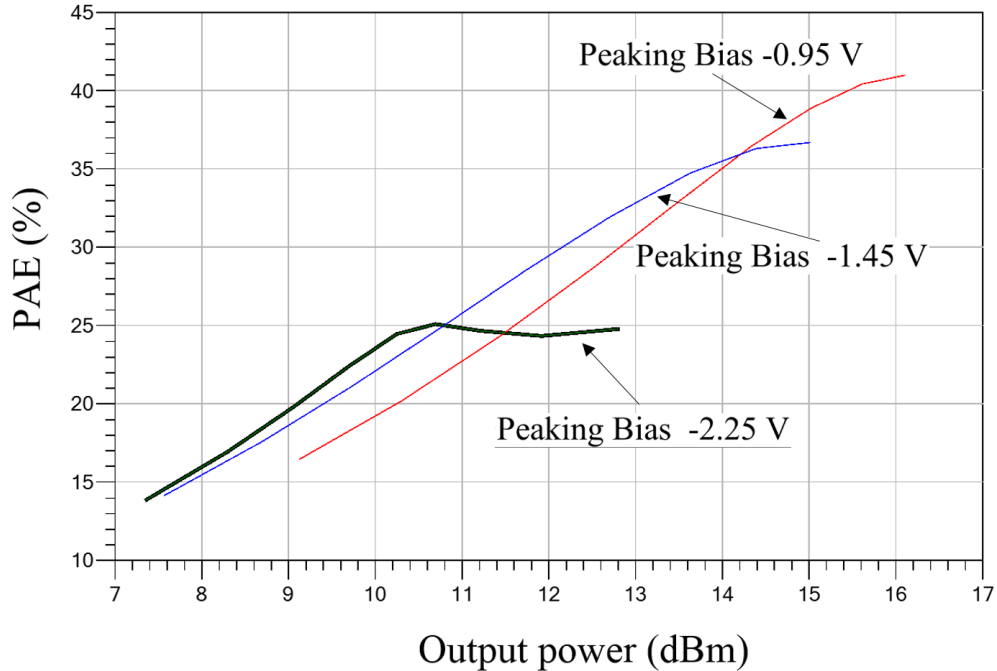


Fig. 48. Simulation results of the overall two-way Doherty power amplifier [29].

As indicated by Fig. 48, final adjustments can be made to the biasing of the peaking path to obtain better performance. The curve at lower bias level for peaking indicates a relatively high PAE at the start and then reaches its saturation (characteristic Doherty PAE curve). Other curves in red and blue at higher bias levels indicate better PAE performance at higher power inputs. The reason for this type of behavior is the activation of the class C branch. At low bias level for the peaking path, the DPA does not waste power into the peaking branch in-other-words load-modulation happens at a later stage. However, at a higher bias level for the peaking path, load-modulation occurs prematurely therefore initially a reduction of PAE is observed until the class C branch is active; when driven with higher input signal magnitudes peaking/class C PA is reached its maximum efficiency this is indicated by higher PAE values at higher output power levels in contrast to lower class C biasing. All of the peaking paths were designed to have the same input bias point, however, for future applications it is possible to alter this to facilitate larger range of back-off operation.

For the proposed application, it is desired to have linear performance as well as high PAE. Therefore, the above mentioned dual-input DPA was designed to fulfill these criteria. However, if indeed further output power is needed, without compromising the

current design goals, a viable solution is to incorporate further amplification stages. By using the previously derived advanced four-way combiner architecture and following a similar procedure to that of the two-way design it is possible to obtain the desired result.

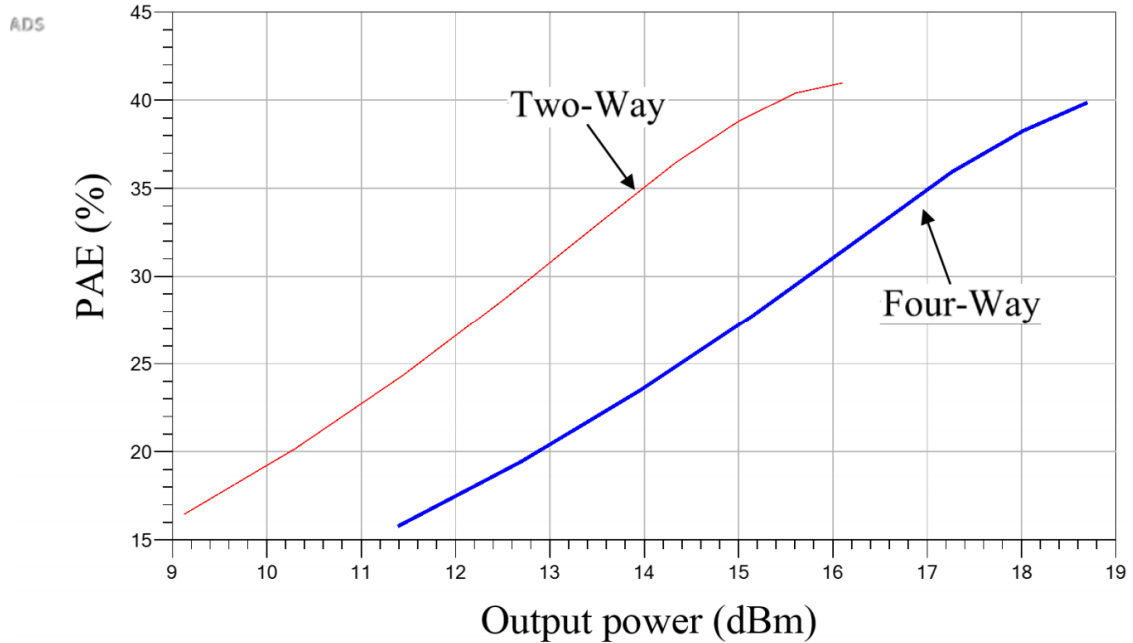


Fig. 49. PAE vs output power curve for two-way and four-way DPA architectures [29].

Fig. 49 indicates the above-discussed advantages in the result. The final test that was performed in testing the digitally-driven four-way amplifier is to supply with a modulated signal input. For the simplicity in this work, the power of the input signal is divided equally between the carrier and all peaking paths. The chosen input signal is of a 64-QAM modulation with a symbol rate of 800 MHz a raised cosine roll-off factor of 0.25. A wide-bandwidth of 800 MHz (approx.) was specifically chosen to represent a more challenging wireless communication signal. Advantages of using this signal have been previously discussed extensively in chapter 1. The main advantage is in its inherent multi-level amplitude and phase characteristics, which enables 64-QAM signal to emulate most of the information-rich wide-band signals such as Digital Video Broadcasting (DVB-S2) type signals commonly used in satellite communications.

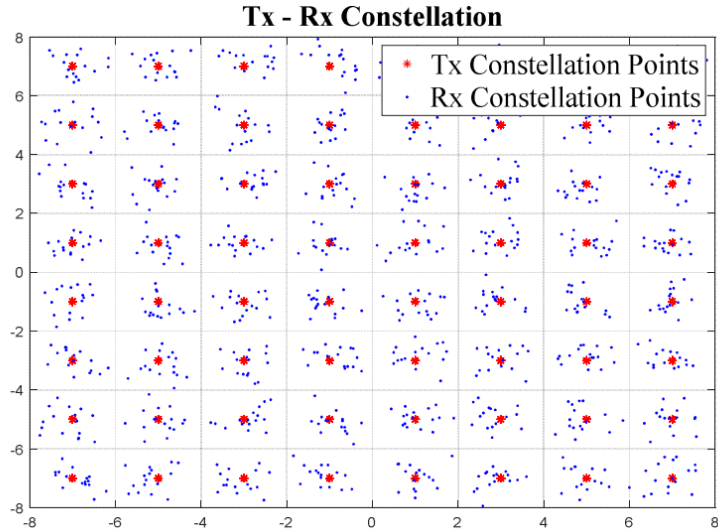


Fig. 50. Transmitted (Tx) and received (Rx) constellation diagram of the 64-QAM signal. (Tx- red, Rx- blue) [29].

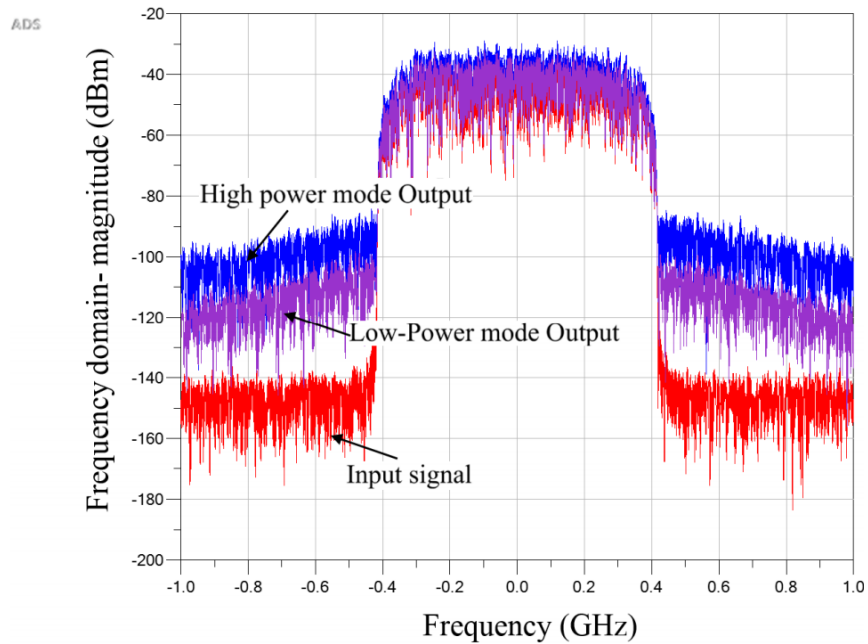


Fig. 51. Magnitude spectrum of the output spectrum [29] (Input signal – red, Low-power mode output, High-power mode).

Fig. 50, and Fig. 51 indicates simulation results for low and high-power mode simulations for the four-way digitally driven Doherty PA. In-terms of the movement of transmitted and received constellation points, results indicate an acceptable movement of received symbol data around the ideal/transmitted constellation point with all transmitted bits being received. In Fig. 51, frequency domain characteristics of the four-way DPA driven by 800 MHz 64-QAM signal is shown. Firstly, it is possible to observe that the

high-power mode introduces a rise in the noise floor. This is mainly due to the active involvement of peaking paths also carrier amplifier driven into its saturation operation regime. However, in both cases, it can be observed that dynamic range is maintained at least at an ~ 50 dBc. Indicating suitability of the matching networks designed, wideband characteristics of the combiner and linear performance of the entire DPA to be operated at designed power levels and frequencies [29].

3.4. CONCLUSIONS

In summary, firstly, followed by the problem statement, a solution has been identified to facilitate the higher data rates, efficiency requirements and linearity performance that is expected from future mobile communication systems. The proposed solution is designed especially to be included in base-stations providing communication links to LEO and MEO satellite constellations. Secondly, previous designs for Doherty power amplifiers including current state-of-the art has been presented. It has also been highlighted the improvements performed on the existing designs to derive the proposed design. Followed by a detailed description of the design methodology. Additionally, a description of the concept of load-modulation has also been presented. At each stage in the design process, the steps were validated by simulations in addition to calculations performed manually based on fundamentals of transmission line theory. The performance of the proposed design was then tested with signal tone and a 64-QAM modulated signal of 800 MHz, a roll-off factor of 0.2 to tests its suitability for wideband operation at Ku-band frequency range. Final measurements indicated a drain efficiency of 53.4 % at a maximum of 19.2 dBm of output power. Moreover, possible future improvements were also discussed in section 5.3.

Based on obtained results it can be concluded that the proposed design offers a solution for addressing the future wireless mobile challenges that are specifically faced by Ku-band applications (such as LEO or MEO). A similar technique can also be used at other frequency bands of operation to facilitate wide-band information-rich signals with a variety of amplitude levels.

Chapter 4

Behavioral Modeling

The aim of this chapter is to discuss available options for device modeling for the proposed application of using models generated by behavioral modeling to be used in distributed arrays and to outline individual advantages between the choices. Experimental testing has been performed in analyzing different behavioral modeling techniques and uses an asymmetrical Doherty Power Amplifier.

4.1. BEHAVIORAL MODELING OF RF POWER AMPLIFIERS

The primary purpose of communication systems is to transmit useful information. Many challenges in wireless system design arise due to the limitations of hardware components that are used in the physical layer of the Open Systems Interconnection model (OSI model). The performance limitations can be spectral constraints, electromagnetic wave propagation properties or due to restrictions in signal processing as described by information theory [36].

Currently, massive multiple-input-multiple-output (MIMO) communication systems are proposed to deliver the additional performance required for 5th generation telecommunications. Massive multiple-input-multiple-output (MIMO) base-stations have multiple transmit paths that increases the spectral and energy efficiency of a network in comparison to traditional networks. A distributed transmission network within MIMO allows benefits such as improved directivity between transmit and received paths, low interference, effective use of antenna diversity [35].

In any Radio Frequency (RF) transmitter, an integral part is the power amplifier. Based on current research methods Doherty power amplifiers provide efficient performance with regards to complex envelope signals with varying Peak to Average Power Ratio (PAPR) [21],[26],[27],[28]. An asymmetrical Doherty power amplifier

stands to be the best choice for single input single output transmission network that is used in a base-station. Therefore, Asymmetrical Doherty power amplifier performance characterization will be an important part of simulating and troubleshooting a distributed array of power amplifiers.

Three types of modeling techniques are used in Computer Aided Design CAD design, physical, circuit level (electrical) and behavioral modeling. Physical models provide more accurate high detailed level of description of the device characterized as they take the device level physics into conservation. Physical properties such as charge distribution and other nonlinear phenomena that govern the operation of a Field effect transistor (FET - commonly used in power amplifiers) are solved as nonlinear partial differential equations in the simulator to yield a model that captures the physical behavior of the device [33],[34]. However, longer development time is required in bringing up a physical model and accurate/devoted study of the nature of the device is necessary. Additionally, computational time and processing power required will also be high [33],[34]. In terms of distributed arrays in a system level, the development time needed to create physical levels model will also be considerably high. An equivalent circuit level model comprises the behavior of the device under test being demonstrated by circuit level components such as transistors, capacitors inductors etc. Simulators use Kirchhoff's laws to solve the interaction between these components to predict the behavior. The main disadvantage in circuit level modeling is that due to various parameters such as fabrication process or physical tolerances of devices the modeled data may not be in good agreement with that of the measured data in a practical testbench [33],[34]. Another constraint in both physical and circuit level models is the intellectual property of the circuit design owned by various companies that are not readily available to the designer. Therefore, as a compromise to physical and circuit level modeling is to perform a behavioral model. This technique offers a high-level mathematical approximation to the device. In characterizing parts of a complex structure separately, behavioral modeling helps to evaluate a complex structure such as a distributed array before it has been implemented in hardware by characterizing individual segments of it separately and finally to perform a combined simulation. This helps to minimize the production cost and further

development costs. In conclusion, behavioral modeling of asymmetrical type PAs is undoubtedly valuable for the proposed application of distributed wireless transmitter arrays. The accuracy of any modeling technique is of high importance as the model must be able to capture both linear and nonlinear behavior.

4.2. MEMORY EFFECT OF A PA

When a nonlinear device is excited with a signal with wide-bandwidth, frequency dependent characteristics such as amplitude roll-off, AM-PM conversion, and group-delay can be observed and must be considered for accurate characterization of the device [45]. These nonlinear frequency dependent characteristics are commonly termed as memory effects. Memory effects of a PA can be described as its current output being dependent upon not only its current input but also on its previous input samples. In-terms of hardware, this is mainly due to charge storage elements, thermal characteristics, and hysteresis present within the active device and its physical assembly [33], [34]. Measured data in Fig. 63 and Fig. 64. (AMAM and AMPM) plots indicates a variation of output amplitude or phase with respect to same value of input signal amplitude for different samples in time. This is due to memory existent in the nonlinear device affecting the performance of the overall system.

Modeling techniques that capture the nonlinear performance of a PA-based only on its instantaneous input and output relations are called memory-less modeling techniques.

4.3. ESTIMATION OF MODEL ACCURACY

Normalized Mean Square Error (NMSE) is a function that calculates the difference between measured data (collected at the output of the nonlinear system to be characterized) and the estimated output from the model with the same input signal applied. NMSE is a time domain estimator for behavioral model accuracy and is presented in dB.

$$\text{NMSE} = 10 \log_{10} \left(\frac{\sum_{n=0}^{N-1} |y(n) - \widehat{y}(n)|^2}{\sum_{n=0}^{N-1} |y(n)|^2} \right) \quad (7)$$

Where N is the number of samples of the stimuli and n is the instantaneous sample number. Since NMSE is calculated as the difference between measured and estimated outputs (like error function), lower NMSE value presents a better model approximation. Although NMSE is a widely used technique to assess quality between behavioral models, the method does have few disadvantages. As NMSE is a time domain estimator both in-band and out-of-band (adjacent channel) components effects are included in the calculation. Additionally, memory effects of the nonlinear system are not assessed separately [39]. Therefore, in addition to performing NMSE calculation, an analysis of output magnitude spectra of the nonlinear system in the frequency domain is required.

Table 4 Models with their NMSE values in comparison to the measured output [42]

Model Name	NMSE (dB)
AM/AM & AM/PM	-24
Volterra Series	-27
VSV with SOM	-29
VSV with k-means	-29

Plots are shown in Fig. 63, Fig. 64 and in two VSV modes indicate superior and similar performance in comparison to other techniques.

4.4. MEMORY-LESS MODELING TECHNIQUES

Under the narrow-band excitation signal, a quasi-memoryless nonlinear system can be characterized by its AM/AM and AM/PM characteristics where the passband response of the system is independent of frequency dependent distortions [39].

4.4.1. AM/AM AND AM/PM

In literature several mathematical expressions are presented to express the AM-AM and AM-PM data, models such as Saleh, Ghorbani, Polynomial based models are widely quoted for memory-less modeling.

$$x(t) = x_1 \cdot \exp(j\omega_c t) \quad (8)$$

$$x_1(t) = A(t) \cdot \exp(j\theta(t)) \quad (9)$$

$$y(t) = g[A(t)] \exp\{j[\theta(t) + \varphi[A(t)]]\} \quad (10)$$

In discrete form,

$$y(n) = g[A(n)] \exp\{j[\theta(n) + \varphi[A(n)]]\} \quad (11)$$

In above equations $x_1(t)$ denotes the complex envelope information signal at baseband of $x(t)$. $x(t)$ is the complex modulated signal at RF frequency that is to be transmitted. ω_c is the angular frequency component that corresponds to carrier frequency f_c . $g[A(n)]$ and $\varphi[A(n)]$ describes the AM/AM (output amplitude) and AM/PM nonlinearities associated with the quasi-memoryless system output response [39]. Output complex envelope of the system is given by $y(t)$.

4.4.1.1. SALEH MODEL

Original publication by Saleh represents $g[A(n)]$ as $A(r)$ meaning output amplitude (normalized input amplitude is “r”) and $\varphi[A(n)]$ is comparable with $\Phi(r)$ in reference [38]. Two formulas have been introduced to quantify the function. Amplitude coefficients of the model are α_a and β_a . Phase coefficients of the model are α_ϕ and β_ϕ . The values for the individual coefficients can be calculated by least-mean-square algorithm (LMS) [39], [45]. According to literature amplitude and phase coefficients of this model can be further advanced to contain frequency dependent characteristics, for broadband applications [39], [45].

$$A(r) = \frac{\alpha_a r}{(1 + \beta_a r^2)} \quad (12)$$

$$\Phi(r) = \frac{\alpha_\phi r^2}{(1 + \beta_\phi r^2)} \quad (13)$$

According to research performed since the original publication by Saleh based on modeling of Traveling-Wave Tube amplifiers (TWTA), more recent developments

concerning modeling of quasi-memoryless systems focuses on solid state power amplifiers (SSPA) that are now widely used for current power amplifier applications. To address the behavior of an SSPA system that has a linear mode of operation under small signal excitations Ghorbani in [38] recommended inclusion of two first-order terms. White, in [40], describes the roll-over effect of the Ghorbani model at high input levels. According to [40] Rapp's model offers a better approximation with measured results at high input power levels leading to saturation. However, it is stated [40] that long linear response and smooth transition into saturation region that is expected to be observed at Ka-band systems; Rapp's model is difficult to be used. Therefore, White has suggested a suitable model for these types of applications.

4.4.1.2. POLYNOMIAL MODEL

Another method to represent a nonlinear function such as AM/AM, and AM/PM is to use a polynomial representation. A power sweep of the quasi-memoryless system yields an input and output relation of the system at different input amplitude levels. The two parameters that capture AM/AM and AM/PM are presented in terms of two independent polynomials of N^{th} order. Coefficients of the two polynomials are termed as a_i and b_i [42], [43].

Following equation (11),

$$g[A(n)] = \sum_{i=0}^N a_i |x_i(n)|^i \quad \text{and} \quad \varphi[A(n)] = \sum_{i=0}^N b_i |x_i(n)|^i \quad (14)$$

$$y(n) = \sum_{i=0}^N a_i |x_i(n)|^i \cdot \exp \left\{ j \left[\theta(n) + \sum_{i=0}^N b_i |x_i(n)|^i \right] \right\} \quad (15)$$

Plots in Fig. 52, Fig. 53 displays the modeled AMAM and AMPM responses using the polynomial model as described above. As seen by the figures for a 5 MHz bandwidth

input the DPA does not indicate a significant amount of memory, therefore, this technique does follow the characteristics of the power amplifier well.

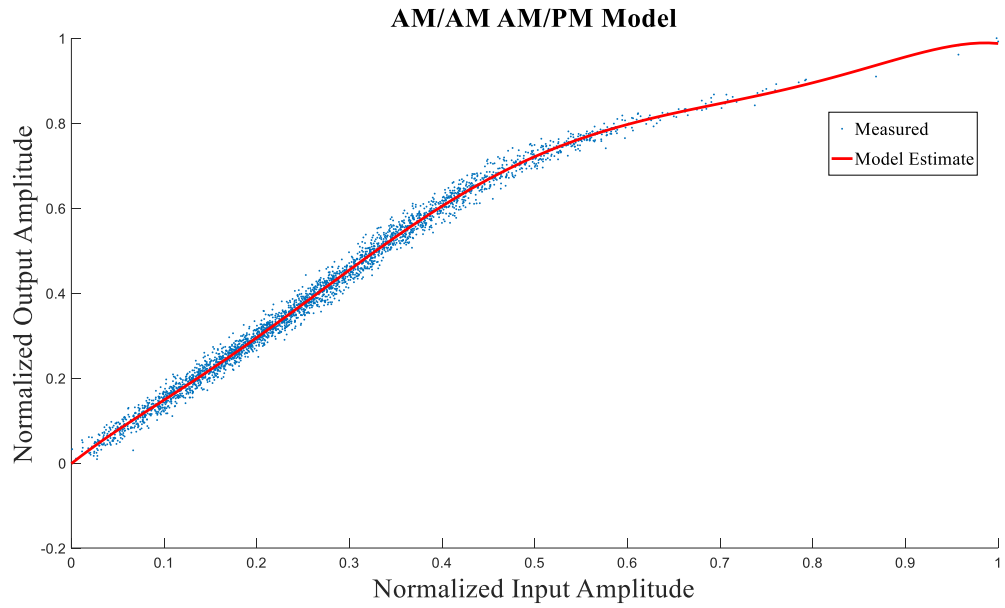


Fig. 52. AM/AM-AM/PM model characterizing the output signal of the DPA in AM/AM distortion curve [42]

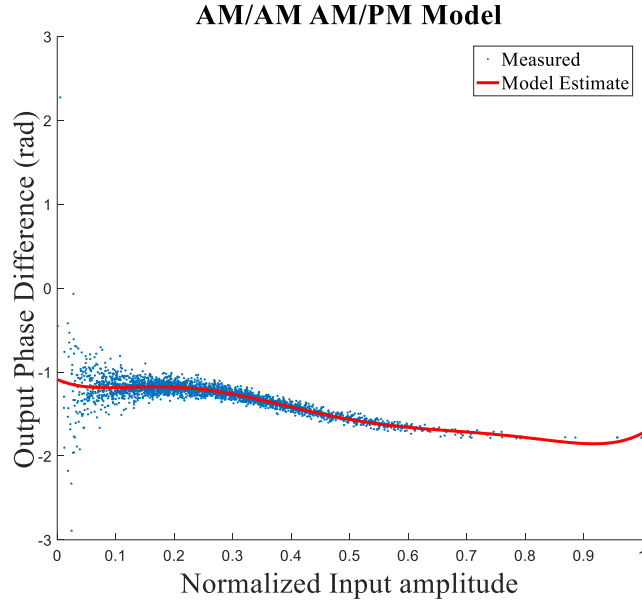


Fig. 53. AM/AM-AM/PM model characterizing the output signal of the PA in AM/PM distortion curve [42]

4.5. MODELS THAT CAPTURE MEMORY-EFFECTS OF PA'S

For accurate characterization of the dynamic effects of PA's as highlighted in section 4.2 inclusion of memory effects into designing of the structure of the model is necessary. Meaning considering not only the current input but also several previous inputs (memory taps) as for the model input. Hammerstein model consists of a memoryless nonlinear block and Linear Time Invariant (LTI) system that is modeled by FIR filter block.

4.5.1. HAMMERSTEIN MODEL

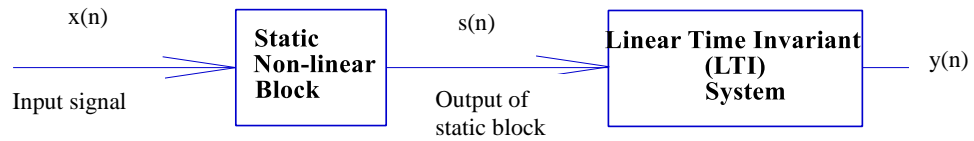


Fig. 54. Hammerstein model an example block diagram¹⁶

$$y(n) = \sum_{m_{len}=0}^M b_{m_{len}} \cdot s(n - m_{len}) \quad (16)$$

$$s(n) = \sum_{i=0}^N a_i \cdot x(n) \cdot |x(n)|^i \quad (17)$$

In the above two equations, discrete sample points are represented by n , $s(n)$ is the output of the static block. The combined response of both static and dynamic behavior of the system characterized is analogous to the output of the LTI block $y(n)$. Memory length of the FIR filter is given by M [39], [42], [43], [44].

¹⁶ References used in understanding Hammerstein model – [39], [42], [44] and [45]

4.5.2. ALTERNATE MODELS

“Weiner model” interchanges the static and dynamic blocks of the Hammerstein model.

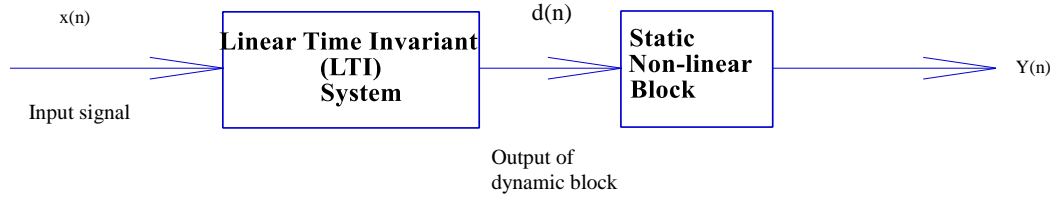


Fig. 55. Wiener model an example block diagram ¹⁷

Final output will then be,

$$y(n) = \sum_{i=0}^N a_i \sum_{m_{len}=0}^N b_{m_{len}} \cdot d(n - m_{len}) \cdot |d(n - m_{len})|^i \quad (18)$$

AMAM characteristics are captured by the “Static nonlinear block” and AMPM characteristics are captured by “LTI” block in both Hammerstein and in Wiener models [45], [39]. Both of these models can be interchanged based on the arrangement of system blocks in the actual hardware used during the test.

4.5.2.1. WEINER-HAMMERSTEIN MODEL

This model is a combination of both above-mentioned models. It contains two nonlinear FIR filter functions at the start and the end and a static memoryless nonlinear block in the middle. The two FIR filter functions are in series, hence can be considered as a single nonlinearity [39], [43]. A variety of further developments to the above-mentioned models exists in literature, ‘Feedforward Hammerstein model’, ‘PLUME model’ etc [39].

¹⁷ References used in understanding Wiener model– [39], [42], [44] and [45]

4.6. VOLTERRA SERIES

A Finite Impulse Response (FIR) filter kernel can describe a causal system with memory as the result of its impulse response convolved with corresponding input response. In contrast, a nonlinear system with no memory can be expressed by a power series. When the response of an above described FIR filter and a power series combined, a time domain series known as Volterra series is made. For a specified number of inputs and a specified order of the nonlinear dynamic polynomial, Volterra series captures all possible nonlinear interactions between all combinations of impulse response functions and the corresponding input samples. All the above-discussed models such as Hammerstein or Weiner etc. can be expressed as a subset of the Volterra series [45], [47].

$$y_n(t) = \int_0^t \cdots \int_0^t \int_0^t h_n(\tau_1, \dots, \tau_n) \cdot \prod_{i=1}^n x(t - \tau_i) d\tau_i \quad (19)$$

Where, $h_n(\tau)$ is the impulse response, (the kernel for the n^{th} term) current output term is $y_n(t)$ and the current input to the system is $x(t)$. In discrete domain, after taking the sampling instance to be equal to 1 for simplification purposes, convolution integrals can be represented as

$$y_{out}(n) = \sum_{k=1}^N \sum_{r=0}^{N-1} \cdots \sum_{r=0}^{N-1} h_n(\rho_1, \dots, \rho_r) \cdot \prod_{i=1}^n x(n - \rho_n) \quad (20)$$

Where, ρ_r , are discrete indices of each of the kernel and corresponding memory length taken, meaning they are the sampling period instances within the time-period concerned [45],[47]. As observed by the equations, Volterra series can quantify both nonlinear and memory effects of nonlinear systems such as power amplifiers. It has been mentioned in [45],[47] that a considerable drawback of this method exists where strong-nonlinearities are present due to non-convergence (divergence). However, for weakly nonlinear systems it provides an accurate and comprehensive characterization.

4.6.1. MEMORY POLYNOMIAL

Extending the concept mentioned in, Hammerstein or Wiener models it is possible to describe memory polynomial to be assisted with separate filters with memory taps at both nonlinear boxes. This implies that each box is dynamic function and the coefficients will form a two-dimensional array taking both lengths of the memory and order of the polynomial [43], [45]. According to an analysis performed by authors in [45] by having non-uniform delay taps in characterizing memory effects yields a more accurate result. It is mentioned that in quantifying long-term memory effects by adopting an optimum non-uniform approach performs better [45]. In [46] authors report that having memory polynomial representation with different memory tap delays are better in performance with respect to uniform tap delay representation by comparing the root-mean-square (RMS) error values for both in-phase and quadrature envelopes. Authors also report that the spectral regrowth, asymmetry, and IMD is better characterized by the proposed method [46],[45].

$$y(n) = \sum_{i=0}^{I-1} \sum_{m_{len}=0}^{M-1} P_{i,m_{len}} \cdot x(n - m_{len}) \cdot |x(n - m_{len})|^i \quad (21)$$

In equation (21), $P_{i,m_{len}}$ represents the polynomial coefficients with both amplitude and phase information. n is the sample number considered and $x(n)$ is the input sample considered and $y(n)$ is the corresponding output sample. Polynomial order is given by i . Memory length is given by M .

In Fig. 56 and Fig. 57 the modeling capability of the classical Volterra series is indicated. As presented by the figures the order of the classical Volterra series does not permit the higher magnitude values, however, does seem to follow very well the lower magnitude values of input. Additionally, the transition region of the DPA is also being modeled to an acceptable level.

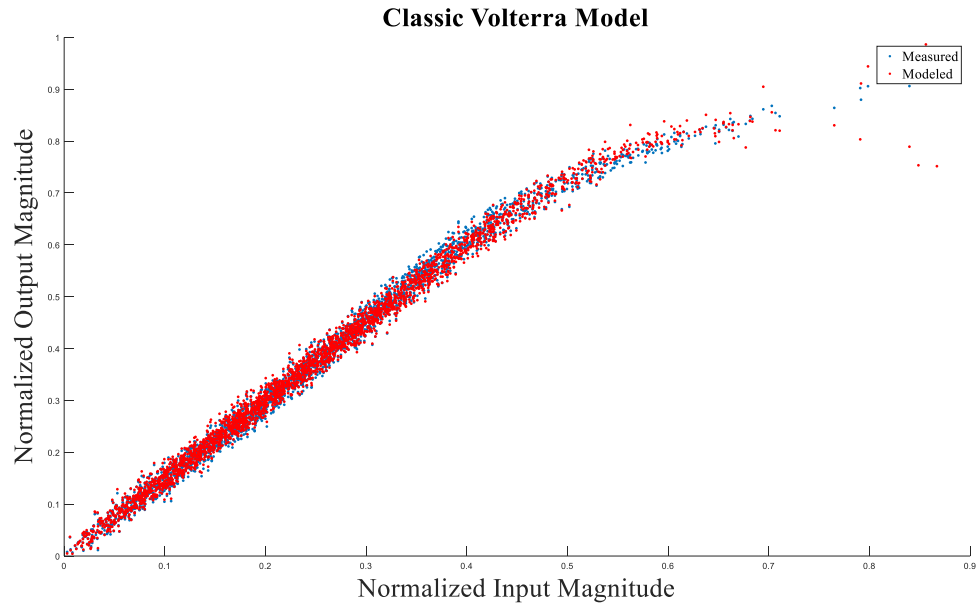


Fig. 56. Classic Volterra model characterizing the output signal of the PA in AM/AM distortion curve [42]

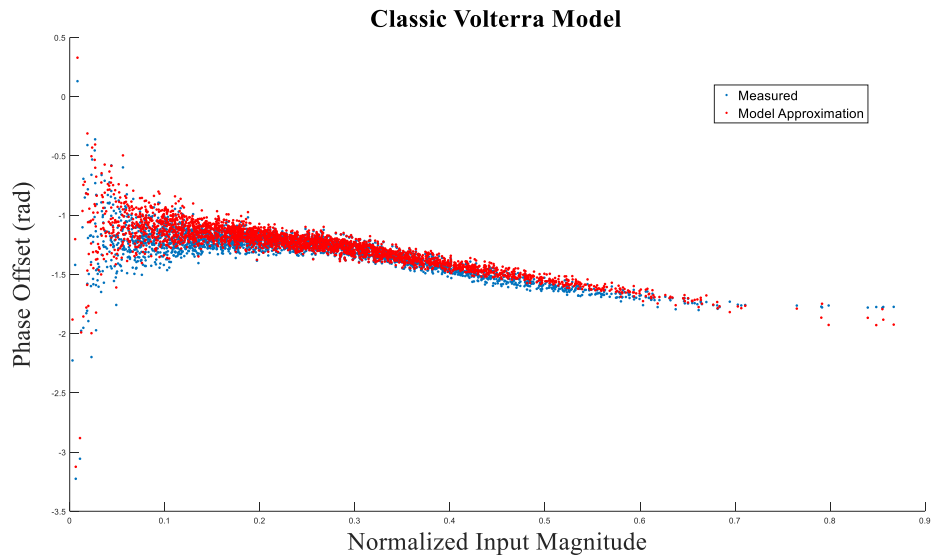


Fig. 57. Classic Volterra model characterizing the output signal of the PA in AM/PM distortion curve [42]

4.7. NEURAL NETWORKS (NN)

Traditional techniques such as AMAM & AMPM model in behavioral modeling suffers from being unable to capture frequency dependent nonlinear effects of a PA. To overcome this issue frequency dependent models have been introduced in [49] addressing several multi-tone products within the signal bandwidth. Additionally, an existing model [37] can be further developed to include frequency dependent behavior as shown by [45]. However, as mentioned in [45] at nonlinear operating conditions long-term memory effects that arise from electrothermal reactions, frequency dispersion characteristics of the nonlinear active device etc. For modeling nonlinear dynamic systems, such as power amplifiers, artificial neural networks are a viable option. Moreover, techniques such as Volterra series-based methods suffer from computational complexity and difficulty in implementing higher order terms for real-time applications [48]. As a solution and as compromise models based on artificial neural networks are considered widely in RF and microwave to model nonlinear behavior for real-time applications.

A biological neural network in the brain or in central nervous system functions as a set of individual neurons (nodes) connected to one another when an activation signal is received, inter-connections are made self-learning process is initiated and the information is processed. An artificial neural network (ANN) model functions in a similar manner to a biological neural network. An ANN processes information within its internal layers and via statistical learning methods (e.g. minimizing an error function) it can estimate an output within an acceptable accuracy for the problem description.

A computational model of a simple neuron can be described as below, [48]

$$y(n) = fn\left(\sum_{k=1}^m \omega_k \cdot x_k + b\right) \quad (22)$$

Where, ω_k denotes the weight applied for each input to the neuron and b is the bias value, the function that computes $y(n)$ is called the activation function fn . Activation function acts based on its input being within a predefined threshold value. Training algorithms, such as back-propagation are commonly used to train the model to accurately fit a model structure to the measured input-output data. A cost function in equation (22) is utilized as

a measure of direction for the training of the model, where it calculates the mean square error between the measured and estimated outputs [43],[48].

$$J = \frac{1}{N} \sum_{n=1}^N (y(n) - \widehat{y(n)})^2 \quad [43],[48] \quad (23)$$

The typical structure of a time-delay neural network (TDNN) consists of an artificial neural network which is fed by a number of delayed input samples [45].

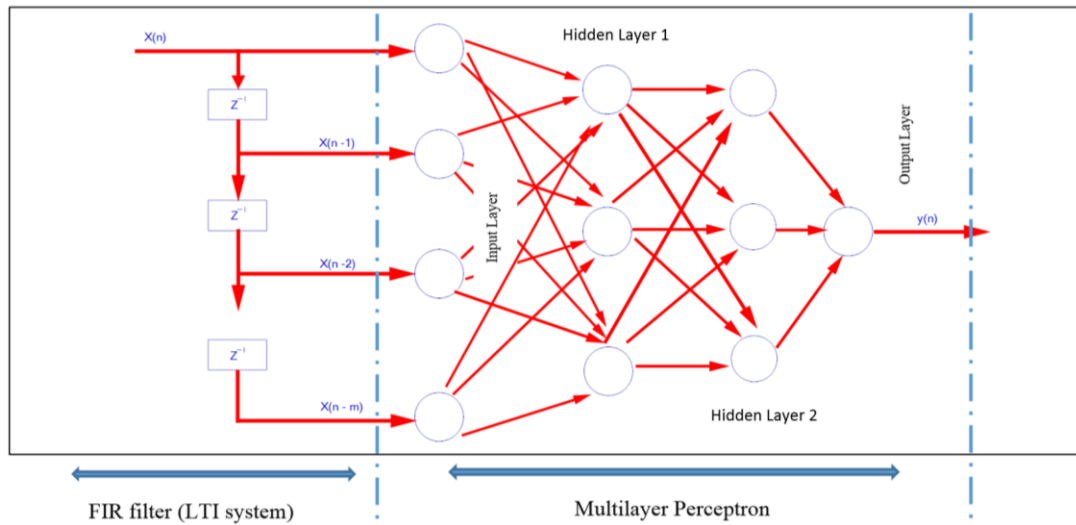


Fig. 58. Block diagram of TDNN model¹⁸

Fundamental formation of an ANN structure with a single input is called a *Perceptron* [50]. Another term commonly used to describe an ANN is *Multilayer Perceptron* (MLP) as it consists of multiple-layers. The input layer accepts input signal(s), the first and subsequent hidden layers consists of a number of neurons whose outputs are connected to the inputs of the following layer of neurons. One of the most common connection strategies is to connect each neuron output from one layer to the input of each neuron in the following layer, thus yielding a *fully-connected* neuron structure. All outputs from the last hidden layer are gathered and summed at the final output neuron. The structure of an MLP in this way has been demonstrated capable of modeling linear and nonlinear RF systems [43], [51].

¹⁸ References used in understanding TDNN model – [43], [45], [50], and [51]

4.7.1. A PIECEWISE SEGMENTED POLYNOMIAL

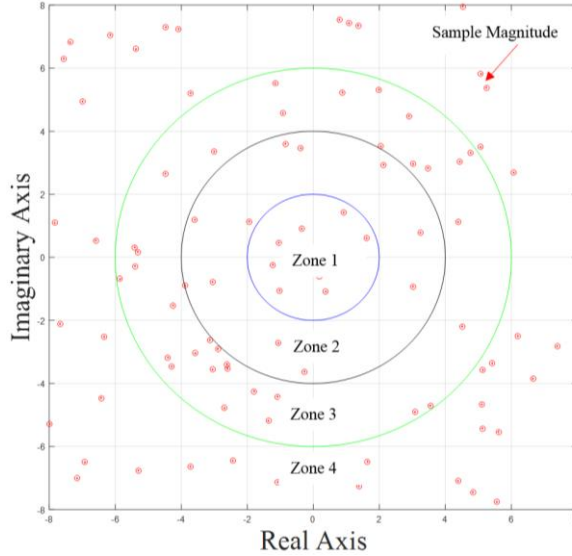


Fig. 59. Example of a piecewise segmentation of each sample in a signal into different zones base on its magnitude.

In a system whose characteristic performance can only be described by several nonlinear blocks (e.g. Doherty or outphasing power amplifier) yields an output, complex nonlinear interactions between them are difficult to be characterized by a single input single output model. Therefore, segmentation of nonlinear system with different intervals allows the designer to more accurately represent unique characteristics of each segment with lower order models with greater accuracy. Fig. 49 describes piecewise segmentation of different samples of an input signal, zones taken as an example classifies signals into magnitudes ($r(n)$) of two, four and six resulting in four zones [43].

$$\begin{aligned}
 H(n) &= h_1 \text{ when } r(n) \leq 2 \\
 H(n) &= h_2 \text{ when } r(n) \leq 4 \\
 H(n) &= h_3 \text{ when } r(n) \leq 6 \\
 H(n) &= h_4 \text{ when } r(n) > 6
 \end{aligned} \tag{24}$$

Following prev. used definition for modeling static nonlinearity by way of polynomial representation piecewise polynomial definition can be derived. The input that was $x(n)$ is now replaced by $H(x, n)$, which gives an optimized Volterra kernel for each segment (following segmentation based on input signal magnitude). Piecewise polynomial after segmentation can be expressed as below, polynomial order is 'N' [43].

$$y_{piec}(n) = \sum_{i=0}^N H(x, n) \cdot |x(n)|^i \quad (25)$$

According to literature [43],[45] piecewise polynomial approximation ($y_{piec}(n)$) offers a better approximation in comparison to classical methods. Due to special observance given into each segment overall characterization of the nonlinear device yields a better approximation.

4.7.2. VECTOR PARTITIONING

As an advancement to piecewise polynomial segmentation, when characterizing a nonlinear device, we can consider a segmented model with memory i.e. selecting on both instantaneous input samples and previous samples. Based on a normalized vector space of previous samples with respect to normalized current sample can be considered as partitioning criteria for each sample input. For a nonlinear device such as power amplifier this has proven to be a better method in comparison to scalar piecewise segmentation as it also encapsulates memory effects into consideration in partitioning [52].

4.7.2.1. K-MEANS

Vector switched Volterra methods use a different Volterra kernel to define each segment of a nonlinear response thus resulting in a better approximated model output. K-means¹⁹ is an iterative method of data clustering, that can be used to select among different Volterra filters according to the input and output characteristics of the nonlinear system. As mentioned by authors in [52] the method applied for behavioral modeling yields fast results. Initially a user defines the number of segments, this sets value for K. The mean position for each partition is termed the *centroid*. Upon each iteration the position of each centroid is adjusted considering the objective function. A common objective function used, is the Euclidean distance between each data point and the nearest cluster center for the data point selected. Upon each iteration, centroids are relocated hence minimizing the

¹⁹ Lloyd's algorithm is a well-known variant of K-means.

resultant value of the objective function. Thus, after several successful iterations centroids are placed on a minimum possible value for objective function for each pre-partitioned segment. Each data point is assigned to its nearest centroid and are stored. These stored values can then be used to select appropriate filter kernel of the Volterra series for each input sample in modeling [43], [53]. A drawback of this technique is randomness in choosing an initial centroid, as this may lead to local minima. Resulting in a partially explored segment, hence non-optimum kernel for VSV series model approximation [53].

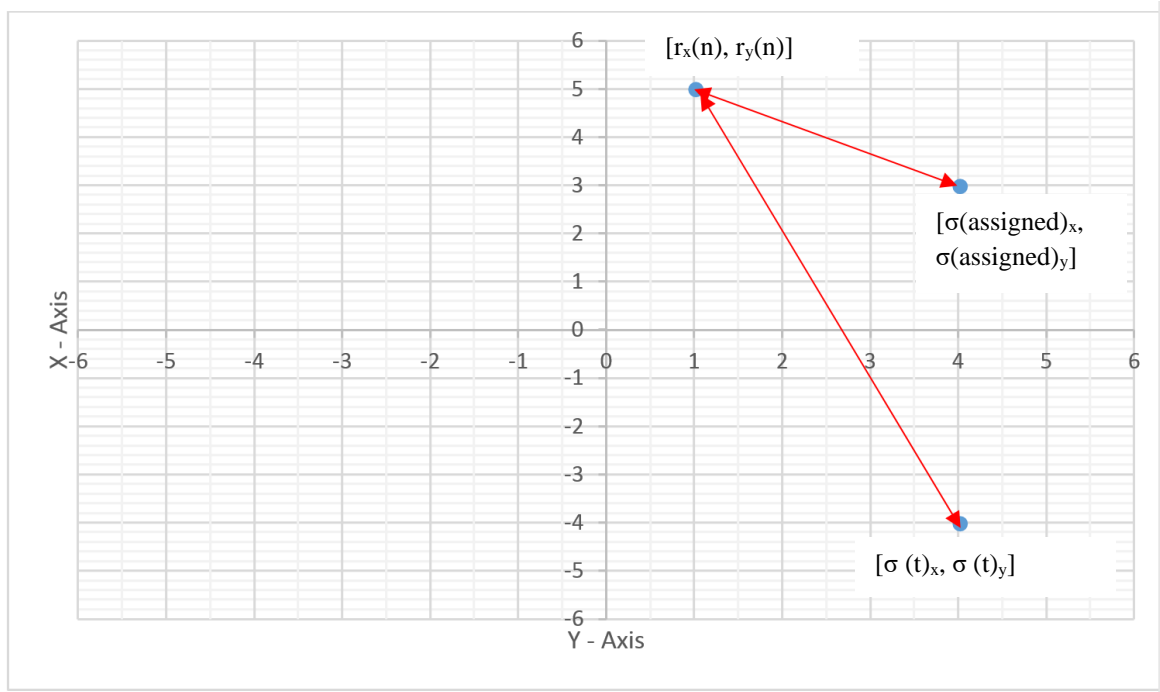


Fig. 60. Euclidean distance calculation

Fig. 60 above illustrates vector partition being performed in order to determine regions for each input value. $r(n)$ represents the magnitude of each input sample ($|x(n)|$). The value $\sigma(\text{assigned})$ is the current assigned associated mean in vector space. Variable $\sigma(t)$ is an iterative value that selects between all other centroids (from 1: K) for the vector distance calculation [41].

$$\overline{\text{distance}}_a = \sqrt{(r_x(n) - \sigma_{(\text{assigned})}(n))^2 + (r_y(n) - \sigma_{y(\text{assigned})}(n))^2} \quad (26)$$

$$\overline{\text{distance}}_t = \sqrt{(r_x(n) - \sigma_t(n))^2 + (r_y(n) - \sigma_t(n))^2} \quad (27)$$

$$r(n) = \{r(n) : \overline{\text{distance}}_a < \overline{\text{distance}}_t \quad \{t = 1 \dots K\} \quad (28)$$

As described by the above equations it is possible to determine the nearest centroid for each sample, thereby assigning each sample with a region in the vector space [41]. In practice for behavioral modeling applications, X and Y axis can be normalized magnitude of the current input sample and normalized magnitude of a previous input sample. This type of partitioning allows the possibility to use a separate Volterra series for each segment (Vector Switched Volterra – VSV). As highlighted before, for applications such as Doherty, outphasing, Digital Doherty or any other type where clear separate nonlinear regions are visible in characteristic plots of the data.

4.7.2.2. KOHONEN’S SELF-ORGANIZED MAPS (SOM)

In comparison to K-means technique, SOM offers better-explored segments due to the weakness of K-means as highlighted above. Consequently, depending on the data set a better-approximated result for a Volterra kernel is found by SOM. SOM also known as Kohonen neural networks is essentially an effective way of mapping separate regions of input data into a grid with N-dimensions (for N-neurons). Both K-means and Self-Organized maps fall into the category of unsupervised learning techniques in ANN. Meaning the training of the ANN network is carried-out entirely by its input data with no knowledge of the desired output data. Training in SOM allows to group data into several clusters. Neurons in SOM relates to their immediate neighbors, this helps each individual neuron to gather data inputs with similar properties to be clustered together and to learn from surrounding neurons. A competitive-learning network is introduced among neurons by the binary function. One of the neurons becomes the *winner* and through negative feedback, the output of other neurons are suppressed. Winners alternate between distinct inputs, after several inputs each neuron adapts itself to a unique domain of input signals and performs as the decoder to input signals within that domain [41]. After the completion of training, when a new set of inputs are supplied to the model they are expected to be

clustered in a similar manner. This helps in the modeling of different types of PAs with complex nonlinear characteristics.

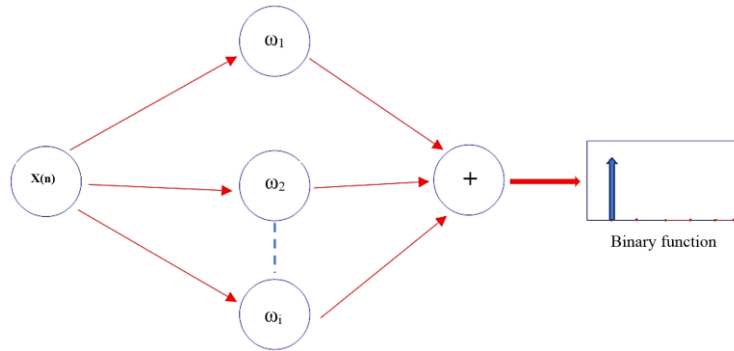


Fig. 61. Neuron structure of a SOM, with several weights (ω_i), inputs ($X(n)$ is the discrete input signal.) and monotonic binary function.²⁰

In the work performed, SOM input data vector (power amplifier measured data) were classified into being fitted to a neuron representing each cluster with minimum cluster points, as defined by the user. A 2D structure of neurons effectively segments the input data set into different groups. As mentioned in literature SOM is computationally more expensive than K-means technique of VSV [43].

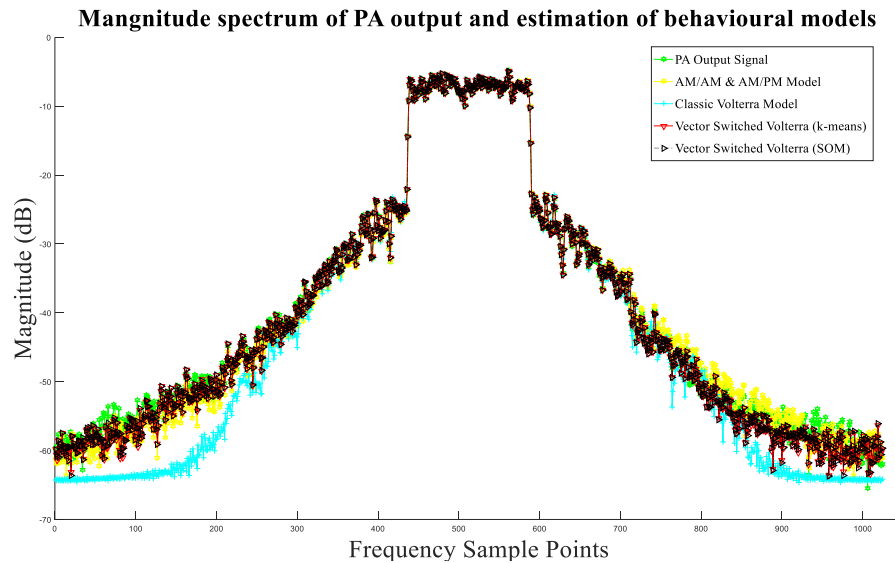


Fig. 62. The magnitude of frequency domain plots of output from each model compared with the measured results [42]

²⁰ References used in understanding neuron structure of a SOM – [41], and [43]

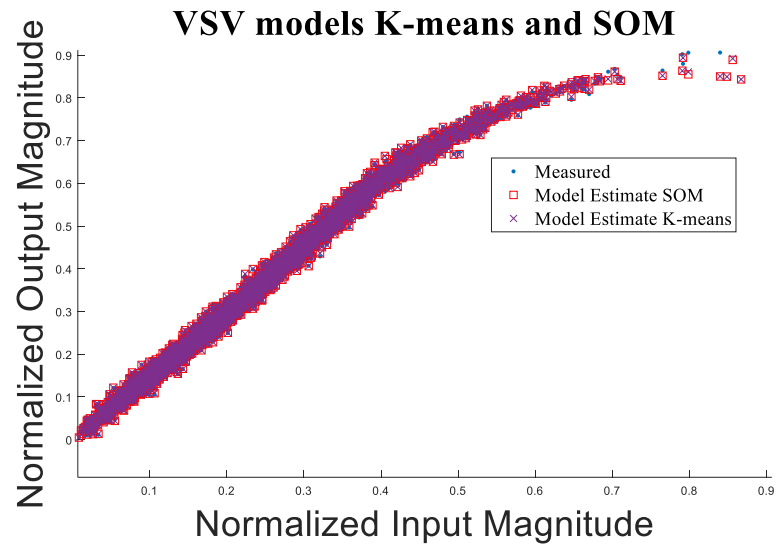


Fig. 63. K-means and SOM model characterizing the output signal of the PA in AM/AM distortion curve.

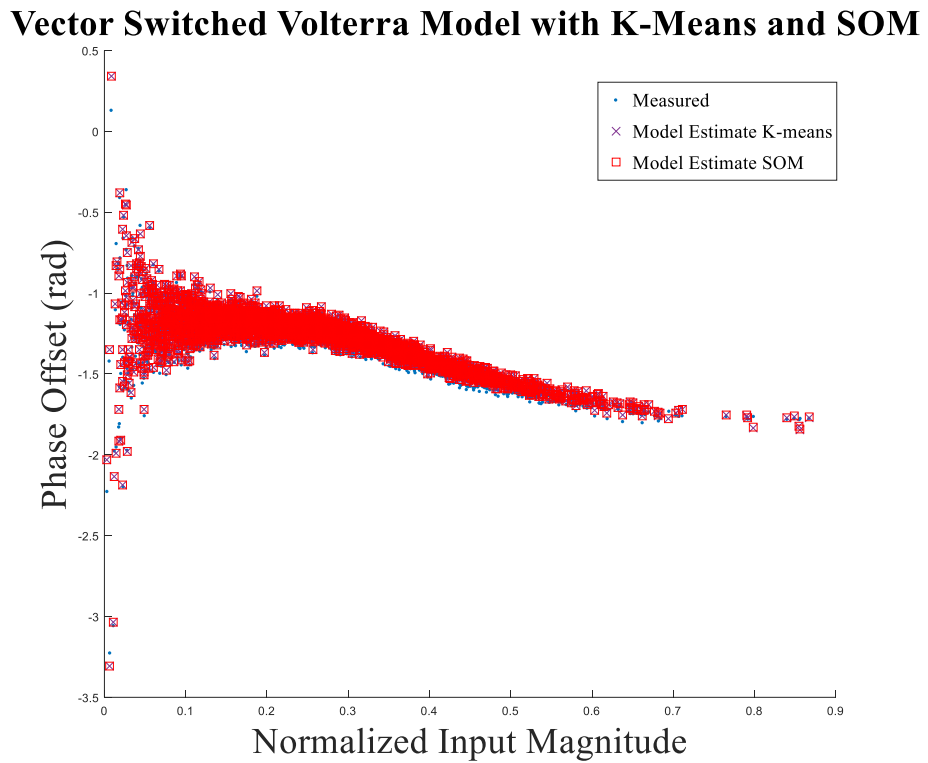


Fig. 64. K-means and SOM models characterizing the output signal of the PA in AM/PM distortion curve.

4.8. CONCLUSIONS

In this work memory less, modeling techniques such as AMAM and AMPM was used to verify the performance of these techniques in accurate modeling of the DPA. Techniques such as VSV was used as models with memory. These four models represents both memory less and with memory modeling in behavioral modeling, therefore other techniques such as Hammerstein or Weiner has not been used however, as the chosen models of that category will result in similar results.

For a single input single output system with complex envelope input signals, asymmetrical Doherty power amplifiers is a suitable choice for the proposed application. As portrayed by the results of Fig. 62 behavioral modeling techniques offer an accurate characterization of the amplifier. As explained VSV models offer much greater accuracy in comparison to classical techniques at the cost of computational efficiency. For an input of 5 MHz bandwidth, the DPA performance can be well approximated via classical techniques (NMSE of -24 and -27 dB for AMAM-AMPM and classical Volterra) as the Doherty transition region indicates a smoother response, indicating a good DPA design. VSV models are introduced, however, for a more challenging scenario of the input signal with higher bandwidth involving more memory effects and a higher number of samples in high power region it is expected to show a better approximation. However, to prove the suggested application, within the boundaries for the work of this chapter, an asymmetrical Doherty PA has been successfully fabricated and has been tested and modeled indicating the validity of such technique for a more complex system level architecture.

Chapter 5

Conclusions and Future work

The aim of this chapter is to summarize the work performed in relation to the enhancement of the performance of RF wireless transmitters using analog and DSP techniques and to present the possible future improvements, interesting research directions that can be undertaken based on the existing work performed.

5.1. CONCLUSIONS

Identified problems in wireless transmitters have been presented in the background and in the introduction of this thesis. These include RF path impairments, higher efficiency power amplifiers for wide bandwidth signals and simulation of complex wireless transmitter architectures. These issues span the full length of the transmitter chain. As such an integrated approach of hardware and DSP techniques for an RF transmitter architecture were required. As seen in full transmitter chain in Figure 65 the work carried out addresses three main areas in developing wireless RF transmitters:

- 1) RF path calibration which leads to an improvement in performance of hardware components in the transmitter
- 2) Advanced N-way digitally driven Doherty power amplifiers to provide more power efficient and application-oriented design of power amplifiers with digital control
- 3) Behavioral modeling of Doherty power amplifiers to overcome large simulation times associated with complex system level simulations e.g. distributed arrays of PAs.

In summary of work performed as presented in individual chapters;

Chapter two portrays a novel calibration technique which performs constellation mapping. This new technique can be applied in a variety of test cases such as weakly and strongly nonlinear systems with detailed methods of identifying unique types of impairments inherent to the system tested. This work helps to make the maximum use of existing hardware components in the RF transmitter by compensating impairments associated with and thus enabling maximum performance. As an example; following experimental results indicated by Fig. 11, Fig. 12, and Fig. 13 for testing performed at S-band, for an 8-PSK test signal an improvement of EVM by 9.62 % and SNR by 15.72 dB was obtained after performing RF path calibration via proposed method. Final values obtained for EVM was 1.881 % with a 34.51 dB of SNR. For the 256-QAM modulated signal after performing RF path calibration it was possible to obtain an EVM of 1.907 % at a SNR of 34.39 dB.

Chapter three presents a significant advancement in RF amplifier hardware used for satellite communications by integrating existing DSP techniques and different types of Doherty power amplifier architectures for the operation in Ku-band. A detailed comparison of performance and previous techniques has been given. Concept of using four-way or N-way Doherty as discrete small signal devices has been presented. It is expected that this work will be of valuable contribution to further advance the performance of power amplifiers used in a RF transmitter as the main power consuming component. In terms of performance a four-way architecture provided a 19.2 dBm of output power with 40% of PAE for a single tone excitation. For a 64-QAM modulated test signal of 800 MHz bandwidth without DPD it was able to have a dynamic range of \sim -50 dBc.

Chapter four highlights the importance of achieving reduced simulation times of a distributed arrays of PAs by using behavioral models and there by shortening the time taken for production and testing of advanced structure that are expected to facilitate the needs of future mobile communication standards for 5G and MIMO. An asymmetrical DPA is a single-input-signal-output nonlinear power amplifier which can provide higher efficiencies, therefore it can be used in the amplification stage of a distributed array to provide better performance in comparison other basic power amplifier architectures. Fig.

63 and Fig. 64 indicates AMAM and AMPM plots for estimated output performance using VSV models and actual output data extracted from the fabricated DPA. The models show good agreement with the measured test data in both cases. Therefore, as a substitute for physical or circuit level models behavioral modeling techniques can be used to approximate the performance of a higher level DPA architecture successfully.

The three methods mentioned as above provides better integration between analogue and digital domains and hence provides the much-needed improvement in overall performance for present and future wireless transmitters. Thus, proving the objective for this research work, which is to utilize and combine advanced capabilities in DSP techniques and advanced architectures of hardware for future wireless transmitter designs.

Analogue and Digital Co-design Methods for Future Wireless Transmitters

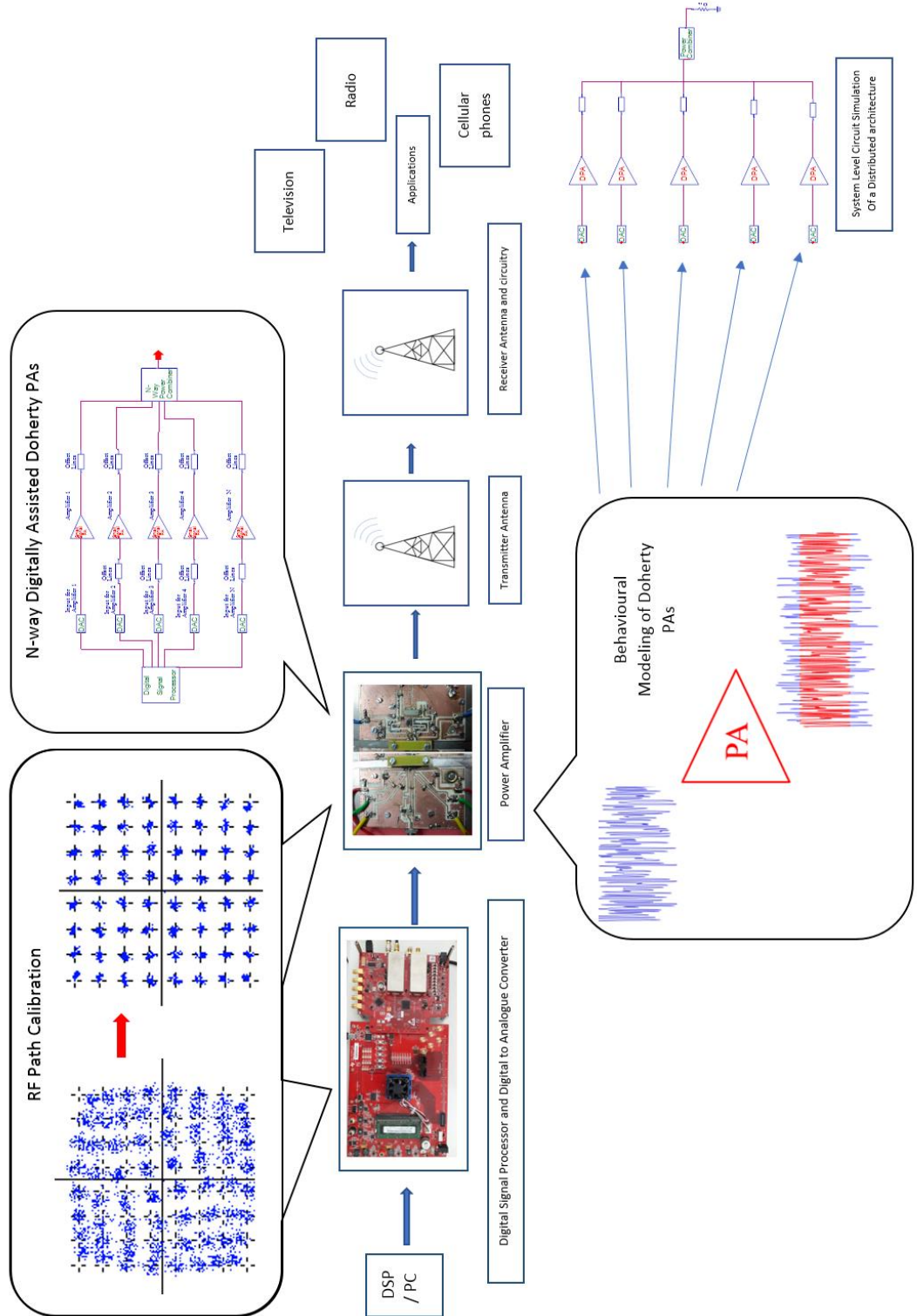


Fig. 65. Overall view of research performed placed in relation to the RF transmit path

5.2. FUTURE WORK FROM NOVEL CALIBRATION TECHNIQUE

Possible further to work to be undertaken from findings in chapter two where a novel RF path calibration technique is introduced based on mapping of constellation points of a 64-QAM signal are presented below.

The bit error rate or EVM is a function of the power level of the received signal. A residual BER calculation can be implemented as depending upon the received signal strength and the error floor. The concept behind residual BER is to offer an indication of the level of signal strength required of the received signal for nominal operation [15]. In comparison to single path calibration performed for weakly, strongly nonlinear systems, a multipath solution can also be implemented to address a variety of different challenges and this will also enable possibility of applying the proposed technique to multiple input and output systems. Further testing may be performed encapsulating different test scenarios such as a complete transceiver calibration or calibration with the over-the-air transmission which emulates a further practical application scenario.

The technique is capable of characterizing both weakly and strongly nonlinear systems including PAs. Therefore, as results indicates an improvement in linearity in the passband, this technique may also be further developed as an alternate practical DPD technique.

5.3. FUTURE WORK FROM N-WAY DIGITALLY DRIVEN DOHERTY AMPLIFIER

Further to current work performed on chapter three, several identified sub-categories that are worth exploring are mentioned below.

Currently, in following the proposed design the carrier amplifier undergoes a transformation ratio of 1:4 in comparison to that of a traditional DPA of 1:2 (Refer to Fig. 42). Meaning at higher transformation ratios (such as 1:4) load-line undergoes a further shift towards left in the output characteristics curve of the device. Further investigation may be executed to find the range of input amplitude levels does the current load-line supports in comparison to that of traditional 1:2. However, without performing any significant design alterations, it is possible to change the biasing of one peaking amplifier branch to be at class AB or class A (essentially a carrier amplifier) to maintain a relationship of a 1:2 as the impedance transformation for each of the carrier paths. Several questions can be answered in doing so. E.g. by selecting bias levels for both carrier amplifiers intelligently, does it help to have a superior linear performance at several input power levels or does it help in obtaining more output power with a fewer number of units?

Currently, power of the input signal is equally distributed among input paths a function to distribute the input power differently may be developed like the operation of an asymmetrical Doherty power amplifier. Does this provide an improvement in performance? Another interesting aspect is to make use of two separate paths to be matched and ready to perform at a different frequency band (other than Ku-band, perhaps K-band or Ka-band); resulting in a multi-band solution. Since the inputs are digitally driven input paths are well isolated from one-another and can readily be controlled by Digital Signal Processing (DSP) techniques. In this scenario, how well does the current design of the combiner perform? What alterations of the combiner can be made to obtain a multi-band solution?

5.4. FUTURE WORK FROM BEHAVIORAL MODELING

In the chapter on behavioral modeling (chapter four) idea of using a behavioral model of a fabricated asymmetrical power amplifier for the used in distributed array of power amplifiers is presented.

Proposed solution has been validated experimentally with measured test results which indicates the validity of the different behavioral modeling techniques in correctly modeling the behavior of the used Doherty power amplifier. The method can be further evaluated in characterizing power amplifiers with multiple input paths, as these advanced architectures are predicted to dominate the wireless amplification stage in future base-stations. Example uses are of multiple input systems are N-way Doherty, multilevel outphasing etc. However, designing and in building such system would take a considerable amount of effort as explained in section 3.1. Validating performance of the different behavioural models with different types of power amplifiers would provide an understanding of which models are better at modelling different power amplifier topologies. In addition, to all possibilities mentioned above a simulation of a distributed array may also be performed in a circuit simulation software such as Keysight's ADS to validate the performance of the behavioural model comparatively to that of a physical and a circuit level model.

References

- [1] M. Deepak Nair, R. Giofre, P. Colantonio, and F. Giannini, "Effects of Digital Predistortion and Crest Factor Reduction techniques on efficiency and linearity trade-off in Class AB GaN-PA," in *2015 European Microwave Conference (EuMC)*, 2015, pp. 1128–1131.
- [2] R. Braithwaite, "The effects of power amplifier nonlinearities and CFR on 64QAM HSDPA Waveforms," in *81st ARFTG Microwave Measurement Conference*, 2013, pp. 1–3.
- [3] X. Ruan, Y. Wang, Q. Jin, "A Review of Envelope Tracking Power Supply for Mobile Communication Systems," *CPSS Trans. Power Electron. Appl.*, vol. 2, no. 4, pp. 277–291, Dec. 2017.
- [4] H. Lee, S. Jang, and S. Hong, "A Hybrid Polar-LINC CMOS Power Amplifier With Transmission Line Transformer Combiner," in *IEEE Transactions on Microwave Theory and Techniques*, 2013, vol. 61, no. 3, pp. 1261–1271.
- [5] Keysight Technologies, Appl. Note, "LTE and LTE-Advanced Solutions." [Online]. Available: <https://literature.cdn.keysight.com/litweb/pdf/5989-7817EN.pdf?id=1366595-1-eng>. [June 30, 2018].
- [6] Keysight Technologies, Appl. Note, "Keysight Technologies Custom OFDM Signal Generation Using SystemVue." [Online]. Available: <https://literature.cdn.keysight.com/litweb/pdf/5990-6998EN.pdf?id=1988473> [June 30, 2018].
- [7] FormFactor Inc (formerly CascadeMicrotech), Appl. Note, "Calibration Tools: Consistent Parameter Extraction for Advanced RF Devices," 2012. [Online]. Available: <https://www.cascademicrotech.com> [June 10, 2018].
- [8] S. Aldoumani, "Calibration Enhancement of Nonlinear VNA System," PhD. thesis, Cardiff University, United Kingdom, 2017.
- [9] X. Zhang, M. Matthaiou, E. Bjornson, M. Coldrey, and M. Debbah, "On the MIMO capacity with residual transceiver hardware impairments," in *2014 IEEE International Conference on Communications (ICC)*, 2014, pp. 5299–5305.

- [10] X. Zhang, M. Matthaiou, M. Coldrey, and E. Bjornson, "Impact of Residual Transmit RF Impairments on Training-Based MIMO Systems," in *IEEE Transactions on Communications*, 2015, vol. 63, no. 8, pp. 2899–2911.
- [11] J. Qi and S. Aissa, "Analysis and compensation of i/q imbalance in MIMO transmit-receive diversity systems." in *IEEE Transactions on Communications*, 2010, vol. 58, no. 5, pp. 1546–1556.
- [12] E. Bjornson, J. Hoydis, M. Kountouris, and M. Debbah, "Massive MIMO Systems With Non-Ideal Hardware: Energy Efficiency, Estimation, and Capacity Limits," in *IEEE Transactions on Information Theory*, 2014, vol. 60, no. 11, pp. 7112–7139.
- [13] A Khandelwal, A Verma, "A Novel Gain, Phase and Offset Calibration Scheme for Wideband Direct-Conversion Transmitters", Vehicular Technology Conference (VTC Spring), 2015 IEEE 81st, DOI: 10.1109/VTCSpring.2015.7145633.
- [14] Prasidh Ramabadrn, Sidath Madhuwantha, Pavel Afanasyev, Ronan Farrell, Lazaro Marco, Sergio Pires and John Dooley, "Digitally Assisted Wideband Compensation of Parallel RF Signal Paths in a Transmitter," 91st ARFTG Microwave Measurement Conference, Philadelphia, PA, USA, 2018.
- [15] Keysight Technologies, Appl. Note, "Lowering Cost and Improving Interoperability by Predicting Residual BER: Theory, Measurements, and Applications."
- [16] K. Nam, Appl. Note, "TI Designs High Speed: CerTified™ Design Direct Down-Conversion System with I/Q Correction." [Online].
Available: <http://www.ti.com/lit/ug/slwu085/slwu085.pdf>. [March 10, 2018].
- [17] Keysight Technologies, Appl. Note, "Keysight Technologies Measuring ACLR Performance in LTE Transmitters." [Online].
Available: <https://www.keysight.com>. [June 18, 2018].
- [18] W.H.Doherty, "A new high efficiency power amplifier for modulated waves," *IRE*, vol. 24, no. 9, pp. 1163-1182, Sept. 1936.
- [19] A.Grebennikov and S.Bulja, "High-Efficiency Doherty Power Amplifiers: Historical Aspect and Modern Trends," *Proc. IEEE*, vol. 100, no. 12, pp. 3190–3219, Dec. 2012.
- [20] W. H. Doherty, "Amplifier," US2210028A, Aug. 1940.

- [21] R. Darraji, F.M. Ghannouchi, and O. Hammi, "A Dual-Input Digitally Driven Doherty Amplifier Architecture for Performance Enhancement of Doherty Transmitters," *IEEE Trans. Microw. Theory Tech.*, vol. 59, no. 5, pp. 1284–1293, May 2011.
- [22] F.M. Ghannouchi, and R. Darraji, "Extended bandwidth digital doherty transmitter," US 2012/0294387 A1, 2011.
- [23] X. Moronval, J.-J. Bouny, and G. Bouisse, "Integrated 3-Way Doherty Amplifier." U.S. Patent US20170230009A1, 2017.
- [24] R. Darraji and F.M. Ghannouchi, "Digital Doherty Amplifier With Enhanced Efficiency and Extended Range," *IEEE Trans. Microw. Theory Tech.*, vol. 59, no. 11, pp. 2898–2909, Nov. 2011.
- [25] Andy Howard, "Presentation on power amplifier design with custom templates," in www.agilent.com/find/eesof, 2000, pp. 1–39.
- [26] P. Colantonio, F. Giannini, and E. Limiti, High efficiency RF and microwave solid state power amplifiers. J. Wiley, 2009.
- [27] C. Burns, "GaN on SiC: RFMD High Power Doherty Design, Modeling & Measurement Webcast Slides," *Innov. EDA Keysight Train. events*, 2013.
- [28] S.C. Cripps, RF Power Amplifier Design for Wirelss Communications, Archtech House, 1999.
- [29] S. Madhuwantha, P. Ramabadran, R. Farrell, and J. Dooley, "N-way Digitally Driven Doherty Power Amplifier Design and Analysis for Ku band Applications," presented at the Conf. in 29th Irish Signals and Systems Conference, Queens University Belfast, UK, June. 21-22, 2018.
- [30] J.M Rollett, "Stability and power gain invariants of linear two-ports", *IRE Trans. Circuit Theory*, 1962, 9, (3), pp. 29–32.
- [31] Keysight Technologies, "Keysight Technologies" [Online].
Available: www.keysight.com
- [32] R. E. Collin, *Foundations for microwave engineering*, 2nd ed. Wiley-IEEE Press, 2001. pp 303-387, pp.713-798.

- [33] P. Aaen, J. A. Plá, and J. Wood. (2007). *Modeling and characterization of RF and microwave power FETs*. (1st edition).[Online]
Available: <https://www.cambridge.org/> [May 05, 2018]
- [34] J. Liu, “Practical behavioral modeling technique of power amplifiers based on loadpull measurements Scholar Commons Citation,” The University of South Florida.
- [35] U. Madhow, D. R. Brown, S. Dasgupta, and R. Mudumbai, “Distributed massive MIMO: Algorithms, architectures and concept systems,” in *2014 Information Theory and Applications Workshop (ITA)*, 2014, pp. 1–7.
- [36] T. L. Marzetta, E. G. Larsson, H. Yang, and H. Q. Ngo, *Fundamentals of Massive MIMO*. Cambridge University Press, 2016.
- [37] A. M. Saleh, “Frequency-Independent and Frequency-Dependent Nonlinear Models of TWT Amplifiers,” *IEEE Trans. Commun.*, vol. 29, no. 11, pp. 171
- [38] Ghorbani and M. Sheikhan, “The effect of solid state power amplifiers (SSPAs) nonlinearities on MPSK and M-QAM signal transmission,” in *1991 Sixth International Conference on Digital Processing of Signals in Communications*, 1991, pp. 193–197.
- [39] F. M. Ghannouchi, O. Hammi, and M. Helaoui, (2015, July, 24) *Behavioral Modeling and Predistortion of Wideband Wireless Transmitters*, (1st edition). [On-line]. Vol 1. Available: <https://ebookcentral.proquest.com> [May 21, 2018]
- [40] G. P. White, A. G. Burr, and T. Javornik, “Modelling of nonlinear distortion in broadband fixed wireless access systems,” *Electron. Lett.*, vol. 39, no. 8, p. 686, 2003.
- [41] T. Kohonen, *Self-Organizing Maps*, vol. 30. Berlin, Heidelberg: Springer Berlin Heidelberg, 2001, pp.1-5,76-104.
- [42] S. Madhuwantha et al., “Behavioural Models for Distributed Arrays of High Performance Doherty Power Amplifiers,” presented at the Conf. in 29th Irish Signals and Systems Conference, Queens University Belfast, UK, June. 21-22, 2018.
- [43] K. Finnerty, “Linear Operation of Switch-Mode Outphasing Power Amplifiers,” PhD. thesis, Maynooth University, Ireland, 2016.
- [44] L. Ding, “Digital Predistortion of Power Amplifiers for Wireless Applications,” PhD. thesis, Georgia Institute of Technology, United States of America, 2004.

- [45] D. Schreurs, M. ODroma, A. A. Goacher, and M. Gadringer, "Overview of power amplifier modelling," in *RF Power Amplifier Behavioral Modeling*, Cambridge: Cambridge University Press, 2008, pp. 1–10, 136-162, 163-185.
- [46] H. Ku and J. S. Kenney, "Behavioral modeling of RF power amplifiers considering IMD and spectral regrowth asymmetries," in *IEEE MTT-S International Microwave Symposium Digest*, 2003, pp. 799–802.
- [47] P. Alper, "A consideration of the discrete Volterra series," *IEEE Trans. Automat. Contr.*, vol. 10, no. 3, pp. 322–327, Jul. 1965.
- [48] T. Liu, S. Boumaiza, and F. M. Ghannouchi, "Dynamic Behavioral Modeling of 3G Power Amplifiers Using Real-Valued Time-Delay Neural Networks," *IEEE Trans. Microw. Theory Tech.*, vol. 52, no. 3, pp. 1025–1033, Mar. 2004.
- [49] F. Launay, Y. Wang, S. Toutain, S. T. D. Barataud, J. M. Nebus, and R. Quere, "Nonlinear amplifier modeling taking into account HF memory frequency," in *2002 IEEE MTT-S International Microwave Symposium Digest (Cat. No.02CH37278)*, pp. 865–868.
- [50] F. Rosenblatt, "The perceptron, a perceiving and recognizing automaton (Project Para)". Buffalo, New York: Cornell Aeronautical Laboratory, 1957, Vol. 85-460-1.
- [51] Qi-Jun Zhang, K. C. Gupta, and V. K. Devabhaktuni, "Artificial neural networks for RF and microwave design—from theory to practice," *IEEE Trans. Microw. Theory Tech.*, vol. 51, no. 4, pp. 1339–1350, Apr. 2003.
- [52] S. Afsardoost, T. Eriksson, and C. Fager, "Digital Predistortion Using a Vector-Switched Model," *IEEE Trans. Microw. Theory Tech.*, vol. 60, no. 4, pp. 1166–1174, Apr. 2012.
- [53] F. Bacao, V. Lobo, and M. Painho, "Self-organizing maps as substitutes for k-means Clustering," in *Computational Science ICCS 2005 (V. Sunderam, G. van Albada, P. Sloat, and J. Dongarra, eds.)*, vol. 3516 of *Lecture Notes in Computer Science*, pp. 476–483, Springer Berlin Heidelberg, 2005.
- [54] A. Ayang, P.-S. Ngohe-Ekam, B. Videme, and J. Temga, "Power Consumption: Base Stations of Telecommunication in Sahel Zone of Cameroon: Typology Based on the Power Consumption—Model and Energy Savings," *Journal of Energy-Hindawi*, vol. 2016, pp. 1–15, Jul. 2016.

- [55] O. Blume, D. Zeller, and U. Barth, "Approaches to energy efficient wireless access networks," in 2010 4th International Symposium on Communications, Control and Signal Processing (ISCCSP), 2010, pp. 1–5.
- [56] Rohde and Schwarz, "R&S®FSQ-K70/FSMR/FSU-B73 Vector Signal Analysis Software Manual," 2014. [Online]
Available: <http://www.rohde-schwarz.com> [June 27, 2018]
- [57] K. Han and X. Luo, "A 9.5–18.5 GHz power amplifier for multi-band microwave point-to-point backhaul communication," *2014 IEEE Radio Frequency Integrated Circuits Symposium*, Tampa, FL, 2014, pp. 339–342.
- [58] Y. S. Noh, M. S. Uhm, and I. B. Yom, "A Compact Ku-Band SiGe Power Amplifier MMIC With On-Chip Active Biasing," in *IEEE Microwave and Wireless Components Letters*, 2010, vol. 20, no. 6, pp. 349–351.
- [59] Bon-Hyun Ku, Sang-Hyun Baek, and Songcheol Hong, "A X-band CMOS power amplifier with on-chip transmission line transformers," in *2008 IEEE Radio Frequency Integrated Circuits Symposium*, 2008, pp. 523–526.
- [60] A. V. Vasylyev, P. Weger, W. Bakalski, and W. Simbuerger, "17-GHz 50-60 mW power amplifiers in 0.13- μm standard CMOS," in *IEEE Microwave and Wireless Components Letters*, 2006, vol. 16, no. 1, pp. 37–39.
- [61] C. Caliskan, I. Kalyoncu, E. Ozeren, M. Kaynak, and Y. Gurbuz, "A wideband low noise SiGe medium power amplifier for X-Band Phased Array applications," in *2016 11th European Microwave Integrated Circuits Conference (EuMIC)*, 2016, pp. 9–12.
- [62] G. Cheng, Z. Li, L. Luo, Y. Yao, X. He, and B. He, "Design of Ku-band SiGe-HBT power amplifier with through-silicon-via applying 3-D EM simulation," in *2017 IEEE Electrical Design of Advanced Packaging and Systems Symposium (EDAPS)*, 2017, pp. 1–3.
- [63] Y. Chen, M. P. van der Heijden, and D. M. W. Leenaerts, "A 1-Watt Ku-band power amplifier in SiGe with 37.5% PAE," in *2016 IEEE Radio Frequency Integrated Circuits Symposium (RFIC)*, 2016, pp. 324–325.
- [64] Triquint, "<http://www.triquint.com/products/p/TGA2510-SG>," TGA2510-SG datasheet.
- [65] Triquint, "<http://www.triquint.com/products/p/TGA2527-SM>," TGA2527-SM datasheet.

- [66] M. L. Bhavsar, P. Srivastava, and A. Bhattacharya, "A Ku-band 1-Watt two stage power amplifier MMIC for space with 52% Power added efficiency," in 2016 Asia-Pacific Microwave Conference (APMC), 2016, pp. 1–4.
- [67] M. Darwish and A.-V. Pham, "Compact and high efficiency Doherty power amplifier using a new modulation load range," in *2017 IEEE MTT-S International Microwave Symposium (IMS)*, 2017, pp. 782–784.
- [68] J. Kim, B. Fehri, S. Boumaiza, and J. Wood, "Power Efficiency and Linearity Enhancement Using Optimized Asymmetrical Doherty Power Amplifiers," *IEEE Trans. Microw. Theory Tech.*, vol. 59, no. 2, pp. 425–434, Feb. 2011.
- [69] C. F. Campbell, "A fully integrated Ku-band Doherty amplifier MMIC," in *IEEE Microwave and Guided Wave Letters*, vol. 9, no. 3, pp. 114–116, March 1999.
- [70] R. Quaglia, V. Camarchia, T. Jiang, M. Pirola, S. Donati Guerrieri and B. Loran, "K-Band GaAs MMIC Doherty Power Amplifier for Microwave Radio With Optimized Driver," in *IEEE Transactions on Microwave Theory and Techniques*, vol. 62, no. 11, pp. 2518–2525, Nov. 2014.
- [71] P. Colantonio, F. Giannini, R. Giofre and L. Piazzon, "Increasing Doherty Amplifier Average Efficiency Exploiting Device Knee Voltage Behavior," in *IEEE Transactions on Microwave Theory and Techniques*, vol. 59, no. 9, pp. 2295–2305, Sept. 2011.
- [72] K. El-Akhdar, S. Ahmed, G. Neveux, D. Barataud and J. M. Nebus, "Calibrated RF time-domain measurement of non-linear devices in digital polar transmitter architecture," 2013 European Microwave Conference, Nuremberg, 2013, pp. 452–455.
- [73] H. Shi, H. Jensen, "Calibrating an RF transmitter," U.S. Patent US20050059361A1, 2005.
- [74] J. van der Geest, "permn(V, N, K) - File Exchange - MATLAB Central." MathWorks File Exchange, 2016.

Appendix

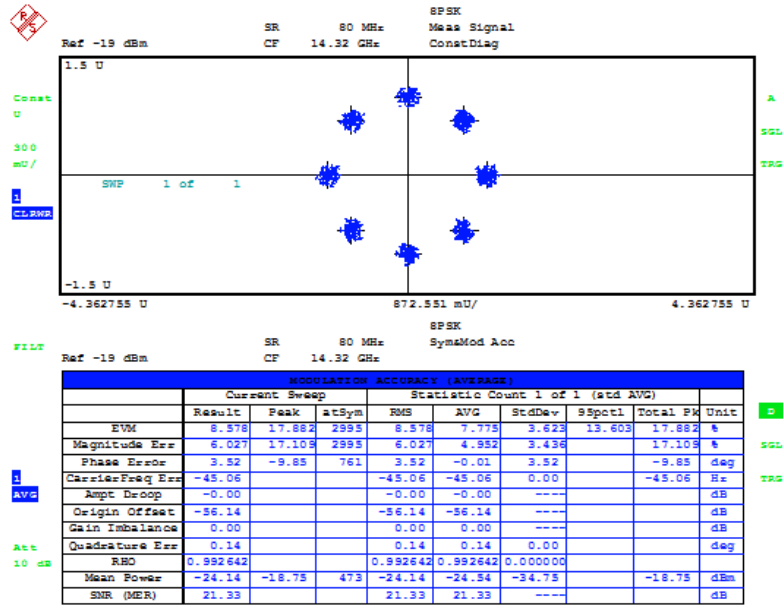


Fig. 66. 8-PSK uncalibrated constellation test result at Ku-band

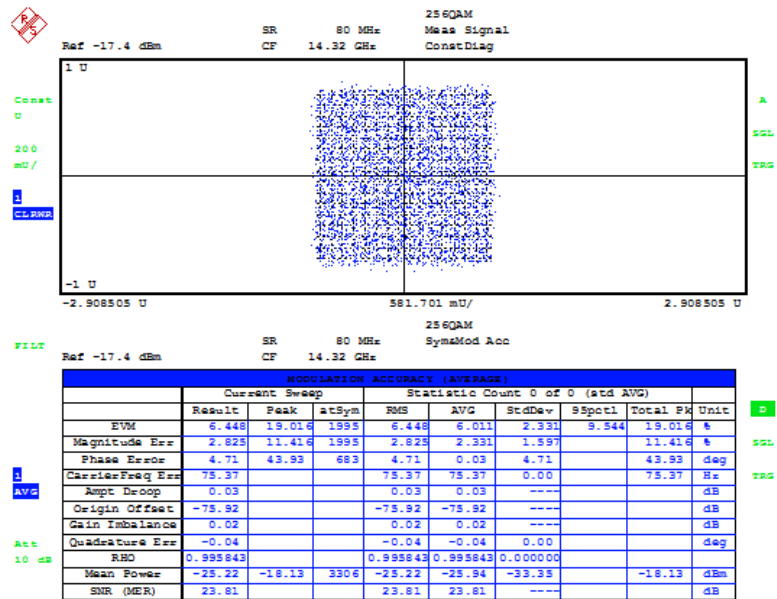


Fig. 67. 256-QAM uncalibrated constellation test at Ku-band. SNR of the signal is lower than that of the Shannon limit for correct demodulation of 256-QAM signal constellation.

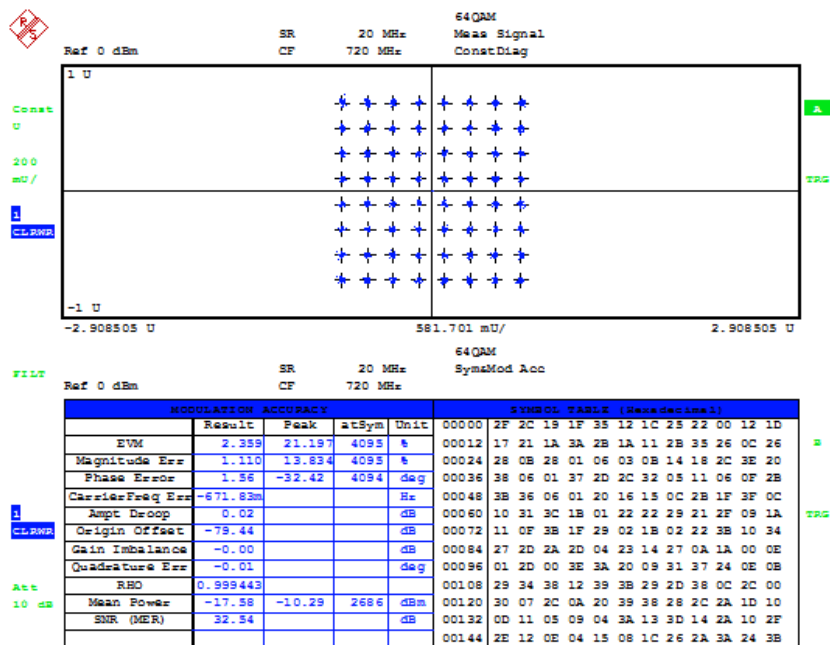


Fig. 68. 64-QAM uncalibrated constellation with DPA at linear conditions at a very low input power level (-10 dBm).

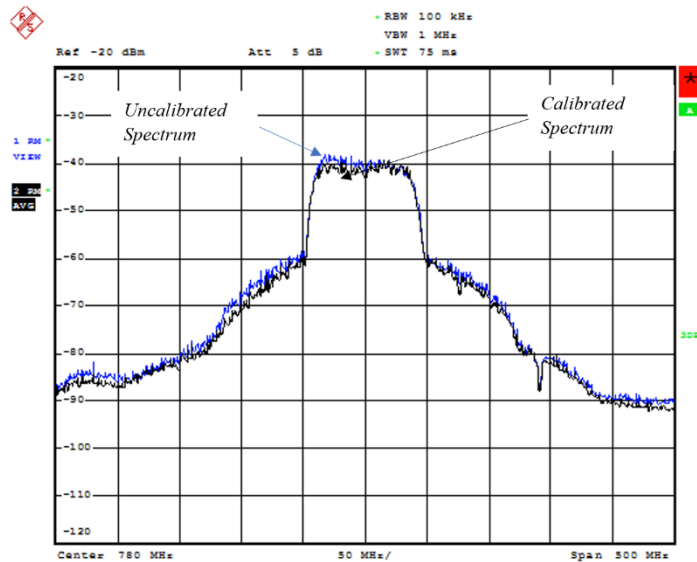


Fig. 69. Magnitude spectrum of uncalibrated and calibrated strongly nonlinear system (with DPA, driver amplifier and DAC board – example test setup is Fig. 19) driven with 80 MHz 64-QAM modulated calibration signal captured at 500 MHz of span (RBW 100 kHz, VBW 1 MHz and SWT 75 ms).

Amplitude tilt can clearly be seen to be compensated within the pass band resulting in a flatter frequency response.